SINGLE-BAND AND DUAL-BAND BEAM SWITCHING SYSTEMS AND OFFSET-FED BEAM SCANNING REFLECTARRAY

A Dissertation

by

JUNGKYU LEE

Submitted to the Office of Graduate Studies of
Texas A&M University
in partial fulfillment of the requirements for the degree of

DOCTOR OF PHILOSOPHY

May 2012

Major Subject: Electrical Engineering

SINGLE-BAND AND DUAL-BAND BEAM SWITCHING SYSTEMS AND OFFSET-FED BEAM SCANNING REFLECTARRAY

A Dissertation

by

JUNGKYU LEE

Submitted to the Office of Graduate Studies of
Texas A&M University
in partial fulfillment of the requirements for the degree of

DOCTOR OF PHILOSOPHY

Approved by:

Chair of Committee,	Kai Chang
Committee Members,	Robert D. Nevels
	Laszlo Kish
	Yongheng Huang
Head of Department,	Costas N. Georghiades

May 2012

Major Subject: Electrical Engineering

ABSTRACT

Single-band and Dual-band Beam Switching Systems and Offset-fed Beam Scanning Reflectarray. (May 2012)

Jungkyu Lee, B.S., Kwangwoon University;

M.S., University of California at Irvine

Chair of Advisory Committee: Dr. Kai Chang

The reflectarray has been considered as a suitable candidate to replace the conventional parabolic reflectors because of its high-gain, low profile, and beam reconfiguration capability. Beam scanning capability and multi-band operation of the microstrip reflectarray have been main research topics in the reflectarray design. Narrow bandwidth of the reflectarray is the main obstacle for the various uses of the reflectarray. The wideband antenna element with a large phase variation range and a linear phase response is one of the solutions to increase the narrow bandwidth of the reflectarray.

A four beam scanning reflectarray has been developed. It is the offset-fed microstrip reflectarray that has been developed to emulate a cylindrical reflector. Unlike other microstrip reflectarrays which integrates phase tuning devices such as RF MEMS switches and another phase shifters to the reflectarray elements and control the reflected phase, the beam scanning capability of the reflectarray is implemented by a phased array feed antenna. This method can reduce the complexity of the design of the beam switching reflectarray. A simple method has been investigated to develop multi-band

elements in this dissertation. In approach to increase the coverage of the operation bands, a six-band reflectarray has been developed with two layers. Each layer covers three frequency bands.

A Butler matrix is one of the useful beamforming networks for a phased array antenna. A Double-Sided Parallel-Strip Line (DSPSL) is adapted for the feeding network of eight array elements. The DSPSL operate very well to feed the microstrip antenna array over the bandwidth to reduce the sidelobe level and a high gain. In another topic of a Butler matrix, a dual-band Butler matrix has been proposed for multi-band applications. A modified Butler matrix is used to reduce a size and a sidelobe level.

The bandwidth of the microstrip antenna is inherently small. A broadband circularly polarized microstrip antenna with dual-offset feedlines is introduced in this dissertation. Aperture-coupled feed method is used to feed the stacked patch antennas and a slot-coupled directional coupler is used for the circularly polarized operation.

The research presented in this dissertation suggests useful techniques for a beam scanning microstrip reflectarray, phased array antenna, and wideband antenna designs in the modern wireless communication systems.

DEDICATION

To my parents, wife, and daughters

ACKNOWLEDGEMENTS

I would like to express my deepest appreciation to Dr. Kai Chang for his support and guidance throughout my Ph.D. education at Texas A&M University. I also appreciate Dr. Robert D. Nevels, Dr. Laszlo Kish and Dr. Yongheng Huang for serving as my committee members and for their helpful comments.

I would also like to thank Mr. Ming-Yi Li for his technical assistance. I gratefully acknowledge Dr. John Huang at the Jet Propulsion Laboratory and Dr. Seongwon Oh at Korea Navy, and Dr. Shih-Hsun Hsu at Reaserch In Motion Inc. for their helpful instructions and comments for the reflectarray design. I gratefully acknowledge Mr. Chanho Kim, Mr. Travis Eubanks, Mr. Jonathan Hansen, Mr. Dongjin Jeong and other members of the Electromagnetics and Microwaves Laboratory at Texas A&M University for invaluable discussions.

Lastly, I would like to express my deep appreciation to my parents and my wife's parents for their constant love, encouragement, and support. Finally, I would like to thank my family, especially my wife, for their love, support, and patience.

TABLE OF CONTENTS

CHAPTER Page

LIST OF FIGURES

Page

Page

Page

Page

Page

LIST OF TABLES

Page

CHAPTER I

INTRODUCTION

1.1 Background

Wireless communications has been a rapidly growing part of the communication industry over the past few years and the range of application has become wider with the potential to provide high-speed high-quality information exchange between portable devices in the world. By means of the rapidly emerging wireless communications systems, based on radio and infrared transmission mechanisms, potential applications enabled by this technology include multimedia Internet-enabled cell phones like GSM and CDMA, smart homes and appliances, automated highway systems, RFID (Radio Frequency Identification) and Bluetooth. Wireless is a method of communication that utilizes radio waves to transmit and receive data between devices. There is significant research and development on smart antennas for wireless systems throughout the world because smart antennas have much potential to improve the performance of the next generation wireless systems. Smart antennas can be characterized into two main categories: adaptive antenna array and switched beam system, or phased antenna array [1]. Switched beam antenna systems form multiple fixed beams with heightened sensitivity in particular directions and switch their beams in different directions

---

This dissertation follows the style of *IEEE Transactions on Antennas and Propagation*.

throughout space by changing the phase differences of the signals used to feed the radiating elements. Adaptive array form an infinite number of patterns that are adjusted in real time using a variety of new signal processing algorithms [2, 3]. Switched beam system has advantages over adaptive antenna array in that the system can be designed in a simpler way and has the ability to select the strongest signal level of multiple beams. These systems cover a wide spectrum of frequency, from 1 MHz up to millimeter wavelengths and are used in a wide range of communication and radar applications, such as cellular telephone, mobile tracking communication system, GPS, and commercial broadcasting linear arrays.

The switched beam system consists of a beam forming network and an antenna array. Several beam forming networks have been proposed, such as the Blass matrix [4], the Nolen matrix [5], the Rotman lens [6] and the Butler matrix [7-11]. The N x N Butler matrix has been used to feed N array antenna elements. The Butler matrix has some good features such as lossless property and simple structure as compared to other matrices. The Butler matrix is composed of branch-line couplers, phase shifters, and cross-overs. In general, the Butler matrix has been realized by microstrip lines [7-11], coplanar waveguides (CPW) [12], waveguides [13], CMOS technology [14]. The N x 2N Butler matrix using the double-sided parallel-strip lines (DSPSL) has been studied. DSPSL has some advantages such as easy realization of high impedance lines, simplicity in circuit structures of wide-band transitions, and good performance of balanced microwave components and can be analyzed using the image theory [15-18]. The DSPSL with an inserted conductor plane are used at the output ports of the Butler

matrix. DSPSL are composed of two identical microstrip lines on top and bottom layers. DSPSL with the inserted common conductor plane has no effect on the identical circuits on the top and bottom layers and the conductor plane is considered as a virtual ground to isolate nonidentical circuits [16]. The beam scanning can be obtained by different feedings with the phase variation provided by the Butler matrix. The elements of the common Butler matrix are branch-line couplers, crossovers, or 0 dB coupler, and phase shifters. This beam forming network (BFN) is more complicate and has more phase error than the modified Butler matrix using only branch-line couplers and phase shifters without any crossovers.

Traditionally, large parabolic reflector antennas have been widely used in high gain antenna applications such as satellite communications, radars, radio astronomy observations, and deep-space communications. The parabolic reflector antenna features high gain over wide frequency bands. However, these antennas are an obstacle for some applications that require small volume, low profile, and mounting simplicity, because they are bulky, heavy, and their geometrical shape. Also, the capability of pattern reconfiguration, beam scanning, and beam shaping, is limited without mechanical devices. To overcome these disadvantage, reflectarray antenna was introduced by D.G. Berry in 1963 [19]. Reflectarray consists of many unit antenna elements placed on a substrate and a feed antenna. Along with developing microstrip patch antennas, a reflectarray using microstrip patch elements, called microstrip reflectarray, has presented as a substitute of parabolic reflector antennas [20-27]. The microstrip reflectarray antenna has the same advantage of microstrip antennas that are low-profile, light-weight,

and conformable to planar and nonplanar surface, and inexpensive to manufacture. According to these advantages, microstrip reflectarray has been intensively studied. However, one drawback of the microstrip reflectarray antenna is its inherent narrow bandwidth due to the limited bandwidth of the microstrip antenna. To overcome this narrow bandwidth of the microstrip reflectarray antenna, multi-band configuration of the reflectarray [22-24] and wide-band reflectarray are presented [25-27].

A reflectarray antenna is a microstrip array antenna, a reflecting element, combined with the feed horn of the reflector antenna. It is a low-cost, low profile, high gain antenna with the beam scanning capability of a phased array antenna if it is integrated with solid-state control devices. Because the feed horn illuminates many isolated microstrip array elements on a thin reflecting surface and eliminates the use of the conventional transmission feeding lines, it also features low insertion loss of the conventional parabolic reflector [28]. The key feature of a reflectarray antenna design is the adjustment of the reflected phase of the microstrip array elements to create a parabolic phase front across the array's surface. The preferred phasing methods depend on the array element and the type of polarization. For a linearly polarized case, the phase correction has been achieved by using identical microstrip patches with different length phase-delay lines [29-31], variable size printed dipoles [32], and variable size microstrip patches [33, 34]. Many papers of microstrip reflectarray have been published on the design of fixed beam antennas. One of the advantages of the reflectarray is an electrically beam switching ability and some interesting developments has been reported. An electrically beam scanning reflectarray using RF MEMS has been proposed in [35]

and aperture coupled elements are used. In [36], switched beam reflectarray with two linear polarized feed arrays has been proposed. Cylindrical reflectors have found use in the area of the advanced precipitation radar antenna and the application of automotive radar. We proposed an offset-fed cylindrical beam switching reflectarray fed by linearly phased array antennas with a Butler matrix.

1.2 Dissertation organization

This dissertation presents a several topics including a single-band beam switching antenna on double-sided parallel strip line and double-sided parallel strip line with the inserted ground plane, dual-band beam switching array system using a modified 4 x 4 Butler matrix, a beam switching microstrip reflectarray fed by a phased array antenna, and a broadband circularly polarized aperture-coupled microstrip antenna using dual-offset feedlines.

Chapter II presents the design of a dual-band switched beam array antenna fed by dual-band Butler matrix. The basic operation mechanism of the Butler matrix is briefly introduced. For low side lobe level and small size, the modified Butler matrix is used. The rectangular microstrip patch antenna and rectangular ring patch antenna connected by four bridges are used.

Chapter III introduces offset-fed beam scanning microstrip reflectarray. The basic operation theory of the microstrip reflectarray is briefly presented. A circular patch with ring element is used as a unit cell of the microstrip reflectarray. This microstrip

reflectarray element has a broad reflection phase. Instead of a horn antenna normally used, a phased array antenna, one of smart antennas, is used as a feed antenna.

Chapter IV proposes a switched beam antennas fed by a 4 x 8 Butler matrix. The conventional Butler matrix has four inputs and four outputs. In this case, a 4 x 8 Butler matrix with the power divider at the output ports of a 4 x 4 Butler matrix is used to reduce a low sidelobe level and obtain a high gain. The Butler matrix is design on double-sided parallel-strip lines (DSPSL).

Chapter V describes broadband circularly polarized (CP) aperture-coupled microstrip antenna. These stacked patch antennas have dual-offset feedlines. The CP patch antennas are fed by a slot-coupled directional coupler for wideband performance.

Chapter VI presents a six-band reflectarray configuration on two layers. The elements of 6.6, 18.7, 57.5, 52.5, 166, 183.3 GHz are located on top and bottom layers. Each substrate layer accommodates three frequency bands. The possibility of this configuration, the achievable phase range and the coupling effect, is investigated.

Chapter VII introduces dual-band branch-line coupler on a DSPSL. Normally the first and third arm of the branch-line coupler with the three arms has the very high impedance. Therefore, these lines with the high impedance have a very narrow width, which is hard to make the very narrow width on the substrate. An offset DSPAL is good for high impedance line with the wider width. Dual-band branch-line coupler on DSPSL and offset DSPSL is proposed.

CHAPTER II

DUAL-BAND SWITCHED BEAM ARRAY FED BY DUAL-BAND BUTLER MATRIX*

2.1 Introduction

In this chapter, the recent advancement in the area of wireless communication systems has increased the demand for multi-band systems. There are two way to take advantage of a multi-beam antenna system: adaptive antenna array and switched beam system as shown in Fig. 1 [1]. Recently, smart antennas have been widely deployed in many of the top wireless communication worldwide to address wireless network capacity and performance challenges. An adaptive array forms an infinite number of patterns that are adjusted in real time using a variety of new signal-processing algorithms. Switched beam systems can form multiple fixed beams with heightened sensitivity in particular directions and switch their beams in different direction throughout space by changing the phase difference of the signals used to feed the radiating elements.

A switched beam system consists of a beam forming network and an antenna array. There are several beam forming networks such as Blass matrix, Nolen matrix, and Butler

---

* Part of this chapter is reprinted with permission from J. K. Lee and K. Chang, "Dual-band switched beam array fed by dual-band Butler matrix", *Electronics Letters*, vol. 47, no. 21, pp. 1164-1165, Oct. 2011, Copyright 2011 by IET.

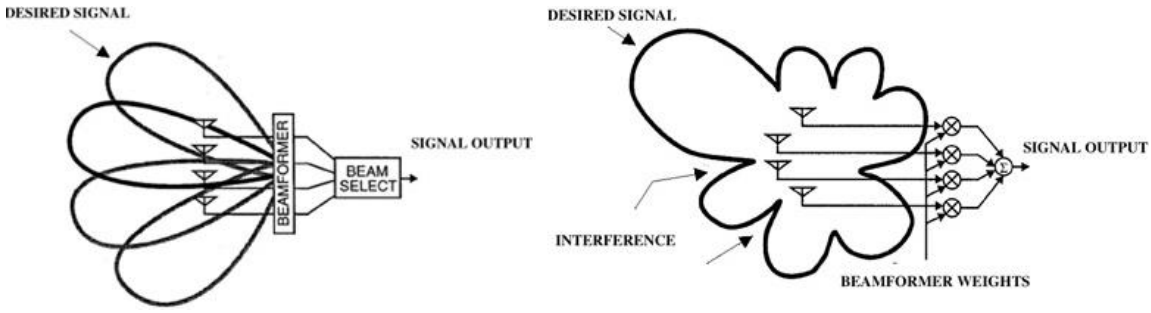

Fig. 1. Two type of the smart antenna: (a) switched beam antenna system and (b) adaptive antenna system.

matrix. A Butler matrix is a beam forming network and has been used in switched beam system to make multi-beams. The conventional Butler matrix consists of branch-line couplers, phase shifters, and crossovers as shown in Fig. 2 (a) [1, 8-11]. This matrix consists of branch-line couplers and phase shifter without any crossovers as shown in Fig. 2 (b) [7].

The conventional Butler matrix is an 2^n x 2^n network with 2^n input and 2^n output (n is a matrix order). The modified matrix has four inputs and four outputs, and it is implemented to excite the array of four patch radiating elements. The beam scanning can be obtained by different feedings with the phase variation of $\pm 45^o$ and $\pm 135^o$ provided by the Butler matrix. Table 1 shows the phase difference of a Butler matrix. This beam forming network is more complicate and has more phase error than the modified Butler matrix using only branch-line couplers and phase shifters without any crossovers. The

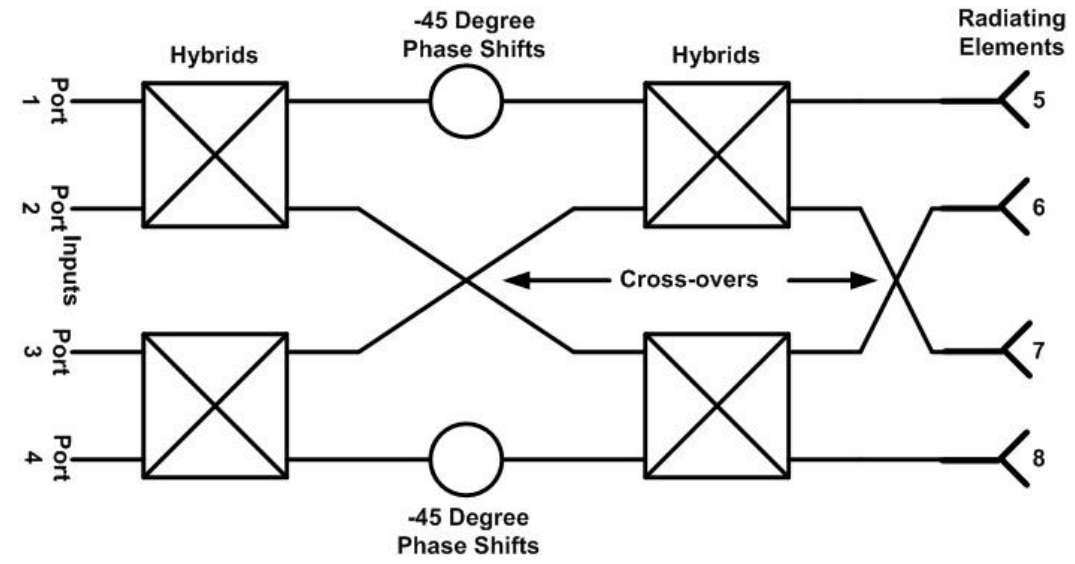

(a)

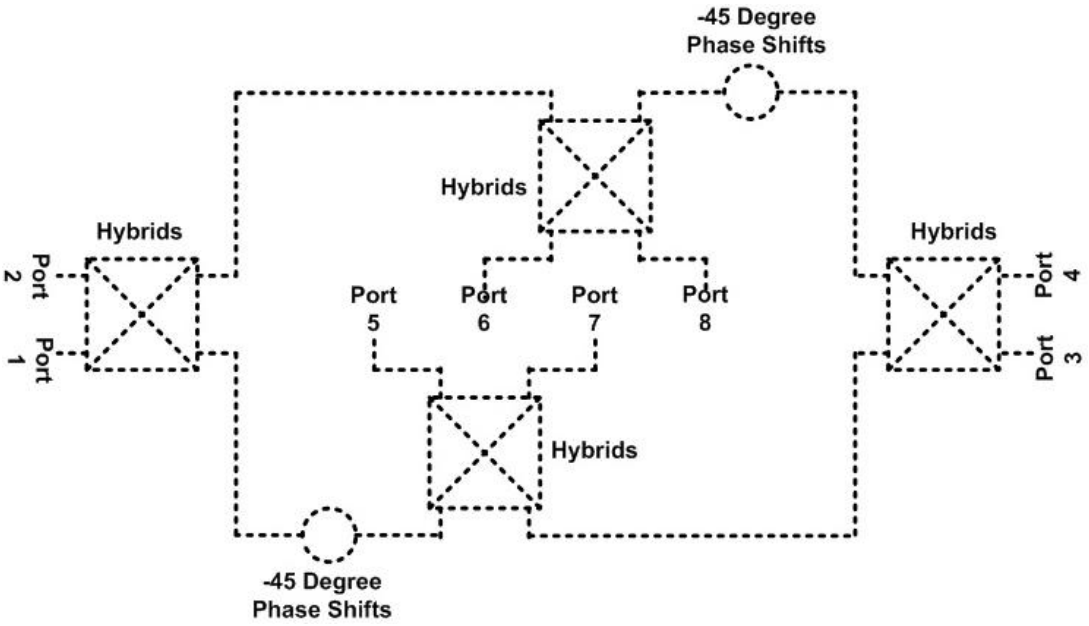

(b)

Fig. 2. Two type of Butler matrix: (a) conventional Butler matrix and (b) modified Butler matrix.

proposed Butler matrix is simple in the design and can reduce phase error by crossover. The antenna array is designed by four microstrip patch antennas. The several elements such as bends and discontinuities in BFN cause spurious radiation, which can reduce the side lobe level [37]. Therefore, as the Butler matrix is implemented behind the antenna array, the system can expect to improve the side lobe level [37].

Recently, dual-band beam switching array has been published. In [8] dual-band antenna array is fed by a broadband Butler matrix. This system uses four diplexers and two antenna arrays for dual-band beam switching operation. A diplexer is used to connect a broadband Butler matrix and antenna array of each band. In [38] dual-band beam forming network is simulated using dual-band couplers and dual-band crossovers. A dual-band beam switching system with two layers is proposed using a dual-band Butler matrix (dotted line) on bottom layer and dual-band antenna array on top layer. Since discontinuity in the Butler matrix such as corners or junctions can cause spurious radiation affecting the array radiation pattern, we decide to implement the matrix on the back side of the antenna array to reduce the sidelobe level. Moreover, this kind of connection can reduce the coupling between the matrix and antenna array.

Table 1. Phase difference of Butler matrix (unit: degree).

	P5	P6	P7	P8	Phase Diff.
P1	135	90	45	0	-45
P2	45	180	315	90	135
P3	90	-45	-180	45	-135
P4	0	45	90	135	45

2.2 Design of dual-band Butler matrix

We present the study of dual-band smart antenna system with frequency ratio to 1:1.85 based on the switched beam system. The beam scanning can be obtained by different feedings with the phase variation of $\pm 45^{o}$ and $\pm 135^{o}$ provided by the Butler matrix at both 4.05 GHz and 7.4 GHz. All elements of the dual-band Butler matrix are branch-line couplers, and phase shifters for simple design and reducing the phase errors at two frequency band. Details of the design of the feeding network together with the antenna array are described. The simulated results are obtained from Ansoft HFSS^{TM} to verify the reliability of the results [39].

The branch-line couplers are one of the most useful passive circuits with wide range of microwave applications. There has been developed for dual-band branch-line couplers for microwave circuit applications. These couplers are a reciprocal four-port network, meaning that they work effectively on waves transmitting in either direction and are 3 dB directional couplers with 90^{o} phase difference in the output at two frequency bands.

In [40], dual-band coupler is presented using two branch-lines, which the electrical length of the horizontal line is twice longer than the vertical length. In [41], the open and short stubs are used to accomplish the dual-band operation with the same length. In [42], dual-band coupler with two additional cross-coupling branches inside is presented. In [43], we can see dual-band coupler with enhanced bandwidth response using three branch-lines. This three branch line coupler has a phase characteristic of different sign at output ports. In this work, we choose the three branch-line coupler which has the same phase sign at output ports and the enhanced bandwidth response at two frequency bands. The branch-line couplers are the first element to be implemented in the matrix. The basic configuration of the dual-band branch-line coupler is shown in Fig. 3. This branch-line coupler is decomposed into the superposition of an odd-mode excitation and an even-mode excitation as shown in Fig. 4.

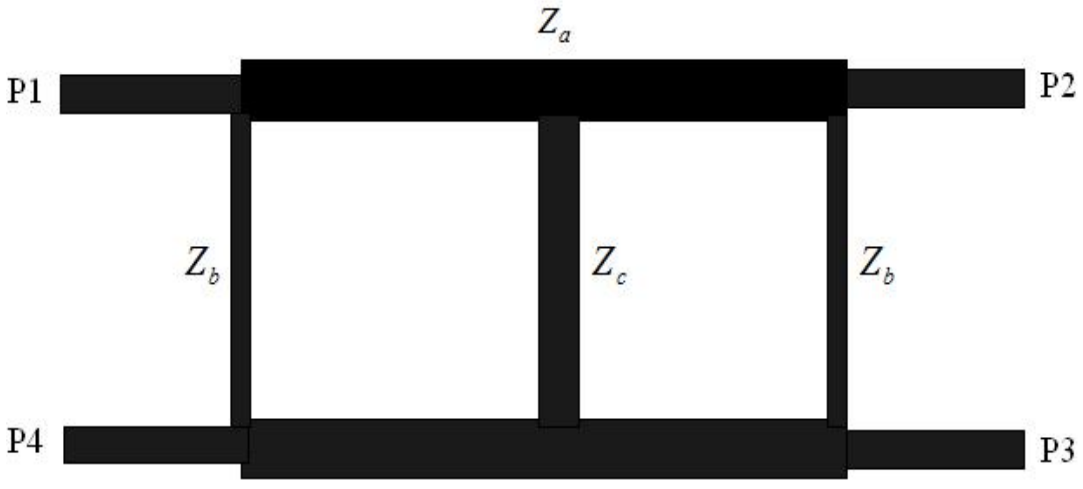

Fig. 3. Geometry of a dual-band branch-line coupler.

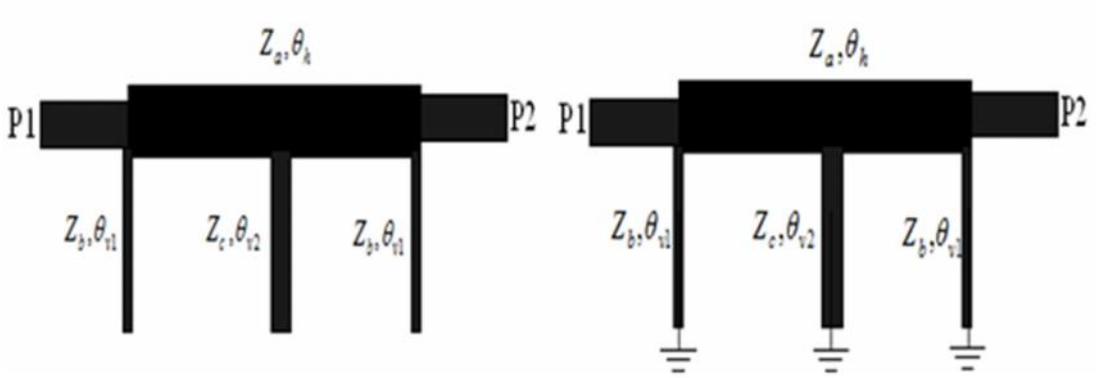

(a) (b)

Fig. 4. Decomposition into (a) even mode and (b) odd mode.

In the even mode half circuit, its ABCD matrix representation is given as follows:

$$\begin{bmatrix} A_e & B_e \\ C_e & D_e \end{bmatrix} = \begin{bmatrix} 1 & 0 \\ \dfrac{1}{-jz_b \cot\dfrac{\theta_{v1}}{2}} & 1 \end{bmatrix} \begin{bmatrix} \cos\theta_h & jz_a \sin\theta_h \\ \dfrac{j\sin\theta_h}{z_a} & \cos\theta_h \end{bmatrix} \begin{bmatrix} 1 & 0 \\ \dfrac{1}{-jz_c \cot\dfrac{\theta_{v2}}{2}} & 1 \end{bmatrix} \times \begin{bmatrix} \cos\theta_h & jz_a \sin\theta_h \\ \dfrac{j\sin\theta_h}{z_a} & \cos\theta_h \end{bmatrix} \begin{bmatrix} 1 & 0 \\ \dfrac{1}{-jz_b \cot\dfrac{\theta_{v1}}{2}} & 1 \end{bmatrix} \tag{1}$$

In the odd mode half circuit, its ABCD matrix representation is given as follows:

$$\begin{bmatrix} A_o & B_o \\ C_o & D_o \end{bmatrix} = \begin{bmatrix} 1 & 0 \\ \dfrac{1}{jz_b \tan\dfrac{\theta_{v1}}{2}} & 1 \end{bmatrix} \begin{bmatrix} \cos\theta_h & jz_a \sin\theta_h \\ \dfrac{j\sin\theta_h}{z_a} & \cos\theta_h \end{bmatrix} \begin{bmatrix} 1 & 0 \\ \dfrac{1}{jz_c \tan\dfrac{\theta_{v1}}{2}} & 1 \end{bmatrix} \times \begin{bmatrix} \cos\theta_h & jz_a \sin\theta_h \\ \dfrac{j\sin\theta_h}{z_a} & \cos\theta_h \end{bmatrix} \begin{bmatrix} 1 & 0 \\ \dfrac{1}{jz_b \tan\dfrac{\theta_{v1}}{2}} & 1 \end{bmatrix} \tag{2}$$

where all impedance values are normalized to the port impedance Z_o.

To simplify the equation, the electrical length of the vertical lines is equal to be half of the horizontal lines. In addition, all vertical lines are the same length ($\theta_{v1} = \theta_{v2} = \frac{\theta_h}{2}$). The ABCD parameters obtained above can be used to calculate the even and odd mode reflection (Γ) and transmission (T) coefficient by the following formula [44].

$$\Gamma_{e,o} = \frac{A_{e,o} + B_{e,o} - C_{e,o} - D_{e,o}}{A_{e,o} + B_{e,o} + C_{e,o} + D_{e,o}} \tag{3}$$

$$\mathrm{T}_{e,o} = \frac{2}{A_{e,o} + B_{e,o} + C_{e,o} + D_{e,o}} \tag{4}$$

If the amplitudes of the incident wave are $\pm 1/2$ at input port, the amplitudes of the emerging wave at each port is expressed as

$$S_{11} = \frac{1}{2}\Gamma_e + \frac{1}{2}\Gamma_o \tag{5}$$

$$S_{21} = \frac{1}{2}\mathrm{T}_e + \frac{1}{2}\mathrm{T}_o \tag{6}$$

$$S_{31} = \frac{1}{2}\mathrm{T}_e - \frac{1}{2}\mathrm{T}_o \tag{7}$$

$$S_{44} = \frac{1}{2}\Gamma_e - \frac{1}{2}\Gamma_o \tag{8}$$

We can calculate Z_a , Z_b , Z_c , and θ that satisfy the equation $|S_{21}| = |S_{31}|$ and $|S_{41}| = 0$. If $\theta = \pi$, from Eq. (5)-(8) the S parameters are independent of the values of the characteristic impedance, Z_0 [43]. Using Eq. (5)-(8), the value of Z_a , Z_b ,and Z_c can be solved at the frequency ratio f_2 / f_1. The operation frequencies are f_1=4.0 GHz and f_2 =7.4 GHz. The optimal impedances are Z_a=41.5 Ω , Z_b=112 Ω , and Z_c=57.8 Ω at the

central frequency, $f_0 = (f_1 + f_2)/2$. We designed this dual-band coupler using Rogers RT/duroid 6006 substrate with a relative permittivity of 6.15 and the thickness of 0.64 mm. Its physical dimension are W_h=1.3 mm, W_{v1}=0.12 mm, W_{v2}=0.708 mm, L_h=11.59 mm, and $L_{v1} = L_{v2}$=6.65 mm.

The simulation results of the coupler are presented. Fig. 5 shows the return loss, isolation, and coupling coefficient of dual-band branch-line coupler. It can be seen that the isolation and return loss is greater than -20 dB at two frequency bands of 4.0 GHz and 7.4 GHz and the insertion loss are -0.1 dB, which are reasonable compared with the theoretical values. Fig. 6 illustrates the phase differences between two output ports, and it is shown that the difference is about -90^o at two frequency bands. The phase differences are almost constant over the operating frequency band.

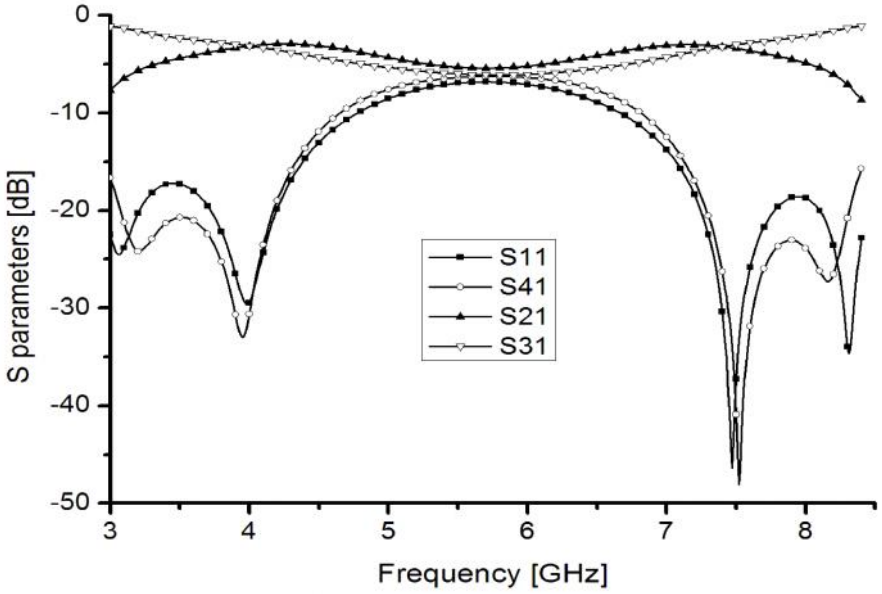

Fig. 5. Magnitude of S-parameters of the branch-line coupler.

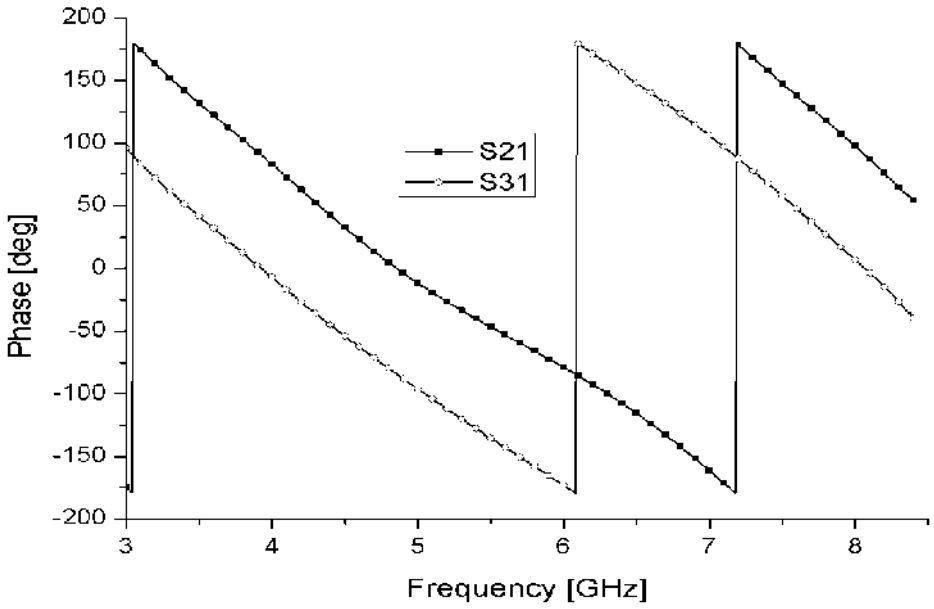

Fig. 6. Phase of S-parameters of the branch-line coupler at output ports.

Phase shifters are used to change the transmission phase angle of a system. Theoretically, phase shifters provide low insertion loss, and approximately equal loss in all phase states. We will concentrate mainly on those that are electrically-controlled. In this work, phase shifters are needed to delay desired phase shift at output ports of the Butler matrix. Transmission line phase shifters are chosen in this work because they are simple in the design and implementation. Eighth wavelength delay line is obtained from $\Delta\theta = \Delta x \cdot \beta$, which is designed by using a simple transmission line at f_0=5.7 GHz. Two 45^o phase shifters are designed as simple transmission lines which yield required phase shifts at the operating frequency. The 50 Ω transmission line of 28 mm plays a part in -45^o phase shifter at both frequency bands.

As in the conventional Butler matrix, by combining the branch-line couplers and -45° phase shifters, we design the modified 4×4 Butler matrix to feed the antenna array. The phase shift is determined by the number of radiating elements n. The phase difference at the output ports is $\delta=(2p-1)/n$, where p is the port number. The simulation results of the 4×4 Butler matrix are presented. As shown in Fig. 7 and Fig. 8, the return losses are greater than -18dB and the insertion losses are 6.4 ± 0.25 dB at 4.0 GHz and 7.4 GHz of the Butler matrix. Table 2 and Table 3 show a summary of the corresponding phase shifts between the inputs and the outputs of the matrix at both frequency bands. The simulated phase errors are within 0.5° at 4.0 GHz and are within 3° at 7.4 GHz. The modified Butler matrix is analyzed by using 3D full wave simulator, Ansoft HFSS v11.

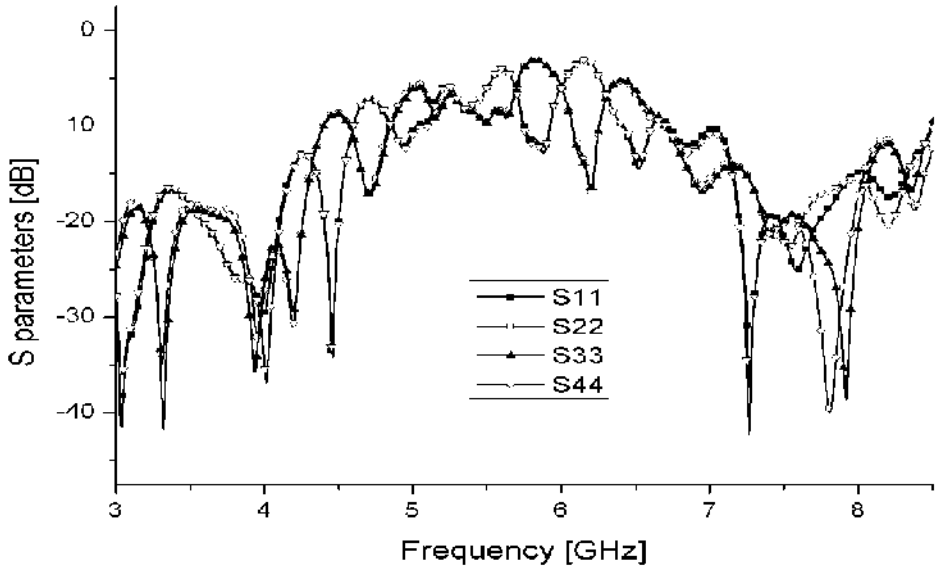

Fig. 7. Return losses of the dual-band Butler marix.

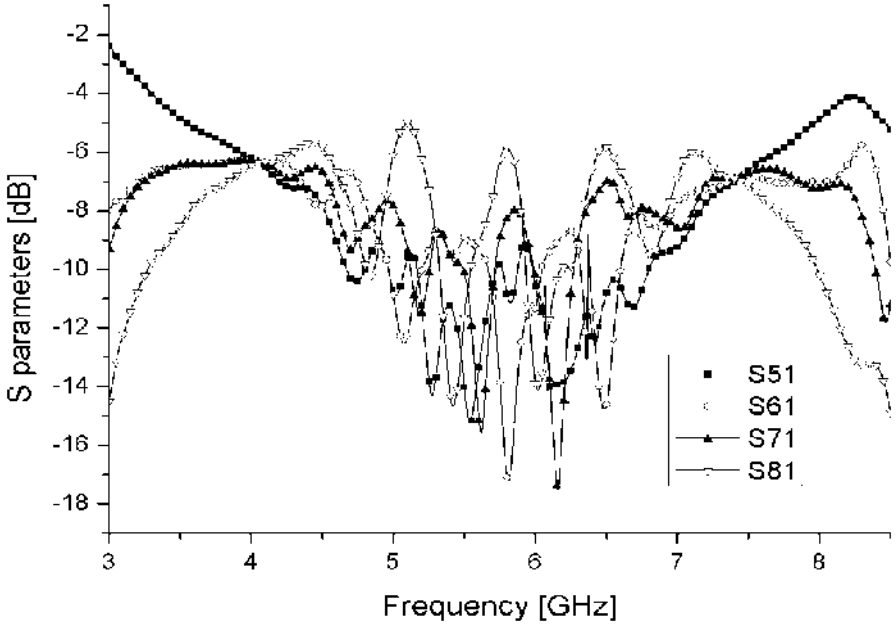

(a)

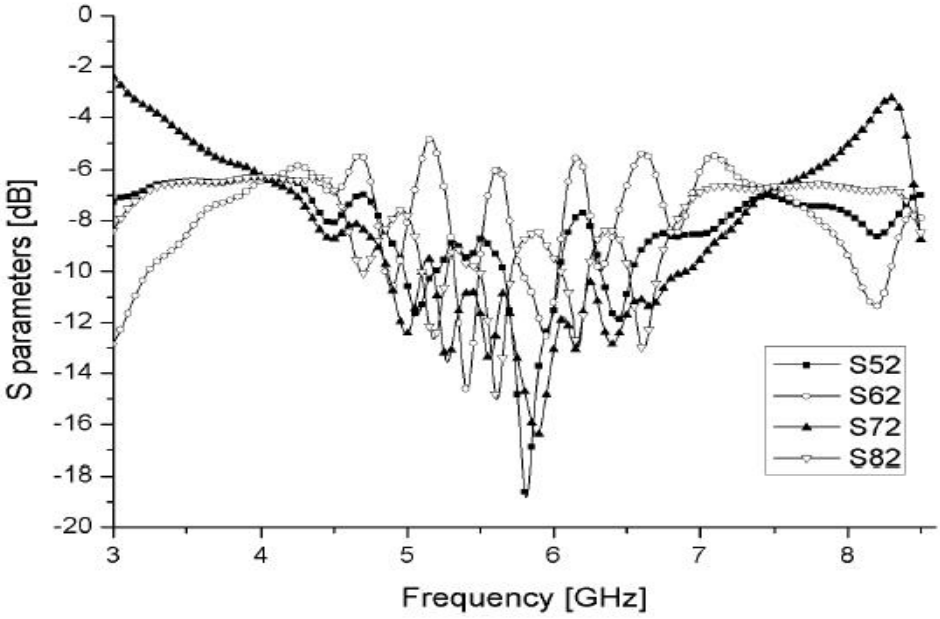

(b)

Fig. 8. Insertion loss of the Butler matrix at (a) port 1 and (b) port 2.

Table 2. Phase at the inputs and outputs of Butler matrix at 4.0 GHz (unit: degree).

Port		5	6	7	8
1	Phase	-5.4	39.27	84.25	128.94
	|Error|		0.33	0.02	0.31
2	Phase	39.68	174.17	-50.6	84.03
	|Error|		0.51	0.23	0.37
3	Phase	84.44	-50.99	174.09	38.95
	|Error|		0.43	0.08	0.14
4	Phase	129.81	84.56	39.73	-5.5
	|Error|		0.25	0.17	0.23

Table 3. Phase at the inputs and outputs of Butler matrix at 7.4 GHz (unit: degree).

Port		5	6	7	8
1	Phase	-86.14	-42.77	3.73	45.83
	|Error|		1.63	1.5	2.9
2	Phase	-43.42	91.99	-133.3	1.77
	|Error|		0.41	0.29	0.07
3	Phase	3.05	-133.3	92.31	-44.17
	|Error|		1.35	0.61	1.48
4	Phase	45.97	2.91	-43.27	-87.69
	|Error|		1.94	1.18	0.58

2.3 Design of dual-band patch antenna array

Recently, dual-band operations of microstrip antenna are needed in various communication systems and radar. In such case, a patch antenna is desirable to operate in multiple bands. In general, there are two kinds of method to obtain the capability of dual-band antenna by using reactively loaded antennas and multi-resonator antennas [45, 46]. Reactively loaded antennas can obtain dual-band operation by including the narrow slots parallel to the radiation element edges or single or double notches [46, 47].

In this work, we use a simple one layer dual-band rectangular patch antenna with single feed. Two rectangular microstrip antennas are connected to each other with four bridges which are located at the center of each radiating element. The feeding point is located at 50 Ω point for two frequency bands. This type antenna has an advantage of obtaining the shift of frequency range by changing the bridge width [48]. The proposed dual-band patch antenna is shown in Fig. 9. Inner patch is designed for a frequency band of 7.4 GHz and outer patch is for a frequency band of 4.0 GHz. A rectangular patch is fabricated on RO 4003C substrate of thickness of 1.524 mm and relative permittivity of 3.38.

Fig. 10 shows the simulated return loss of a dual-band rectangular patch antenna using 3D full-wave simulator, Ansoft HFSS software. It can be seen that radiation occurs at the interested dual-frequency, 4.05 GHz and 7.4 GHz with good impedance matching. The return loss is greater than -14 dB at the 4.05 GHz and 7.4 GHz. Fig. 11 shows the simulated radiation pattern of a patch element in E-plane at two frequency bands.

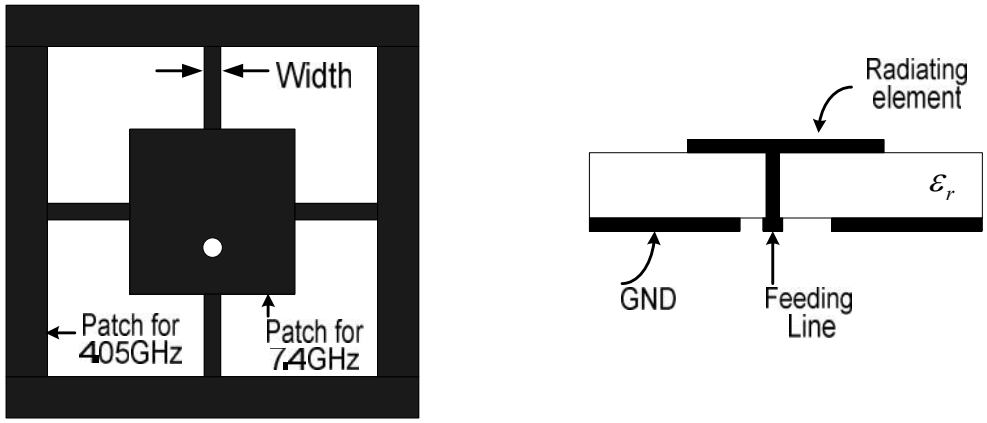

Fig. 9. Geometry of the proposed dual-band patch antenna.

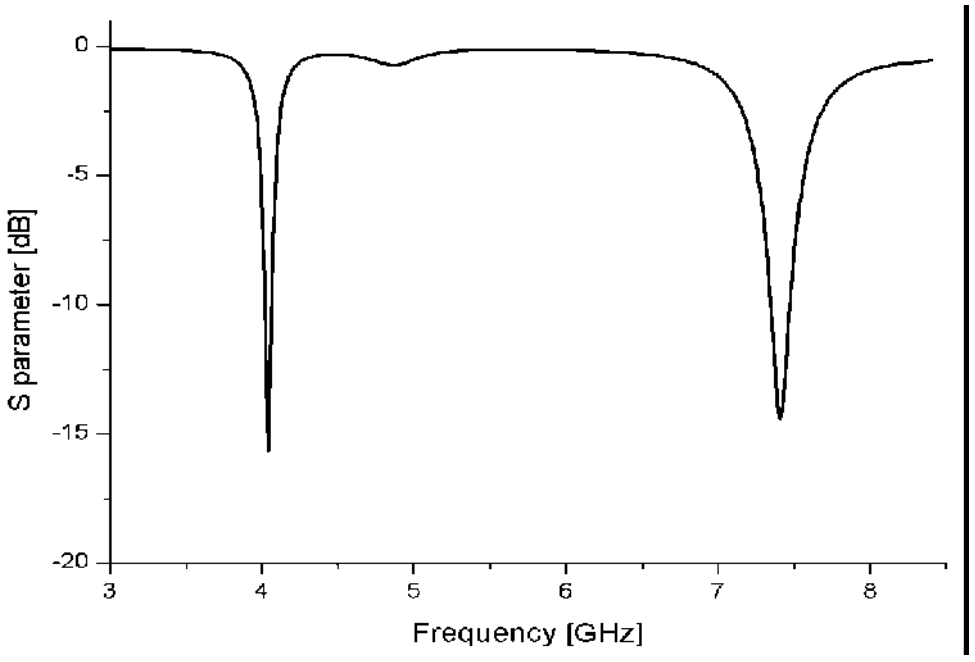

Fig. 10. Return loss of the dual-band patch antenna.

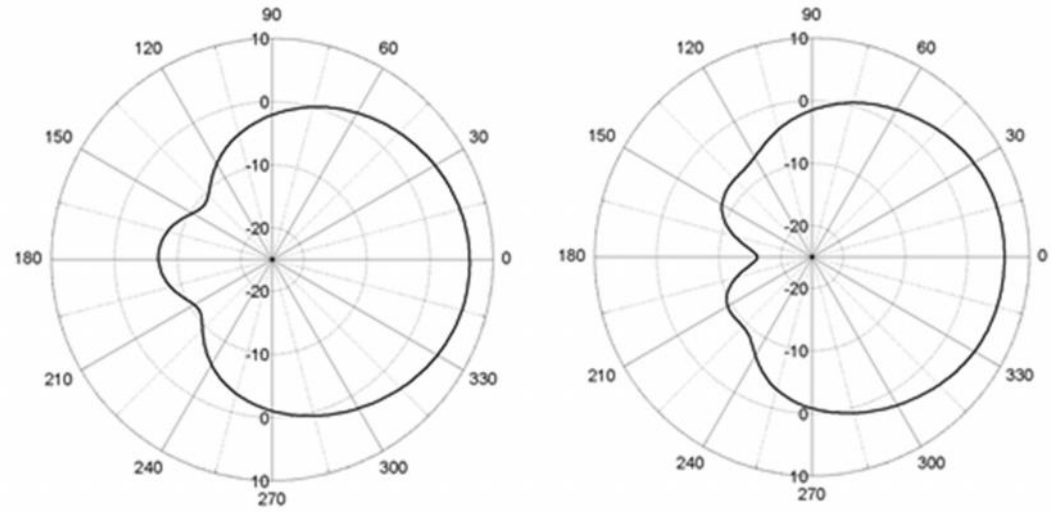

(a) (b)

Fig. 11. Simulated radiation patterns at (a) 4.05 GHz and (b) 7.4 GHz

By controlling the progressive phase difference of the radiating elements, the maximum radiation can be tilted in any desired direction for scanning. The radiation characteristics of the array are determined by the type of each element used, its position in space, and the amplitude and phase of the currents feeding it. The total field is determined by the vector addition of the fields radiated by the each element. The fields from the individual elements of the array interfere constructively in the space to provide very directive patterns. In this work, the linear array in which the centers of antenna element lie along a straight line is used. The element distance between the single antennas is playing a crucial role in the mutual coupling between the elements. Mutual coupling affects impedance, the gain and radiation characteristics such as far-field pattern and polarization. It is difficult to control the distance of two frequency bands for

a good performance. The distance between the antenna elements is about $0.5\lambda_0$ at the center frequency of f_0=5.7 GHz. As shown in Fig. 12, the simulation results of return losses of all radiating elements are greater than -15 dB at two frequency bands of 4.05 GHz and 7.4 GHz.

2.4 Measurement of dual-band switched beam system

In this work, we proposed the dual-band switched beam system which is composed of a modified Butler matrix using branch-line couplers and phase shifters and the microstrip antenna array. An antenna array and the Butler matrix have a dual-band characteristic. The Butler matrix is connected to the antenna array by using two back-to-back substrates with feed through pins to improve the side lobe level. This would allow plenty of surface area, and have the critical advantage of allowing the use of one substrate with a low dielectric constant for the antenna elements. Fig. 13 (a) and (b) show a photograph of the antenna array and the proposed Butler matrix. The total area is 16.5 x 9 cm2.

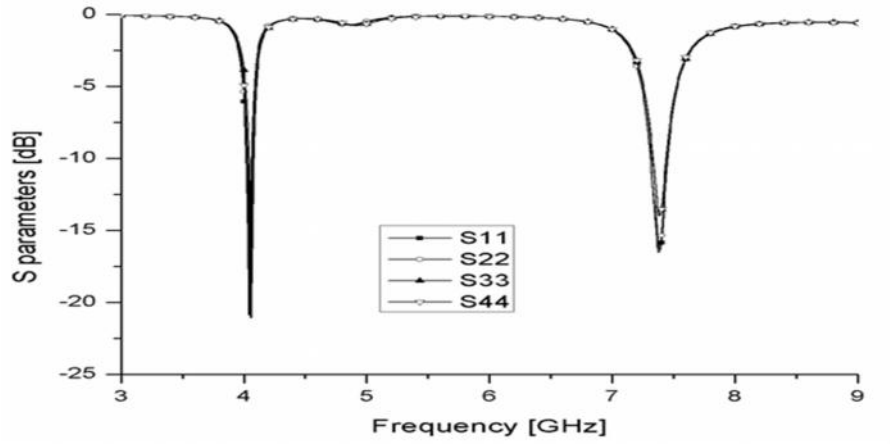

Fig. 12. Return losses of the dual-band antenna array.

(a) Top view

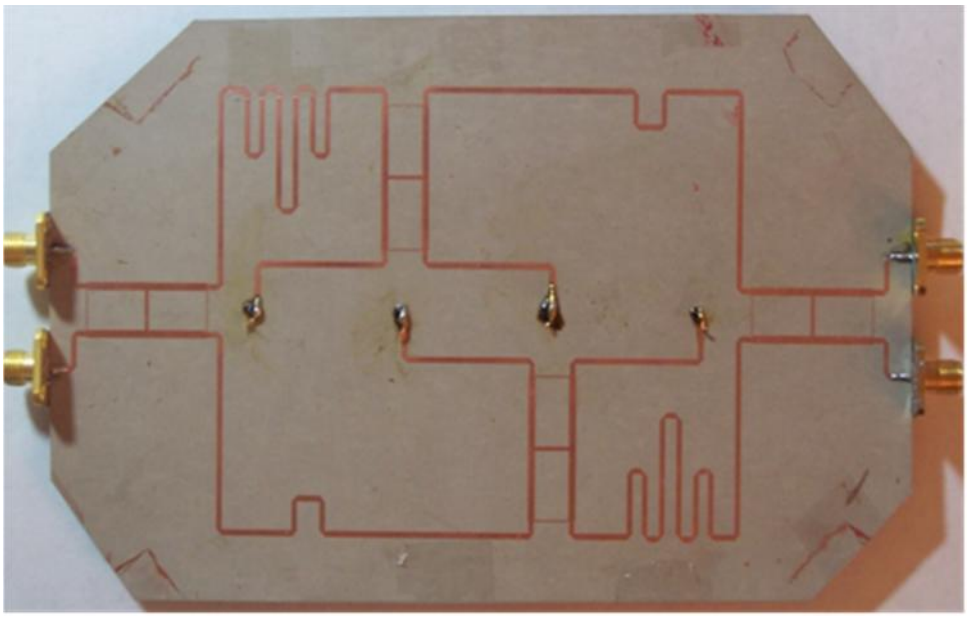

(b) Bottom view

Fig. 13. Photograph of the proposed beam switching system: (a) the antenna array and (b) the Butler matrix.

The measured return loss of the fabricated Butler matrix with microstrip array antenna is shown in Fig. 14. The measured result shows that the return losses at each input port are better than -8 dB at two frequency bands. The normalized radiation patterns of the beams are measured using far-field method in the anechoic chamber. Fig. 15 illustrates the normalized radiation patterns when port 1, port 2, port 3 and port 4 are excited respectively at (a) 4.0 GHz and 7.3 GHz. The side lobe level (SLL) of 4.0 GHz array antenna is -13 dB at port 1 & 4 and -7.5 dB at port 2 & 3. The SLL of 7.3 GHz system is -12.5 dB at port 1 & 4 and -7.2 dB at port 2 & 3. The main beam direction of 4.0 GHz antenna array is $\pm 14^{o}$ for port 1 & 4 and $\pm 47^{o}$ for port 2 & 3. The main beam direction of 7.3 GHz antenna array is tilted by $\pm 10^{o}$ for port 1 & 4 and $\pm 28^{o}$ for port 2 & 3.

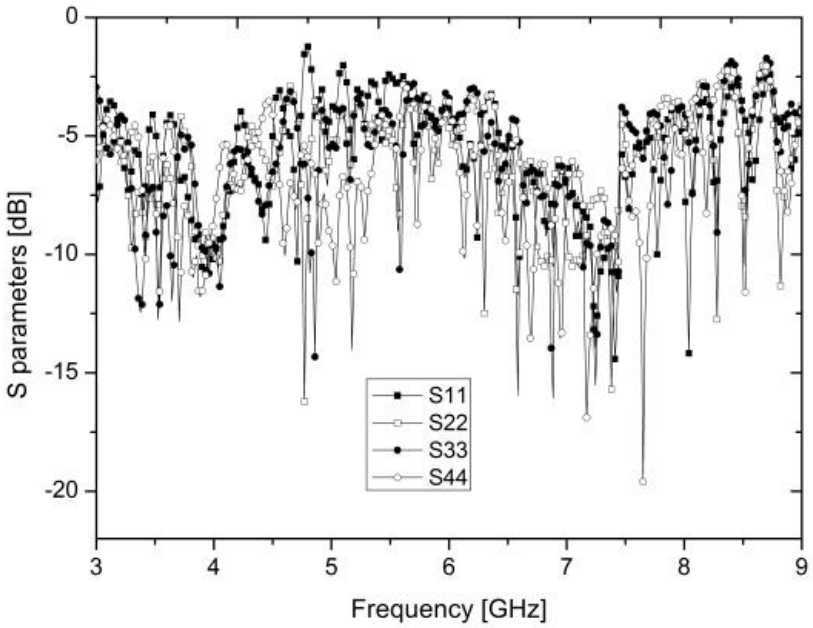

Fig. 14. Measured return losses at each input port.

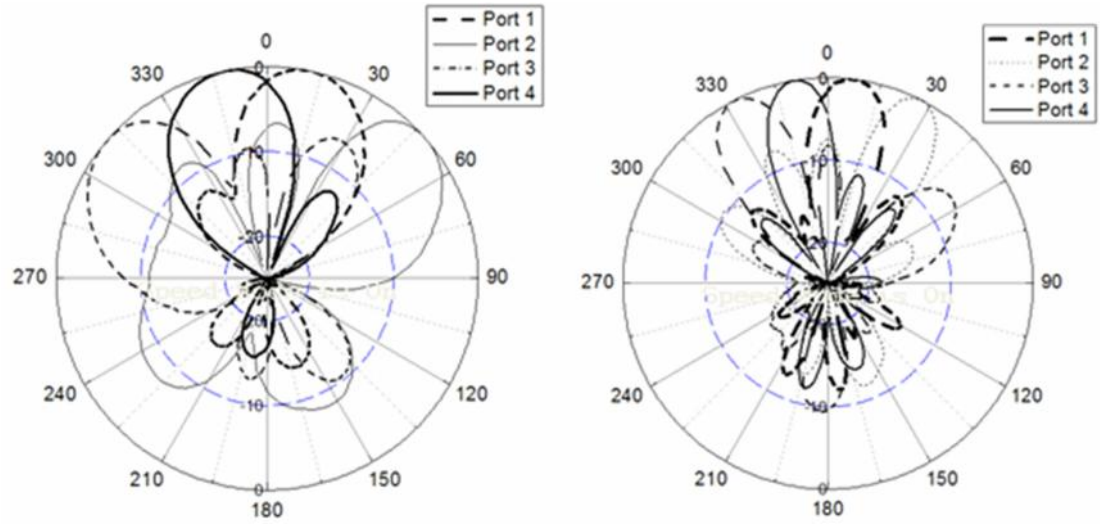

(a) (b)

Fig. 15. Measured radiation patterns at (a) 4.0 GHz and (b) 7.3 GHz when each port is fed respectively.

2.5 Conclusions

Dual-band beam switching antenna array with two layers is proposed and measured. The Butler matrix and antenna array have dual-band characteristic and connected back-to-back substrate. A modified Butler matrix is used for this system, which has simple schematic and can reduce phase error due to crossover. The frequency ratio between the two frequency bands is around 1:1.85. The measured results show good properties for dual-band multi-beam system.

CHAPTER III

OFFSET-FED BEAM SCANNING MICROSTRIP REFLECTARRAY FED BY PHASED ARRAY ANTENNA

3.1 Introduction

Large parabolic reflector antennas have been used in satellite communications and radio astronomical system due to high gain. Although they are efficient antennas, these antennas are bulky and heavy, and the main beam can be tilted only a few degrees from broadside direction. Recently, reflectarray antennas have been studied to replace the conventional high gain parabolic reflectors because of their low profile structures and light weight. A microstrip reflectarray is composed of many microstrip radiating elements which are designed to reradiate the incident field with proper phases [34]. The phase range is required up to 360° to compensate the spatial phase delay between the parabolic curvature and each radiating element location on the flat reflectarray. Due to the less metallization as compared to patches, microstrip rings are commonly used as reflectarray unit cells. The use of the ring element has several advantages such as compact size, broader circular polarization bandwidth, and little blockage of the incident field in multi-layer structures [49].

Many papers of microstrip reflectarray have been published on the design of fixed beam antennas. One of the advantages of the reflectarray is an electrically beam switching ability and some interesting developments have been reported. An electrically beam scanning reflectarray using RF MEMS devices has been proposed in [35] and

aperture coupled elements are used. In [36], switched beam reflectarray with two linear polarized feed arrays has been proposed. Cylindrical reflectors have been useful in the area of the advanced precipitation radar antenna and the applications of automotive radar. In this work, we proposed an offset cylindrical beam switching reflectarray fed by linearly phased array antennas with a Butler matrix, which is one of the beam forming networks.

3.2 Basic reflectarray operation theory

In this section, some basic theoretical aspects concerning a microstrip reflectarray are described, and then a method to calculate a reflection phase from a reflected wave is introduced. The fundamental theory of the microstrip reflectarray antenna in this section is cited from [50, 51]. Fig. 16 shows the geometry of a parabolic reflector antenna and a microstrip reflectarray. Contrary to a metallic curved surface of parabolic reflector antenna, a microstrip reflectarray is composed of a microstrip radiating elements, printed on a ground substrate. The feed antenna of both antennas is located at the focal point of a parabolic curve and they illuminate the curved reflector or the microstrip antenna array. When the wave from the feed antenna is incident on the microstrip reflectarray surface, the elements of the reflectarray will reradiate the incident wave into the space. However as can be seen from Fig. 16 (b), the incident path lengths for the field propagating from the feed antenna to the elements are all different. Therefore the reradiated field will not be coherent in a desired direction. In a microstrip reflectarray, the path adjustment of different paths is done by the microstrip array elements instead of geometrical shape of

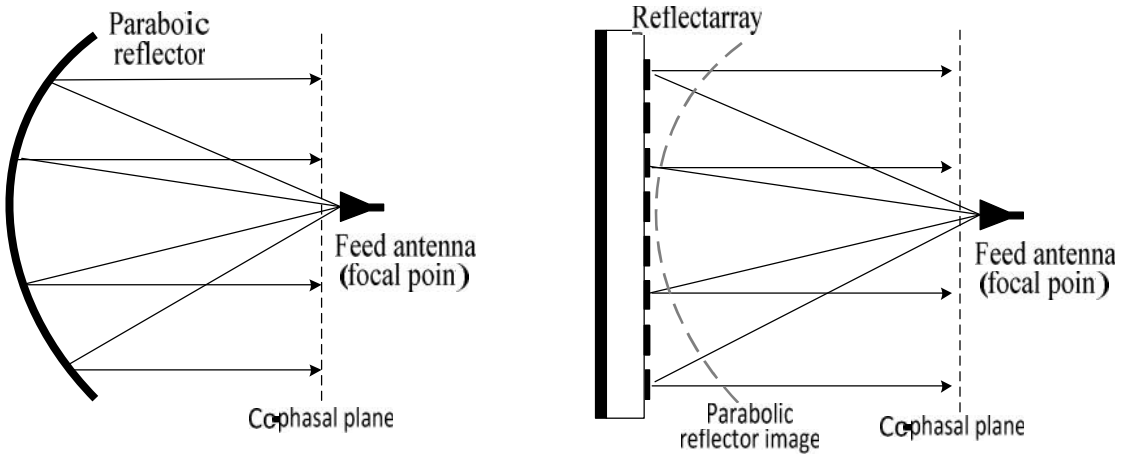

Fig. 16. Geometry of (a) parabolic antenna and (b) microstrip reflectarray antenna.

the parabolic reflector antenna. The key to the microstrip reflectarray design is to adjust the reflection phase of each element to compensate for the path differences so that the reradiated fields from each element should be collimated towards a desired direction.

The analysis of a microstrip reflectarray antenna can be derived by comparing the configurations of a parabolic antenna. Fig. 17 shows the geometry of a microstrip reflectarray with its virtual parabolic curve. An incident plane wave is incident on the parabolic reflector's metal surface and then bounces to a focal point a distance f above the center of the parabolic reflector. Each reflectarray elements are located at a position (x', y') from the center of the array (0, 0). The distance between the focal point and any antenna element is denoted as r_{mn}. The angle θ' is the angle between the path connecting the focal point and the array center and the path connecting the focal point and the antenna element.

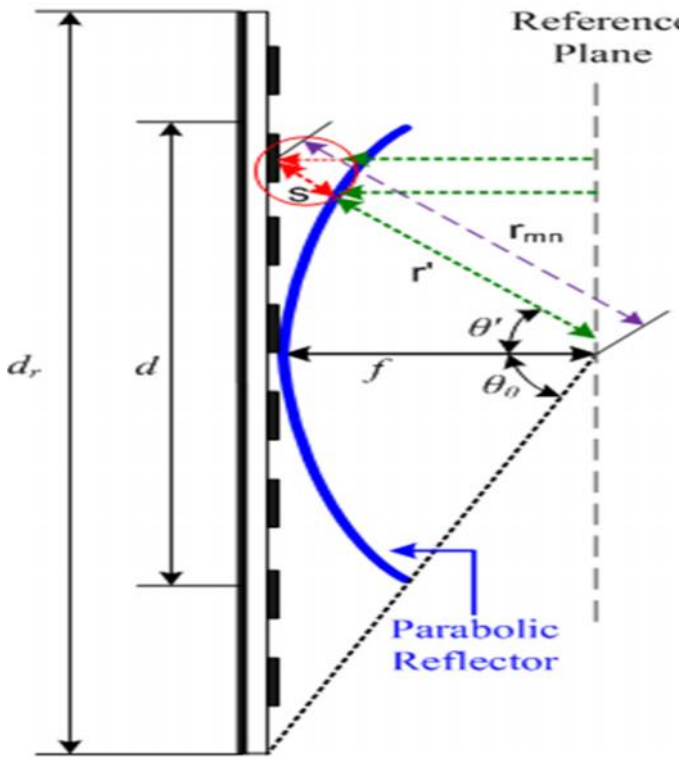

Fig. 17. Geometry of the front-fed microstrip reflectarray.

The parabolic curve equation is as follows;

$$r' = \tan^{-1}\left(\frac{2f}{1+\cos\theta'}\right) \tag{9}$$

The dimensions of the reflector (*d)* and the largest angle (θ_0) from the center of the parabolic reflector are related [15] as

$$\theta_0 = \tan^{-1}\left(\frac{\left|0.5\frac{f}{d}\right|}{\left(\frac{f}{d}\right)^2 - \frac{1}{16}}\right) \tag{10}$$

For any angle θ', the distance from the reference plane of the reflectarray element to the focal point is ($s + s \cos \theta'$) longer than the corresponding ray trace from the reference plane of the parabolic antenna to the focal point. This additional path length must be compensated in the design of the reflectarray element in order to provide the parabolic phase front across the surface of the array.

The distance s is equal to

$$s = \frac{f}{\cos\theta'} - r' = \frac{f(1-\cos\theta')}{\cos\theta'(1+\cos\theta')} \tag{11}$$

Therefore, the total path difference (S_{path}) can be obtained as follows;

$$S_{path} = s + \cos\theta' = \frac{f}{\cos\theta'} - f \tag{12}$$

From the equation (12), the total phase from the feed to an aperture in front of the reflectarray can be calculated.

The disadvantage of the front-fed parabolic reflector is that the feed antenna blocks the transmitting or receiving wave. To solve this problem, offset-fed parabolic reflector antenna has been presented [52-58]. The analysis to calculate the needed phase delay is derived based on the comparison of the geometrical configurations between an offset parabolic reflector and a flat microstrip reflectarray. Fig. 18 shows the geometry of the offset-fed microstrip reflectarray with its virtual parabolic surface. The microstrip reflectarray elements are placed at (x_{re}, y_{re}, z_{re}) in the (x, y, z) coordinate system.

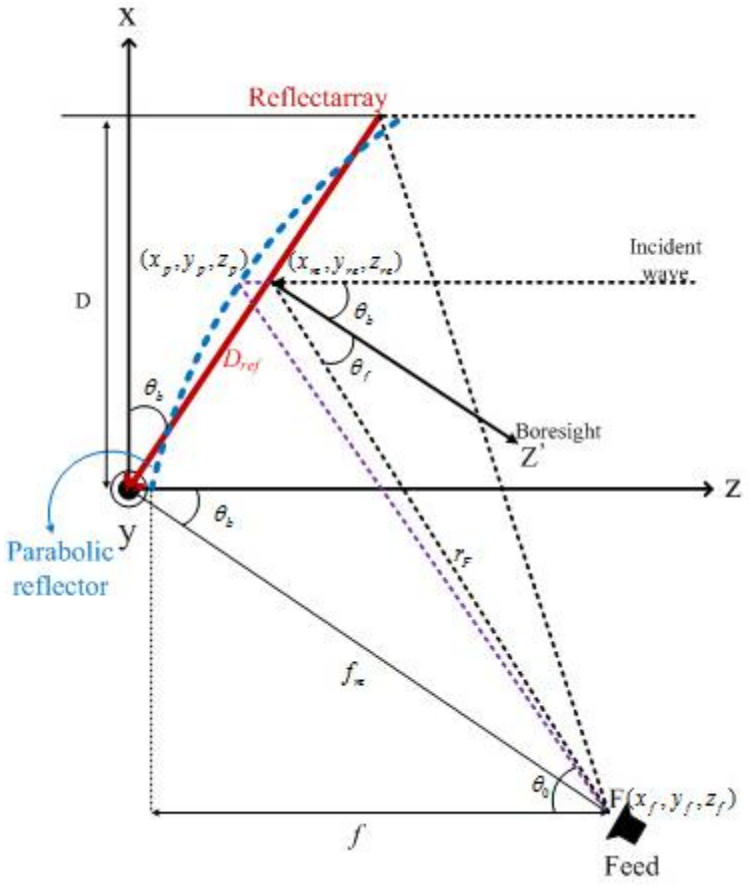

Fig. 18. Geometry of the offset-fed microstrip reflectarray.

From Fig. 18 and specifying the reflectarray dimension D_{ref}, the vertical distance f_{re}, and the desired scan angle θ_b, the phase center of the feed is ($-f_{re}\sin\theta_b$, 0, $f_{re}\cos\theta_b$) in the (x_f, y_f, z_f) coordinate system. From the center of the feed antenna, the center of the microstrip array element on the reflectarray surface is obtained such that the incident angle of the feed horn θ_f, relative to the normal of the reflectarray surface is very close to the main beam angle θ_b. By choosing the value of θ_f very close to θ_b, the

effect of beam squint of the microstrip reflectarray can be minimized to a great extent for an offset-fed reflectarray system. Since the center of the microstrip array element on the reflectarray surface lies on the surface formed by the parabolic antenna, the subtended angle θ_0 can be determined with its corresponding focal length defined as [52];

$$F = \frac{r_F(1+\cos(\theta_0))}{2} \tag{13}$$

Now the origin in the (x, y, z) coordinate system is redefined such that the center (x_f, y_f, z_f) of the feed antenna can be placed at $(0, 0, F)$ and the (x_{re}, y_{re}, z_{re}) coordinates of the microstrip reflectarray elements are also transformed. The surface of a parabolic antenna is formed simply by expressing the value of z_{sh} coordinate in terms of x_{re} and y_{re} [52]. That is,

$$z_{sh} = \frac{{x_{re}}^2 + {y_{re}}^2}{4F} \tag{14}$$

Finally, the path difference is as follows;

$$\Delta l = \sqrt{{x_{re}}^2 + {y_{re}}^2 + (z_{re} - F)^2} - \sqrt{{x_{re}}^2 + {y_{re}}^2 + (z_{sh} - F)^2} + z_{sh} - z_{re} \tag{15}$$

The aperture efficiency is one of major factor to predict the microstrip reflectarray system performance. The efficiency of the microstrip reflectarray is similar to that for the parabolic antenna. The design of the microstrip reflectarray antenna usually begins with a specific gain. The gain of a reflectarray antenna can be obtained by the product of the aperture directivity and the aperture efficiency. The aperture directivity D_r is determined by the aperture area A as

$$D_r = \frac{4\pi A}{\lambda^2} \tag{16}$$

Then, the gain of the reflectarray antenna is defined as

$$G = D_r \cdot \eta_a = \frac{4\pi A}{\lambda^2}\eta_a \tag{17}$$

where η_a is the aperture efficiency.

There are two types of the aperture efficiency, the illumination efficiency and the spillover efficiency [50, 59-61]. The illumination efficiency is caused by the unequal illumination of the array aperture due to the feed's tapered pattern. This efficiency is a function of the subtended angle (θ_0) and the feed pattern of reflector. The spillover efficiency is the ratio of the amount of feed energy that illuminates the entire array to the total amount of energy that is radiated by the feed antenna.

Let us define the total aperture efficiency (η_a) as

$$\eta_a = \eta_i \eta_s \tag{18}$$

where η_i is a illumination efficiency and η_s is spillover efficiency.

From Silver [62],

$$\eta_i = \frac{\left| \int_{\theta=0}^{\theta} \int_{\phi=0}^{2\pi} \vec{E} \cdot P\hat{x} ds \right|^2}{s \int_{\theta=0}^{\theta} \int_{\phi=0}^{2\pi} \left| \vec{E} \right|^2 ds} \tag{19}$$

where $s = \pi f^2 \tan^2 \theta$, and

$$\eta_s = \frac{\left| \int_{\theta=0}^{\theta} \int_{\phi=0}^{2\pi} \left| \vec{E} \right|^2 ds \right|^2}{\int_{\theta=0}^{\pi/2} \int_{\phi=0}^{2\pi} \left| \vec{E} \right|^2 ds} \tag{20}$$

Among various radiation models, the analysis assumes the feed has a $cos^q\ \theta$ pattern. The parameter q determines the pattern shape and the directivity of the feed antenna. Fig. 19 shows the directivity of the feed antenna versus the q value. The larger q value, the higher directivity is. Once the feed antenna is designed with a specific directivity, the q value is obtained. From the power distributed across the reflectarray aperture, the total power radiated by the feed, and the total power radiated by the feed antenna, Eq. (19) and (20) can be calculated as follows [50]:

$$\eta_i = \frac{[((1-\cos^{q+1}\theta)/(q+1)) + ((1-\cos^{2q+1}\theta)/q)]^2}{2\tan^2\theta[(1-\cos^{2q+1}\theta)/(2q+1)]} \tag{21}$$

and

$$\eta_s = 1-\cos^{2q+1}\theta \tag{22}$$

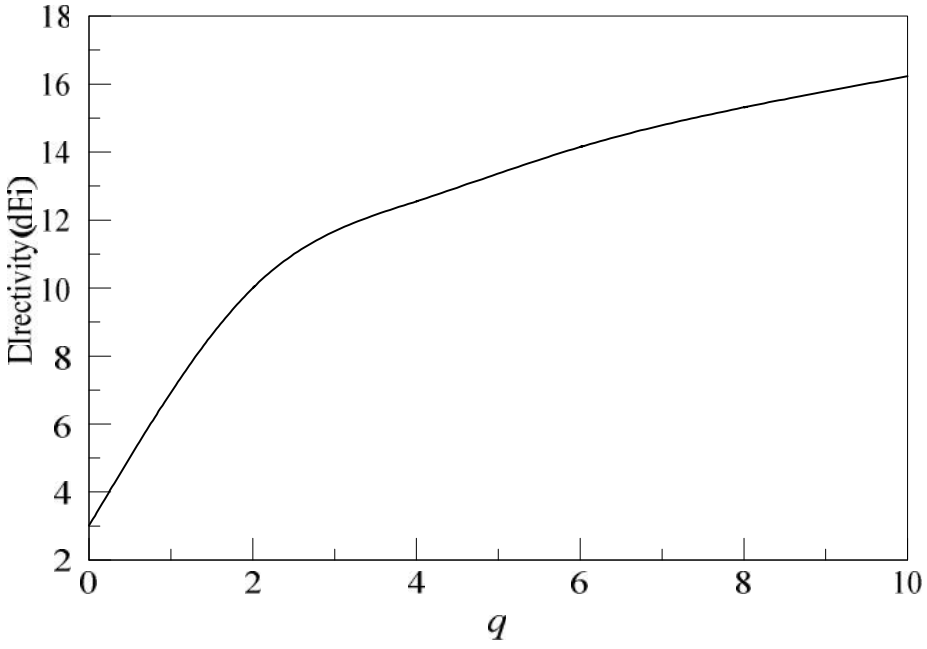

Fig. 19. Directivity vs. q factor of the feed antenna.

By using Eq. (21) and (22), the efficiencies are plotted against the feed antenna pattern in Fig. 20 with a given reflectarray diameter of 0.5 m at 32 GHz and a *f*/D ratio of 1.0. These curves indicate that the illumination and the spillover efficiencies are complementary to each other [50].

In the design of a reflectarray, it is desired to find the maximum aperture efficiency with the given design parameters. The feed antenna location is an important parameter and is described by the offset angle θ_0 and the height F.

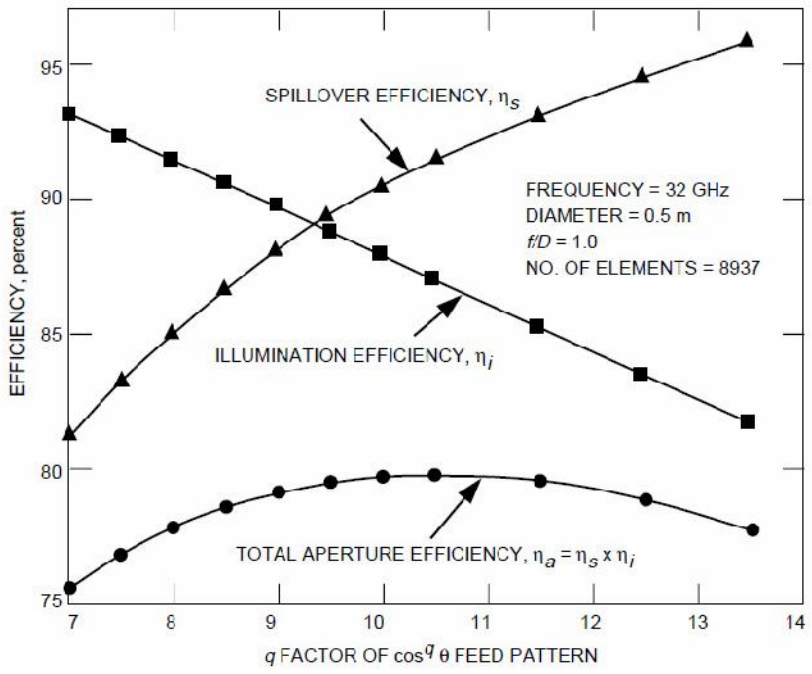

Fig. 20. Illumination and spillover efficiencies vs. feed pattern shape [50].

3.3 Design and performance of the feed array

A. Introduction

The development of a 0.25 m square offset fed beam switching reflectarray antenna has been presented. The reflectarray is a flat aperture to emulate parabolic right cylinder and ring-patch elements are used to obtain the wide phase variation. A linearly polarized microstrip patch fed by a Butler matrix is placed along the focal line to feed the reflectarray antenna. Large parabolic reflectors have been used in satellite communications and radio astronomical system due to high gain. Although they are efficient antennas, these antennas are bulky and heavy, and the main beam can be tilted only a few degrees from broadside direction. Microstrip reflectarray has been studied as a substitute for parabolic reflectors due to flat surface, light weight, easy fabrication, and broad beam scanning [20-36]. This reflectarray consists of feed antenna and microstrip array of reflecting elements. The feed antenna illuminates microstrip array elements, which are designed to make the reradiated wave phase coherent wave. For this, there are several ways such as loading patches with stubs of variable length [31], using patches of variable size [34], using patches with rotation angles [32].

Many papers of microstrip reflectarray have been published on the design of fixed beam antennas. One of the advantages of the reflectarray is an electrically beam switching ability and some interesting developments has been reported. An electrically beam scanning reflectarray using RF MEMS has been proposed in [35] and aperture coupled elements are used. In [36], switched beam reflectarray with two linear polarized feed arrays has been proposed. Cylindrical reflectors have found use in the area of the

advanced precipitation radar antenna and the application of automotive radar. In this paper, we proposed an offset cylindrical beam switching reflectarray fed by linearly phased array antennas with Butler matrix, which is one of the beam forming networks.

B. Design of Butler matrix elements

The Butler matrix is a 2^n x 2^n network with 2^n input, 2^n output, 2^{n-1} $\log_2 2^n$ branch-line couplers and some phase shifters (n is a matrix order). A 4 x 4 Butler matrix has been used to feed N array elements and has some good features such as lossless property and simple structure [7-14]. This matrix is composed of branch-line couplers, -45^o phase shifters, and crossovers as shown in Fig. 2. A signal incident at input port is divided into output ports with equal magnitude and the constant differential phase shift ($\pm 45^o$ and $\pm 135^o$). The Butler matrix is implemented on substrate with a relative permittivity of 2.33 and a thickness of 0.508 mm.

The conventional planar branch-line couplers are used for the matrix. The branch-line couplers are the simplest type of a quadrature coupler, since the circuitry is entirely planar. These couplers are a reciprocal four-port network, meaning that they work effectively on waves transmitting in either direction and are 3 dB directional couplers with 90^o phase difference in the output port. They have a symmetry shape, as any port can be used as the input port and the output ports (P2 and P3) are on the opposite side from the input port (P1). The isolated port (P4) is the remaining port on the same side as the input port at the center frequency.

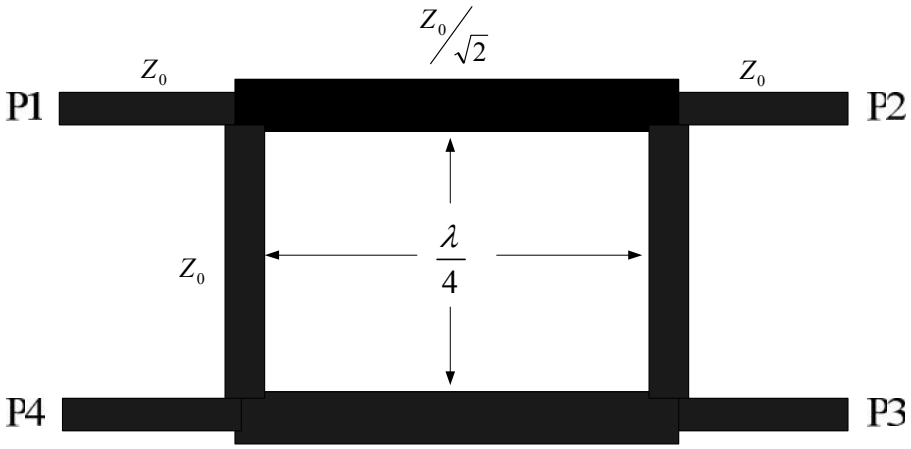

Fig. 21. Geometry of a conventional branch line coupler.

The branch-line couplers are the first element to be implemented in the matrix. The basic configuration of the branch-line coupler is shown in Fig. 21. The branch-line couplers can be decomposed into the superposition of an odd-mode excitation and an even-mode excitation. The length of each arm of the branch line coupler is quarter-wavelength. One pairs have the characteristic impedance of Z_o, and the other pairs have the characteristic impedance of $Z_0/\sqrt{2}$. A part of the wave traveling from port1 to port 2 is coupled to port 3, but not port 4. Port 1 and 4 are decoupled as are port 2 and 3. With all ports matched, power entering port 1 is evenly divided between port 2 and 3 with a 90^o out of phase between these output ports. No power is delivered to port 4, which means it is the isolation port. The line widths of 50 Ω and 35.4 Ω are 1.51 mm and 2.47 mm and the length of two branch lines is the quarter-wavelength, 6.68 mm. The simulation results of the coupler are presented. Fig. 22 shows the return loss, isolation, and insertion loss of branch-line coupler. It can be seen that the isolation and return loss

is greater than -20 dB at 8 GHz and the couplings are 3.05 dB, which are reasonable compared with the theoretical values. Fig. 23 illustrates the phase between two output ports, and it is shown that the phase difference between the output ports is about -90°. The phase differences are almost constant over the operating frequency band. These simulation results are obtained by using Ansoft HFSS V12.

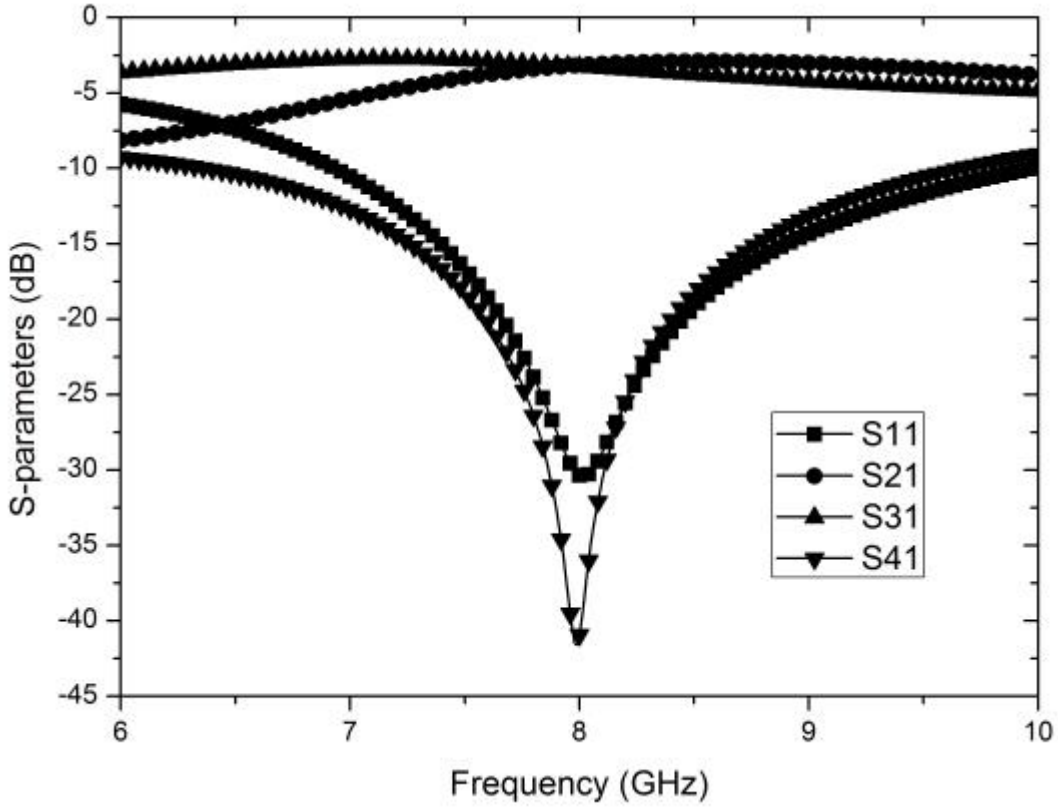

Fig. 22. Simulated magnitude resopnses of the branch-line coupler.

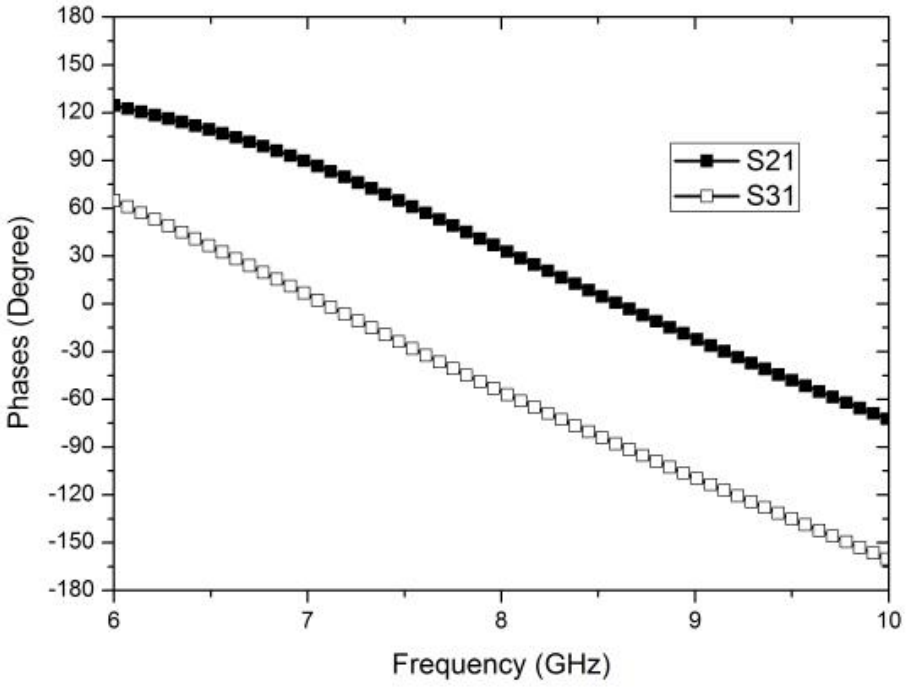

Fig. 23. Phase responses of the branch-line coupler at output ports.

A planar crossover, 0 dB coupler, can be designed by cascading two branch-line couplers. The main role of crossover is to isolate signals at the crossing of lines. Fig. 24 shows the simulated results of 0 dB coupler. As shown in Fig. 24, S_{31} is about -0.1 dB and $S_{11,}$ $S_{21,}$ and S_{41} are greater than -25 dB at the center frequency. Theoretically phase shifters provide low insertion loss, and approximately equal loss in all phase states. Most phase shifters are reciprocal networks, meaning that they work effectively on waves passing in either direction. Phase shifters can be controlled electrically, magnetically or mechanically by using PIN diodes. We will concentrate mainly on those that are electrically-controlled. In this work, phase shifters are needed to produce desired phase shift at output ports of the Butler matrix. Transmission line phase shifters are chosen in

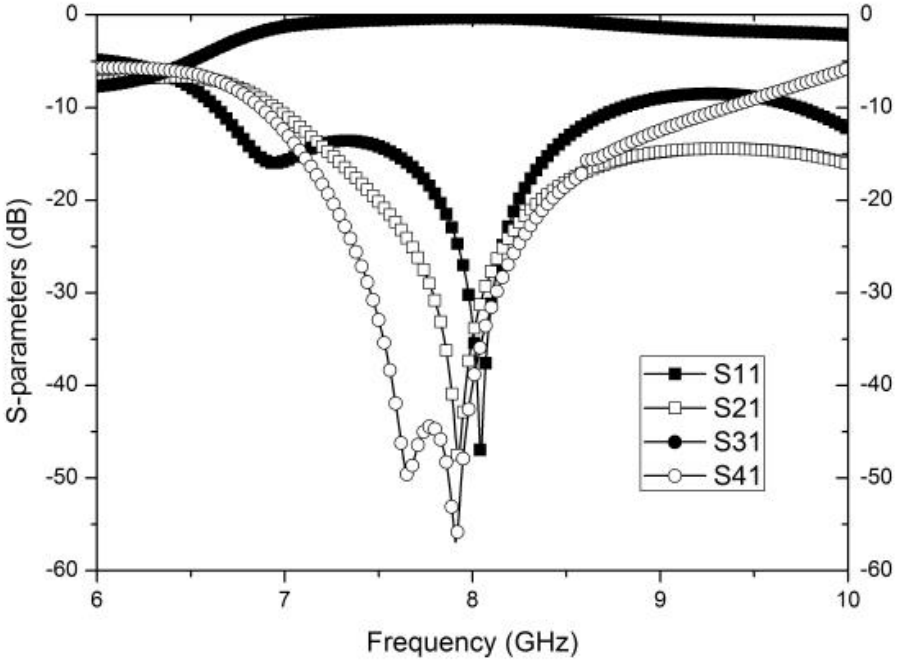

Fig. 24. Simulated S-parameters of the 0 dB coupler.

this work because they are simple in the design and implementation. Eighth wavelength delay line is obtained from $\Delta\theta = \Delta x \cdot \beta$, which is designed by using a simple transmission line at 8 GHz. The phase shifter is used to delay the signals equal to the needed phase shift (-45^{o}), plus the delay of the crossover. The simulated phase of the crossover is -149.3^{o} at 8 GHz. Therefore, the required phase of the phase shifter is -194.3^{o} . A 50 Ω transmission line of the length of 39.02 mm and the width of 1.51 mm produces the required phase.

By combining the branch-line couplers, -45^{o} phase shifters, and crossovers, we design the Butler matrix on Rogers RT/duroid 5870 substrate with a relative permittivity of 2.33 and thickness of 0.508 mm. The schematic of the Butler matrix is shown in Fig.

25. We consider the matrix that has the same number of bends in all paths because of reducing the effects of amplitude and phase differences between all paths. The simulation results of the Butler matrix are presented. As shown in Fig. 26 and Fig. 27, the return losses are greater than -18 dB and the insertion losses are 6.6 ± 0.2 dB at 8 GHz when port 1 is applied. Table 4 shows a summary of the corresponding phase shifts between the inputs and the outputs of the matrix. The simulated maximum phase errors are about -3.6^{o} at 8 GHz.

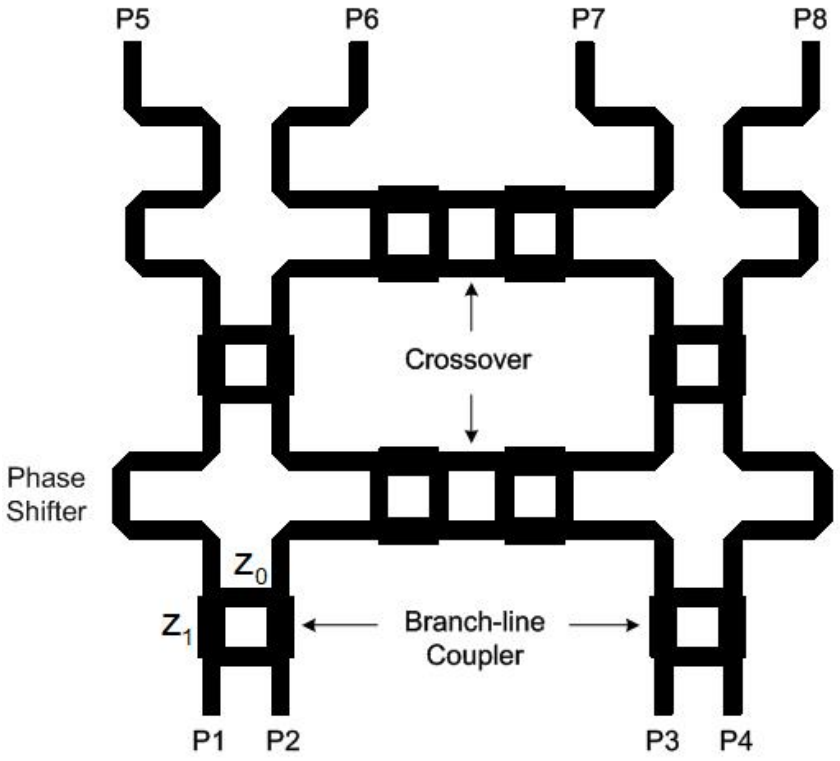

Fig. 25. Schematic of the conventional 4 x 4 Butler matrix.

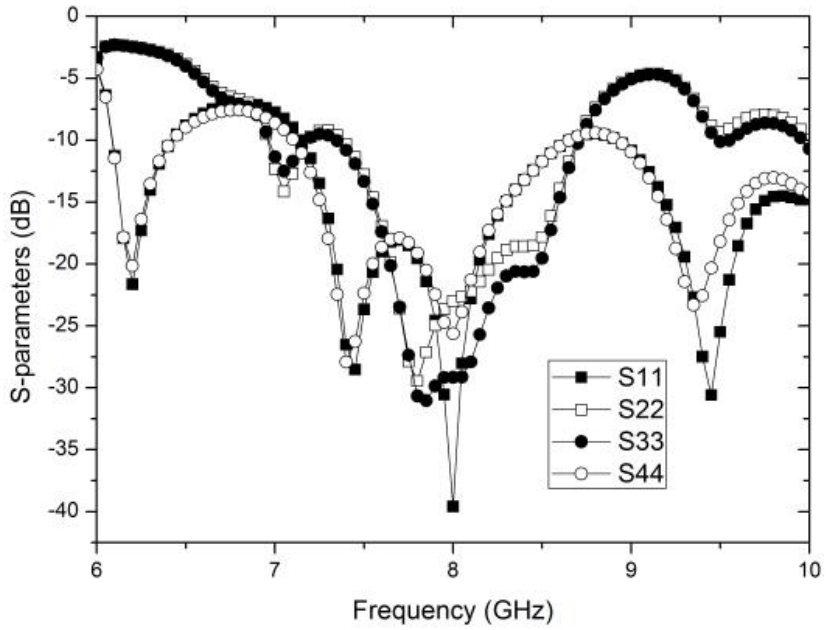

Fig. 26. Return loss of the Butler matrix.

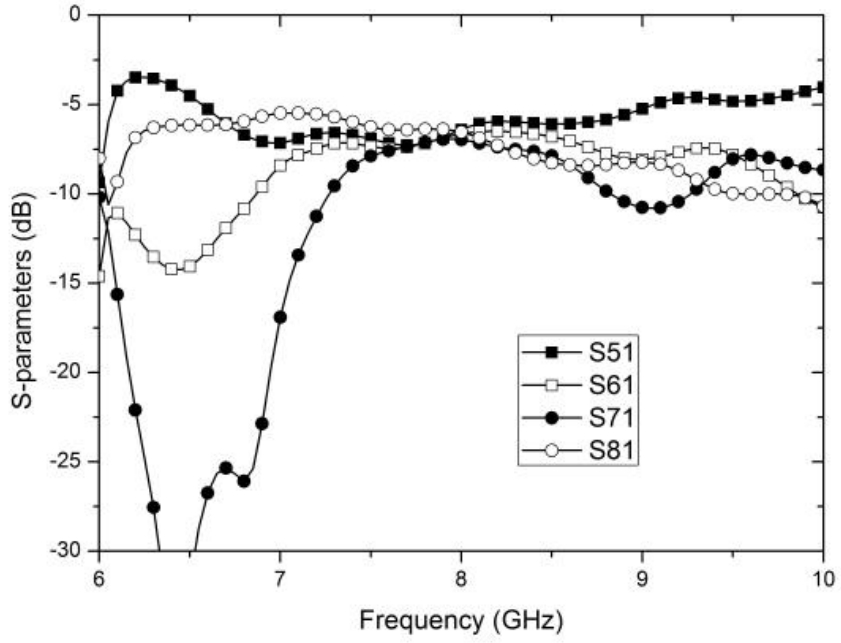

Fig. 27. Insertion loss of the Butler matrix when port 1 is applied.

Table 4. Phase shifts at the input and output port of the Butler matrix (unit: degree).

Port		5	6	7	8
1	Phase	132.89	90.51	44.51	-2.59
	|Error|		2.62	1.1	2
2	Phase	41.82	-180.0	-45.63	87.18
	|Error|		3.18	0.63	2.19
3	Phase	87.43	-45.67	179.64	41.04
	|Error|		1.9	0.31	3.6
4	Phase	-3.34	43.6	88.82	131.01
	|Error|		1.94	0.22	2.81

A patch antenna is fabricated by etching the antenna element pattern in metal trace bonded to a dielectric substrate that has dielectric constants usually in the range of $2.2 \le \varepsilon_r \le 12$. The patch antenna is one of the resonant antennas and when the particular shape and mode are chosen, they are very versatile in terms of resonant frequency, polarization, pattern and impedance. It is easy to analyze using both the transmission-line and cavity model, which are most accurate for thin substrate. The feeding mechanism plays an important role in the design of microstrip patch antennas. The resonant input resistance of the patch antenna can be changed by using an inset feed, recessed a distance from the slot. By using a transmission line model, it is possible to accurately model and analyze microstrip line inset fed patch antenna designs. In addition, by using modal-expansion analysis, it is possible to locate the exact recessed length of a

50 Ω input impedance. Microstrip line feeding is suitable for developing high gain microstrip array antennas and the recessed length determines the input impedance. Microstrip edge feed antennas with inset are used for an antenna array as shown in Fig. 28 (a). The dimensions of array element are as follows: the width of 7.92 mm, the length of 5.84 mm, the inset width of 0.32 mm, and the inset length of 1.86 mm. The return loss is greater than -25 dB at 8 GHz as shown in Fig. 28 (b).

C. Measurement of the feed array antenna

Feed array antenna consists of beamforming network and microstrip array antenna. The radiating elements are spaced at a free space half-wavelength at 8 GHz. The measured return loss of each port is greater than -20 dB as shown in Fig. 29. Fig. 30 shows the normalized radiation pattern of the feed array antenna at 8 GHz. The boresight angles of four beams are 16^{o}, -32^{o}, 31^{o},and -15^{o}, respectively. The sidelobe level is -

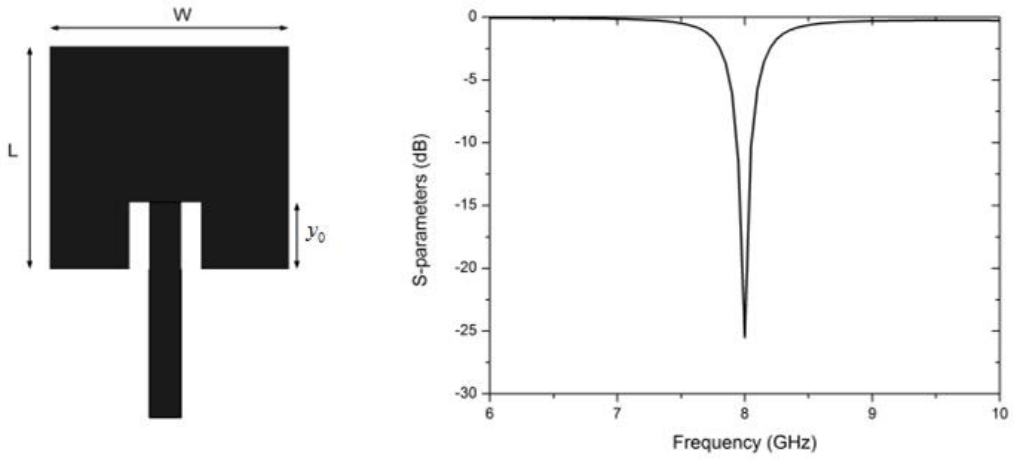

(a) (b)

Fig. 28. (a) Geometry of array element and (b) return loss of the antenna.

11.5 dB for port 1 & port 4 and -8.8 dB for port 2 & port 3. The size of the feed antenna is 11.8 cm x 12.5 cm.

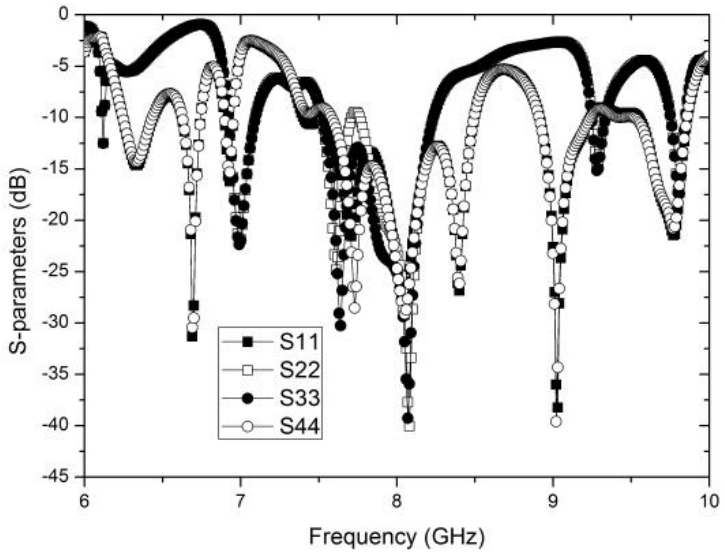

Fig. 29. Measured return losses of the feed array antenna.

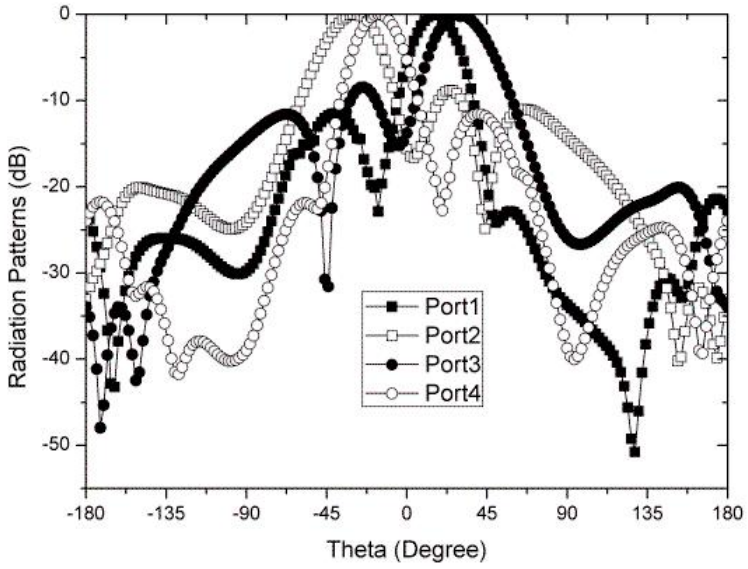

Fig. 30. Measured radiation patterns of the feed array antenna.

3.4 Design and performance of the microstrip reflectarray antenna

Space borne radar is an important technology to the research in the meteorology and topography of the Earth and other planets in the solar system. Cylindrical reflect antenna fed by linear phased array antennas have found use in the area of radar applications. A prototype model of the advanced precipitation radar antenna using parabolic cylindrical reflect antenna made of a polymer membrane material is reported in [63]. An offset cylindrical reflect antenna has been designed for the application of automotive radar [64]. An offset feed configuration is used to reduce the aperture blockage. The analysis of line-source-fed single layer microstrip reflectarray is presented by Sze [65]. Many papers of the microstrip reflectarray antenna have fixed beam direction [35, 36]. In this work, the scannable microstrip reflectarray has the four main beams with one feed array antenna.

The radiating element of the proposed microstrip reflectarray is shown in Fig. 31. The unit cell consists of one multi-resonant element using a ring and a circular patch on the substrate. The microstrip reflectarray is implemented on substrate with a relative permittivity of 2.2 and a thickness of 0.787 mm. The foam layer (ε_r =1.06) is inserted to reduce the rapid phase change between the substrate and ground plane. The height of the foam layer is 1.6 mm. In this design, the radius of a ring (r_1) is variable and the gap between the ring and the circular patch are fixed of 1 mm and r_1-r is fixed at 1 mm. The unit cell is a square lattice with a side length of 18.75 mm, which is 0.5 λ_0 at 8 GHz. The reflection phase of the microstrip reflectarray element changes with this variable and is simulated with Ansoft HFSS using E and H wall waveguide approach mentioned in [66].

While the size of a unit cell differs from that of its neighboring elements, this simulation method assumes an infinite periodic array environment with normal incident wave to optimize the size of a unit cell. Fig. 32 shows the simulated reflection phase of the microstrip reflectarray element at 8 GHz. The phase range is obtained around 612^{o} in case of normal incidence.

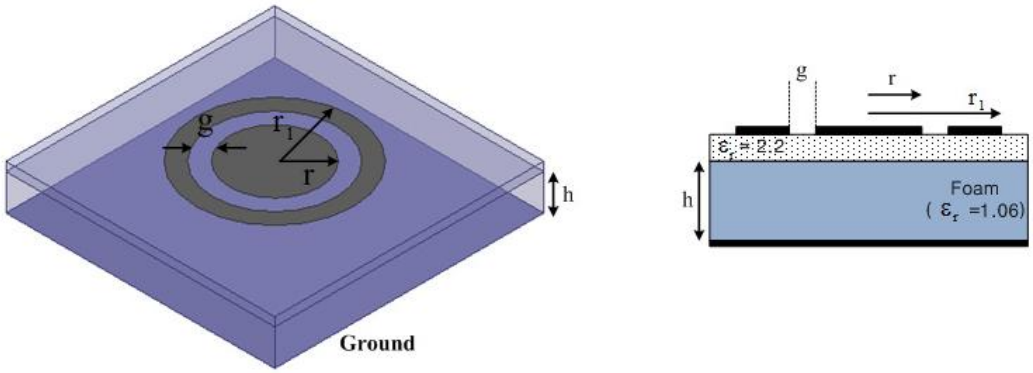

(a) (b)

Fig. 31. Unit cell of the microstrip reflectarray: (a) 3D view and (b) side view.

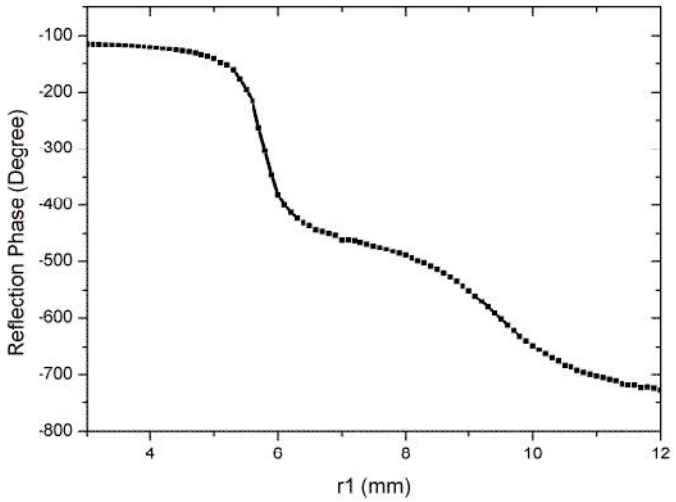

Fig. 32. Reflection phase of the microstrip reflectarray element at 8 GHz.

Measurements of the beam scanning reflectarray fed by the phased array antenna are conducted in the anechoic chamber at Texas A&M University with the range of 10 meters. The photograph of the measurement setting of 0.25 mm offset-fed microstrip reflectarray is shown in Fig. 33. The scan angle designed is 20^{o} in the H-plane. The boresight angles of four beams generated by the feed array antenna are 14^{o}, -29^{o}, 35^{o},and -12^{o} as shown in Fig. 34. The sidelobe levels are -12.9 dB for port 1 & port 4 and -5.1 dB for port 2 & port 3.

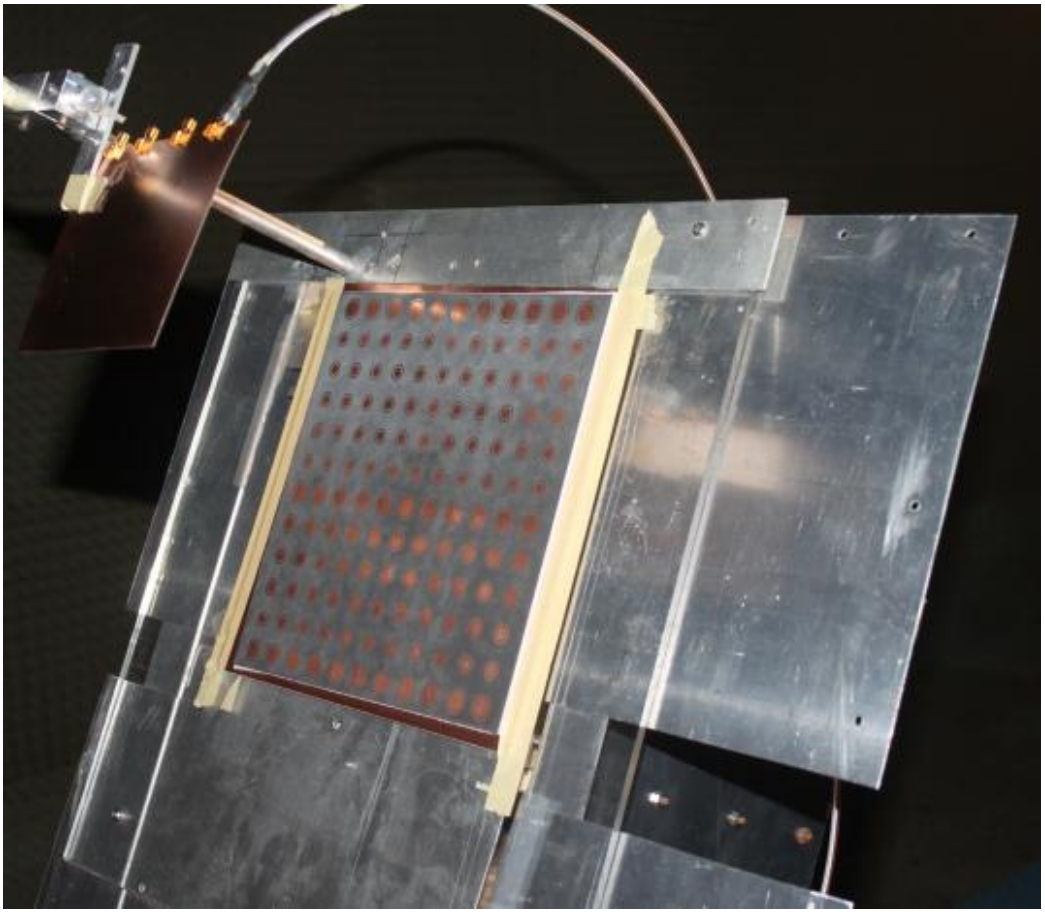

Fig. 33. Photograph of the measurement setup.

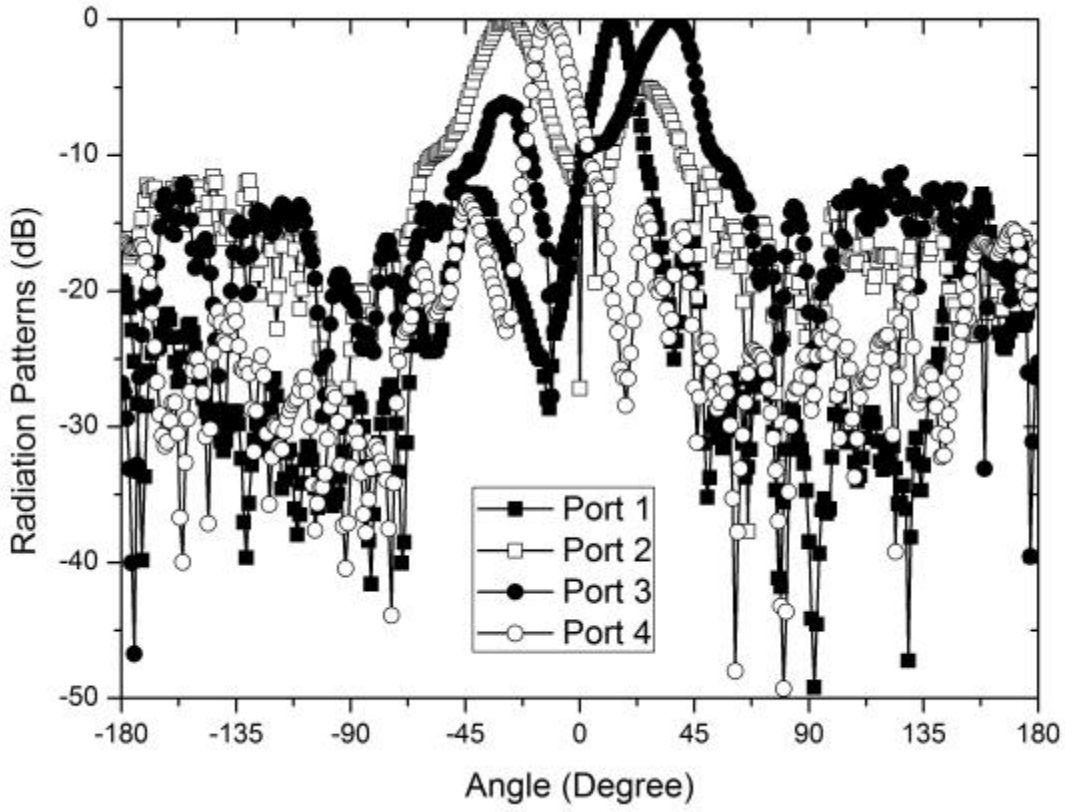

Fig. 34. Measured normalized radiation patterns of the offset-fed beam scanning microstrip reflectarray.

3.5 Conclusions

An offset cylindrical reflectarray fed by linear polarized phased array has been developed. An electrically beam scanning microstrip reflectarray has been designed and fabricated. The microstrip reflectarray shows four main beam directions depended on the feed array antenna with Butler matrix. Further study will consider low sidelobe levels of feed array antenna and the increase of the number of elements for low sidelobe level of the microstrip reflectarray.

CHAPTER IV

SWITCHED BEAM ANTENNAS FED BY 4 X 8 BUTLER MATRIX USING DOUBLE-SIDED PARALLEL-STRIP LINE

4.1 Introduction

There has been a rapid growth in the development of smart antenna in wireless communication systems to reduce multipath fading and interference. The two types of smart antennas are adaptive array antennas and switched beam antennas. Adaptive array antennas aim to steer automatically the beam to any. Although adaptive array has some advantages such as the improvement of speech quality and the continuous beam patterns, the technical realization of these algorithms is more complex than switched beam array systems. The switched beam systems have multiple fixed beam patterns, but these systems can be easily implemented and can also improve the channel capacity and range.

The switched beam system consists of a beam forming network and an antenna array. Several beam forming networks have been proposed, such as the Blass matrix [4], the Nolen matrix [5], and the Butler matrix [7-13]. The N x N Butler matrix has been used to feed N array antenna elements. The Butler matrix has some good features such as lossless property and simple structure as compared to other matrices. The Butler matrix is composed of branch-line couplers, phase shifters, and cross- overs. In general, the Butler matrix has been realized by microstrip lines [7-11], coplanar waveguides (CPW) [12], and waveguides [13]. In this work, we propose the N x 2N Butler matrix using the double-sided parallel-strip lines (DSPSL). DSPSL has some advantages such

as easy realization of high impedance lines, simplicity in circuit structures of wide-band transitions, and good performance of balanced microwave components and can be analyzed using the image theory [15, 67]. The DSPSL with an inserted conductor plane are used at the output ports of the Butler matrix. DSPSL are composed of two identical microstrip lines on top and bottom layers. DSPSL with the inserted common conductor plane has no effect on the identical circuits on the top and bottom layers and the conductor plane is considered as a virtual ground to isolate nonidentical circuits [16].

According to the array theory, it is difficult for microstrip antenna arrays to obtain a low sidelobe level (SLL) due to mutual coupling between array elements and coupling and mismatch between elements and feed network [37]. In this work, power dividers based on DSPSL with the inserted ground plane are used to increase the number of the output ports of feed network. This type of power divide has a good performance over the broadband range [68, 69]. The proposed switched beam array antenna is designed with low sidelobe level and high gain operating at 8 GHz compared to the conventional 4 x 4 Butler matrix.

4.2 Analysis of double-sided parallel strip line

Double-sided parallel-strip line (DSPSL) was analyzed by Wheeler using the conformal transformation mapping method [70]. Fig. 35 shows the side view of the conventional DSPSL and the microstrip line. The conventional DSPSL is a symmetric structure. The RF voltage on the top strip is positive (+) if the voltage on the bottom strip is negative (-). According to the image theory, the voltage in the middle of the substrate

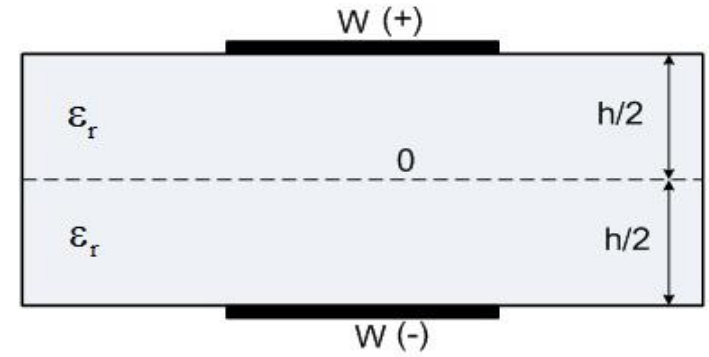

(a)

(b)

Fig. 35. Side view of the conventional DSPSL and microstrip line.

can be considered to be zero (0) and the inductance per unit length of the DSPSL (L_d) is twice of that of the microstrip line (L_m). Moreover, the capacitance per unit length of the DSPSL (C_d) is one half of that of the microstrip line (C_m). It means that the middle plane of the substrate can be considered as a virtual ground plane as shown in Fig. 35 (a) and the characteristic impedance of the two cases can be given by

$$Z_{cd} = \sqrt{\frac{L_d}{C_d}} = \sqrt{\frac{2L_m}{C_m / 2}} = 2\sqrt{\frac{L_m}{C_m}} = 2Z_{cm} \tag{23}$$

where Z_{cd} and Z_{cm} is the characteristic impedance of the DSPSL and microstrip line.

4.3 Design of the 4 x 8 Butler matrix on DSPSL

In this section, the conventional Butler matrix is designed on DSPSL. The DSPSL with an inserted conductor plane are used at the output ports of the Butler matrix. DSPSL are composed of two identical microstrip lines on top and bottom layers as shown in Fig. 36 (a). DSPSL with the inserted common conductor plane as shown in Fig. 36 (b) has no effect on the identical circuits on the top and bottom layers and the conductor plane is considered as a virtual ground to isolate nonidentical circuits. Fig. 37 shows the characteristic impedance of micro- strip line and DSPSL. These impedances versus the width (W) are extracted by Zeland IE3D software [71]. A signal incident at the input ports is divided into the output ports with equal magnitude and the constant differential phase shift ($\pm 45^{o}$ and $\pm 135^{o}$) depending on the input port signal. The superposition of all differential phase makes a beam more directional to a certain direction.

The proposed Butler matrix is composed of the branch-line couplers, crossovers, phase shifters, and power dividers. Fig. 38 shows the circuit configuration of the proposed 4 x 8 planar Butler matrix based on DSPSL and DSPSL with inserted conductor plane. Since DSPSL is a balanced line as shown in Fig. 36, two circuits on both sides of a substrate have the same dimensions. A RT/Duroid 6010 with a relative dielectric constant of 10.2 and thickness of 0.762 mm is used to design the branch-line couplers, crossovers, and phase shifters.

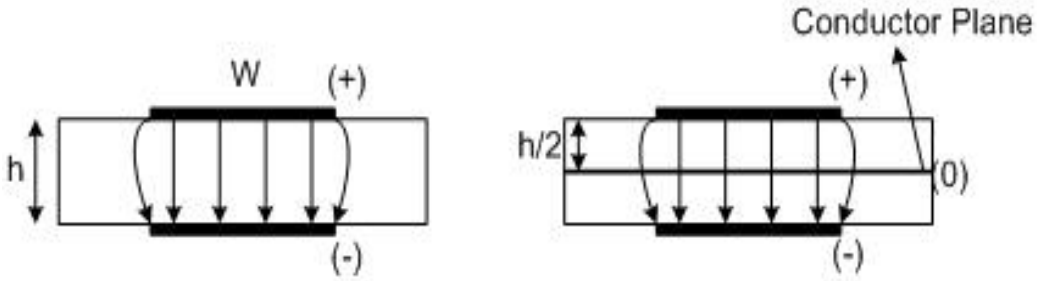

(a) (b)

Fig. 36. Cross section view and E-field distribution of (a) conventional DSPSL and (b) DSPSL with an inserted conductor plane.

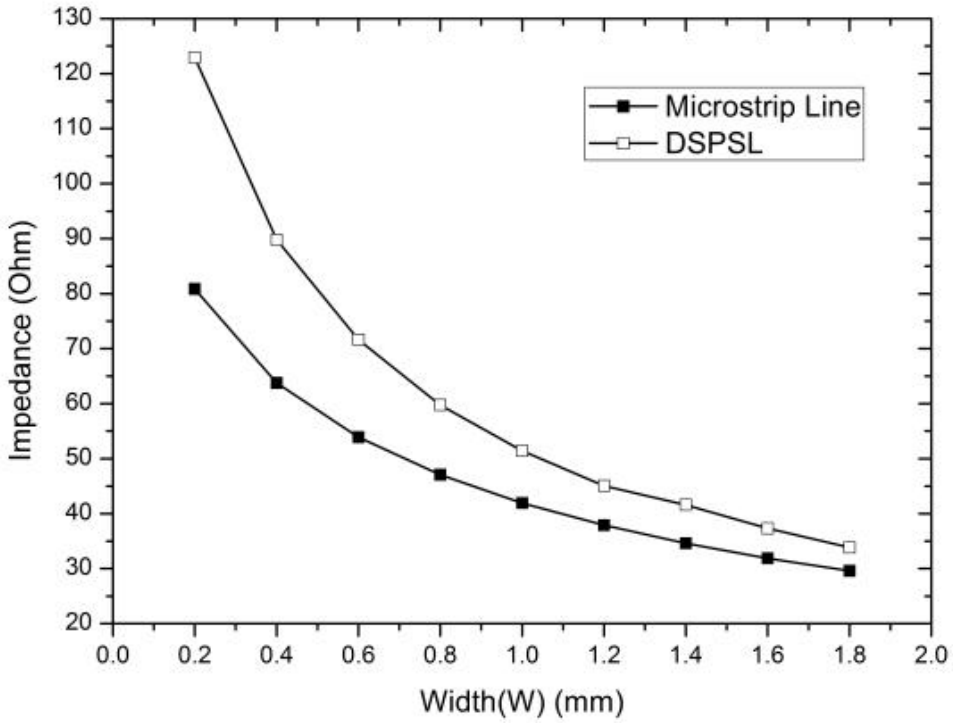

Fig. 37. Characteristic impedance of the microstrip line and DSPSL.

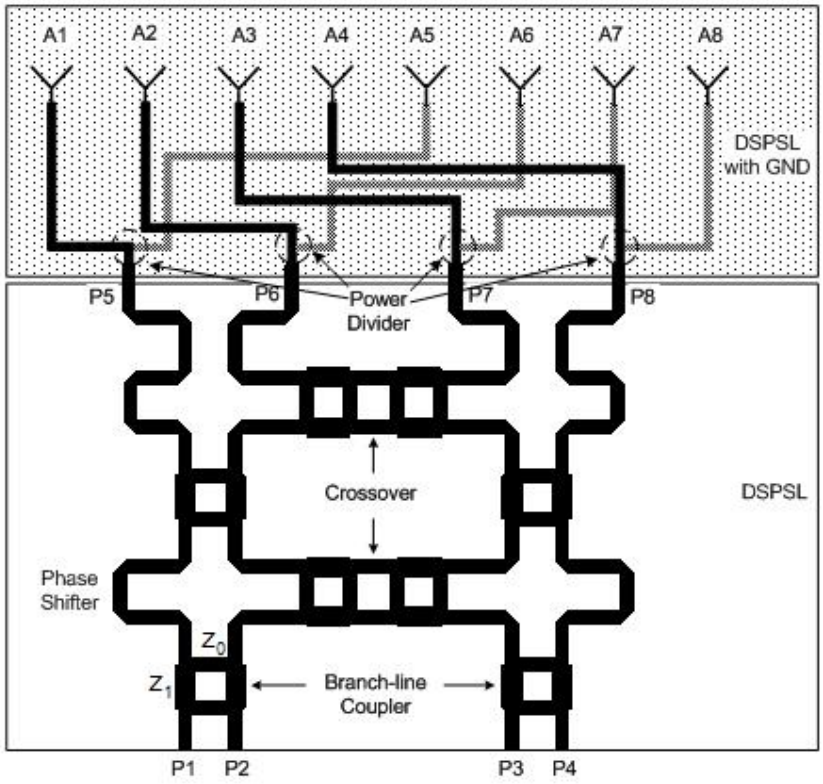

Fig. 38. Geometry of the proposed 4 x 8 Butler matrix (clean box: DSPSL and dotted box: DSPSL with ground plane).

The conventional planar branch-line couplers are used for the proposed matrix on DSPSL as shown in Fig. 39. With all ports matched, a signal incident on input port (P1) is evenly divided between output ports with 90^{o} phase shift and no power is coupled to insolation port (P2) as shown in Fig. 38. The line width of each impedance can be founded using Fig. 37. The line widths of Z_0 (50 Ω) and Z_1 (35.4 Ω) are 1.06 mm and 1.62 mm. The line length of each impedance is the quarter-wave length of DSPSL, 2.60 mm. The simulated results are the insertion loss of 0.18 dB and the return loss and isolations of over 20 dB at 8 GHz as shown in Fig. 40 (a). Fig. 40 (b) shows that the

phase difference is -89.5^{o} between output ports at 8 GHz. These results show a good performance. These results are achieved using Ansoft HFSS V12.

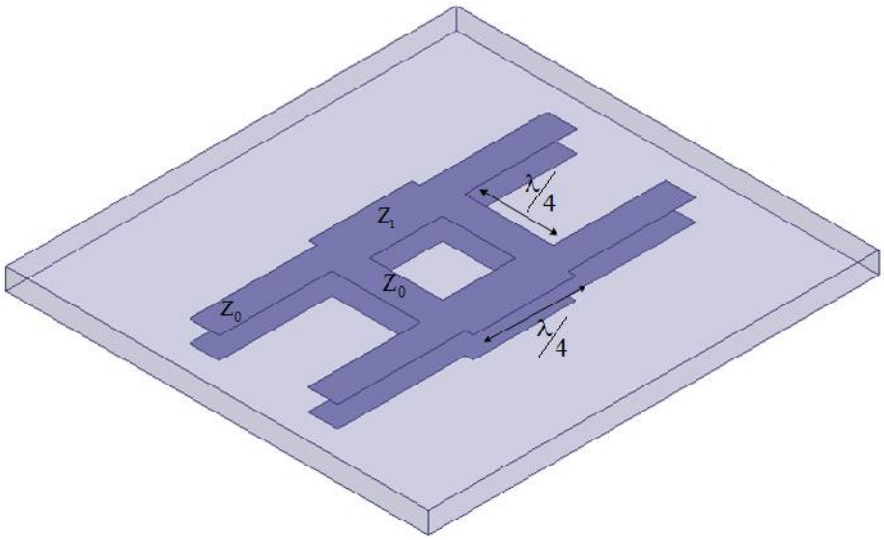

Fig. 39. Geometry of the branch-line coupler on DSPSL.

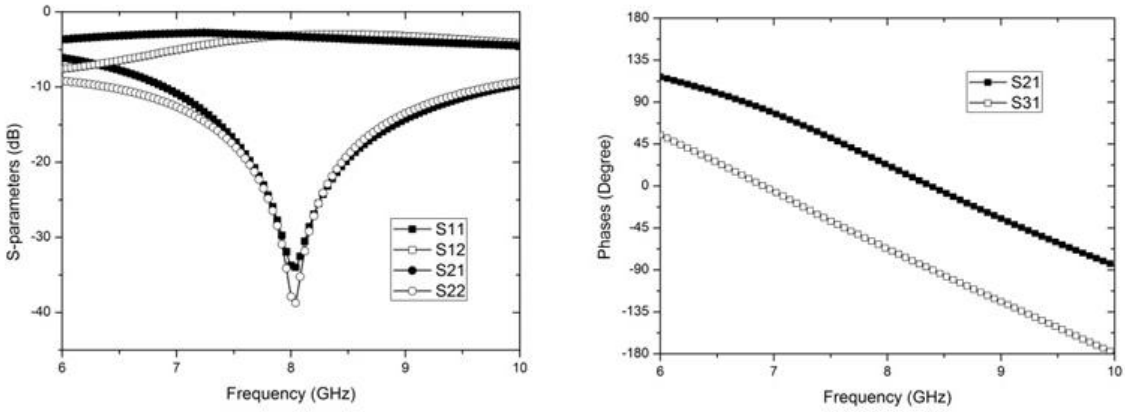

(a) (b)

Fig. 40. Simulated S-parameters of the branch-line coupler: (a) magnitude responses and (b) phase responses.

A planar crossover, 0dB coupler, can be designed by cascading two branch-line couplers. The main role of a crossover is to isolate signals at the crossing of lines. The layout of the crossover is seen by in Fig. 38. The insertion loss is 0.23 dB and the return loss and isolation are over 25 dB at 8 GHz as shown in Fig. 41. The simulated phase of the crossover shows 40.7^{o} at 8 GHz.

After designing the branch-line coupler and crossover, we design a phase shifter for controlling phase. The phase shifter is used to delay the signals equal to the needed phase shift, plus the delay by the crossover. The simulated phase of the crossover is 40.7^{o} at 8 GHz. Therefore, the required phase of the phase shifter is -4.3^{o}. A 50Ω transmission line of the length of 10.4 mm and the width of 1.06 mm produces the required phase shift.

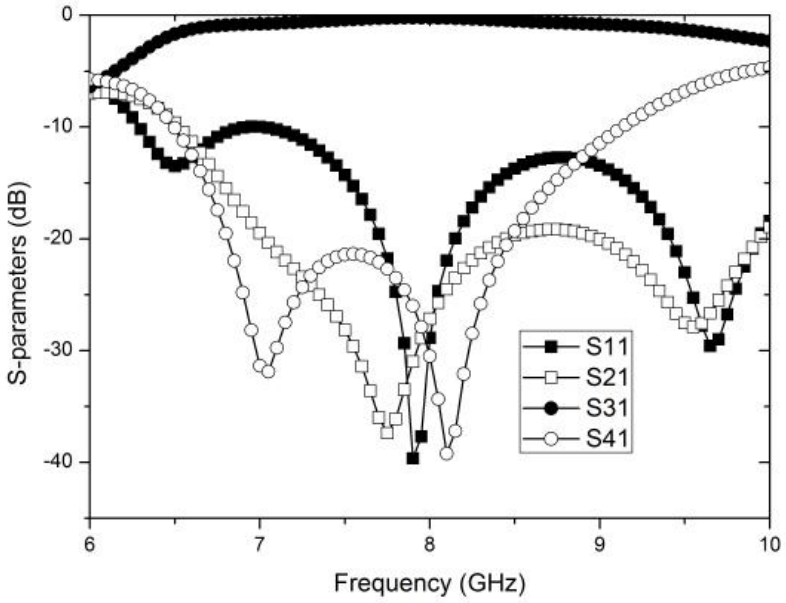

Fig. 41. Simulated S-parameter responses of the crossover.

Fig. 42 shows the S-parameters of the proposed Butler matrix on DSPSL when port 1 is applied. The insertion loss is 0.73 dB ± 0.16 dB for port 1 as shown in Fig. 42. The insertion loss for port 2, port 3, and port 4 is 0.75 dB ± 0.18dB, 0.82 dB ± 0.2 dB, 0.83 dB ± 0.23 dB, and 0.74 dB ± 0.17 dB, respectively. The return loss for all ports is greater than -20 dB at 8 GHz. Table 5 shows the phase of each output port and maximum phase error is less than 2^{o} . These results show the good performance in terms of magnitude and phase of S-parameters.

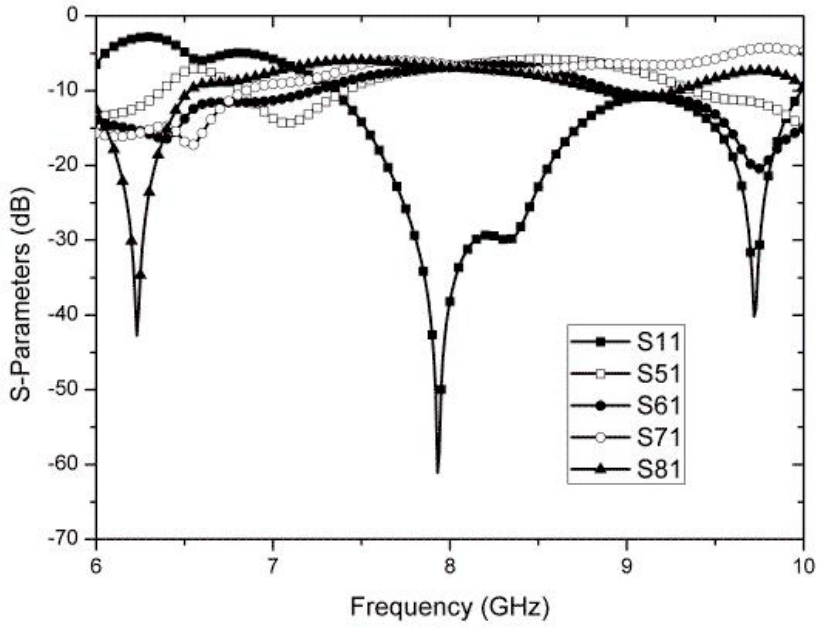

Fig. 42. Simulated S-parameters of the proposed 4 x 4 Butler matrix when port 1 is applied.

Table 5. Phase and phase error of each port (unit: degree).

	P5	P6	P7	P8	Maximum phase error
P1	161.5	116.6	72.1	27.6	0.5
P2	72.4	-151.6	-15.6	117.8	1.6
P3	117.4	-16.1	-151.9	72.2	1.5
P4	27.6	72.3	116.5	161	0.8

The power divider is a fundamental and important component used in the microwave and millimeter wave applications. In this work, the power divider on a DSPSL and a DSPSL with the inserted ground plane is used to increase the output ports of the 4 x 4 Butler matrix. Fig. 43 shows the 3-D view of the power divider, which consists of DSPSL at port 1 and the back-to-back microstrip lines at port 2 and port 3. The inserted ground plane, located in the middle of the substrate, has no effect on the DSPSL, which can be considered as two identical microstrip lines placed back-to-back as shown in Fig. 44. As shown in Fig. 38, the output port, P5, of the Butler matrix is connected with the power divider and the output ports of the power divider are used to feed antennas A1 and A5 with 180^{o} phase difference. The ground plane is inserted in the middle layer (h/2) and divided into two parts by gap. The two circuits on the top and bottom layers are identical. When the input port signal is applied to, the phase between top line (port 2) and bottom line (port 3) is 180^{o} out-of-phase as shown in Fig. 36. A resister R is located between two grounds to isolate the output port [68]. Using the even

and odd mode analysis method, the impedances of each section can be calculated: Z_0 =50 Ω of DSPSL,

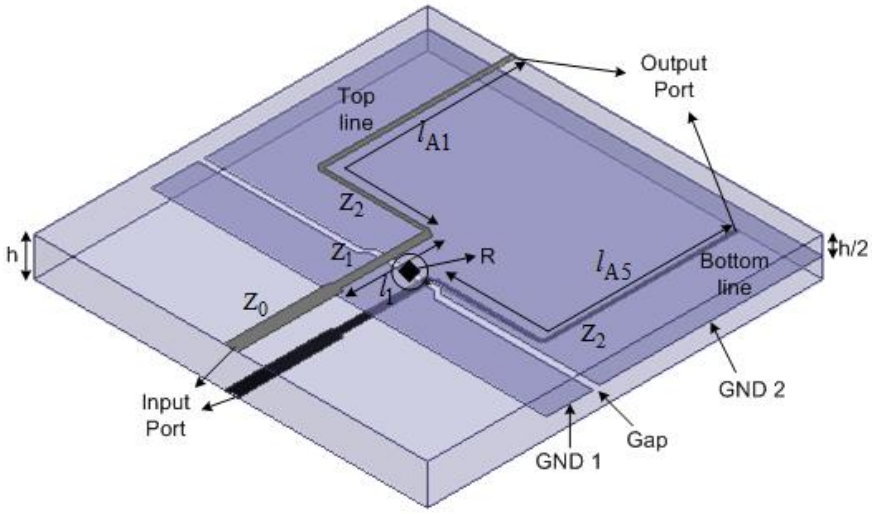

Fig. 43. 3-D view of the power divider on a DSPSL and DSPSL with the inserted ground plane.

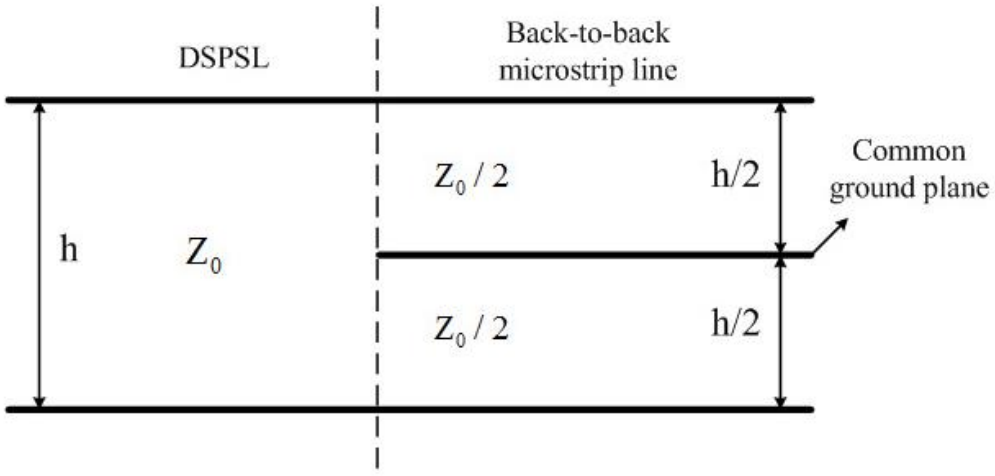

Fig. 44. Side view of the power divider.

Z_2 = 50 Ω of the inserted DSPSL, or the microstrip impedance line with h/2, and Z_1 = $Z_0 / \sqrt{2}$ with R= Z_0 /2 [68]. The power divider is designed on RT/Duroid 6010 with a dielectric constant of 10.2 and a thickness of 0.762 mm. The dimensions of the circuit are as follows: w_0=1.06 mm, l_0=8 mm, w_1 = 0.63 mm, l_1=3.5 mm, w_2=0.35 mm. The output port with the length l_{A1} on the top layer is used to feed an antenna A1 and the output port with the length l_{A5} on the bottom layer is used to feed an antenna A5 on the top layer. The phase difference of the power divider must be 180^o out-of-phase to have a constant differential phase shift. The lengths of the output ports on the top and bottom layer should be same for 180^o out-of-phase shift. In this design, the phase delay due to via should be considered. The lengths of the output port on top layer are 66.35 mm and the lengths of the output port on bottom layer are 64.4 mm. The simulated results show the insertion loss of ± 0.14 dB and the return loss of over 20 dB at 8 GHz as shown in Fig. 45. The simulated phase difference of the output port is 179.4^o at 8 GHz as shown in Fig. 46.

4.4 Design of the microstrip antenna array

Microstrip edge feed antennas with inset are used for an antenna array. Fig. 47 shows the layout and side view of an antenna array element. All antenna array elements are located on the top layer. Antennas A1 to A4 are fed by the output port of the power divider on same layer and antennas A5 to A8 are fed by that of the power divider from the bottom layer. An array antenna with eight elements produces the beam with low SLL

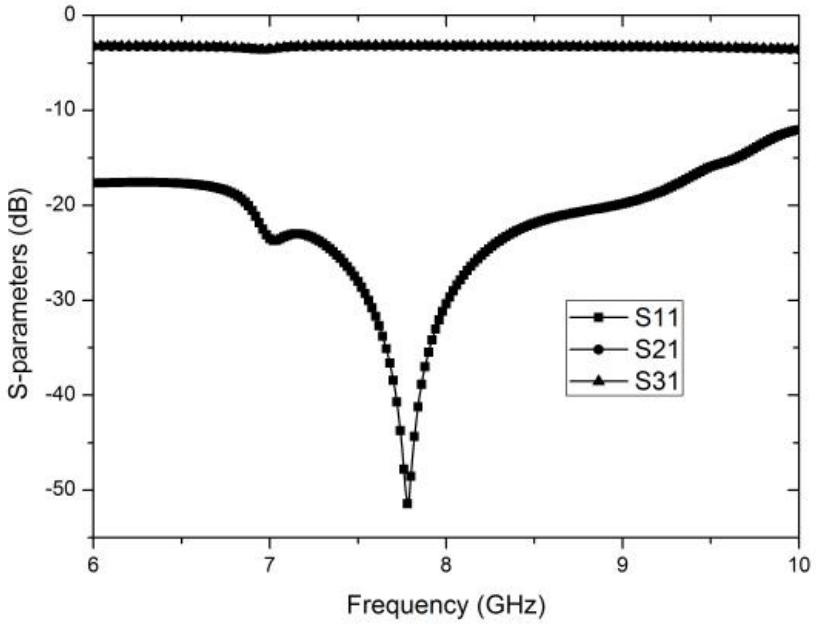

Fig. 45. Simulated magnitude responses of the power divider.

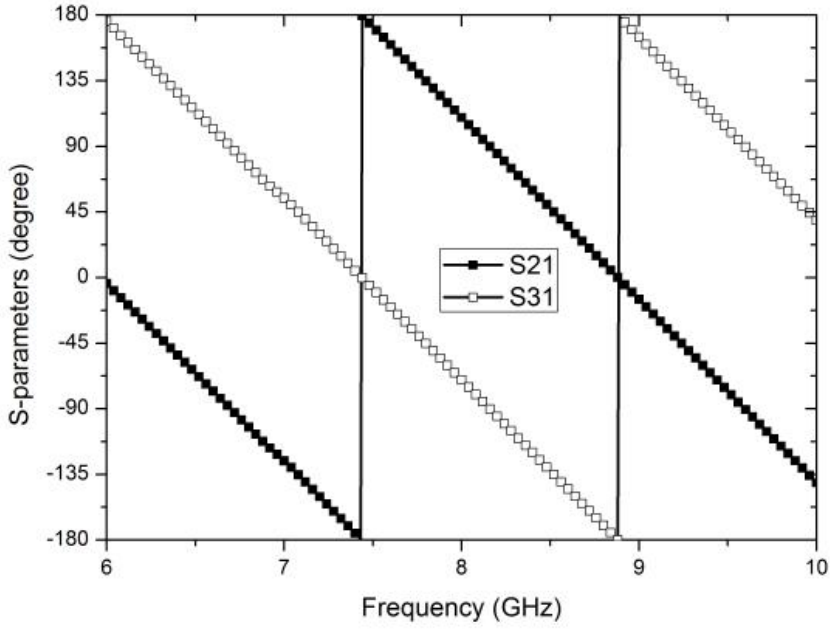

Fig. 46. Simulated phase responses of the power divider.

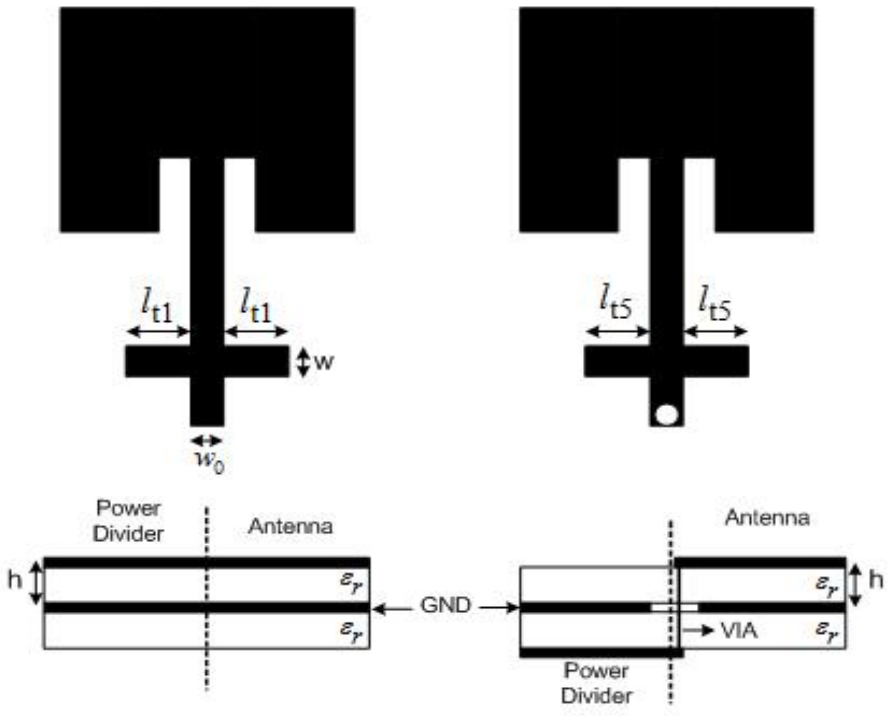

(a) (b)

Fig. 47. Layout and side view of an antenna array: (a) antenna A1 to A4 and (b) antenna A5 to A8.

and high gain compared to an array antenna composed of four elements. Moreover, to reduce sidelobe level (SLL), -20 dB Dolph-Chebyshev distribution is adopted for the array antenna design and the length of from l_{t1} to l_{t5} is used for this distribution. The method was introduced by Dolph [72]. Its excitation coefficients are related to Chebyshev polynomials [59]. The array factor of an array of even or odd number of elements with symmetric amplitude excitation is written as:

$$(AF)_{2M} = \sum_{n=1}^{M} a_n \cos[(2n-1)u] \tag{24}$$

$$(AF)_{2M+1} = \sum_{n=1}^{M+1} a_n \cos[(2n-1)u] \tag{25}$$

where $u = \frac{\pi d}{\lambda}\cos\theta$

If the number of array antenna is eight, Eq. 24 should be

$$(AF) = \cos(7u) = 64\cos^7 u - 112\cos^5 u + 56\cos^3 u - 7\cos u \tag{26}$$

If we let,

$$z = \cos u \tag{27}$$

Eq. 26 can be written as

$$\cos(7u) = 64z^7u - 112z^5u + 56z^3u - 7z = T_7(z) \tag{28}$$

And Eq. 28 is related to a Chebyshev polynomial $T_m(z)$, which is valid only in the $-1 \le z \le +1$ range. This polynomial is related to the hyperbolic cosine functions. Each polynomial can be computed using [59]:

$$T_m(z) = \cos[m\cos^{-1}(z)] \qquad -1 \le z \le +1 \tag{29}$$

$$T_m(z) = \cosh[m\cosh^{-1}(z)] \qquad z < -1,\ z > +1 \tag{30}$$

Since the array factor is a summation of cosine function, the unknown coefficients of the array factor can be determined by equating the series denoting the cosine terms of the array factor to the proper Chebyshev polynomial.

The excitation coefficients of the array factor are calculated by using the above formulas. If we set a major-to-minor lobe ratio of 20 dB, the current excitation

coefficients are a_1=1, a_2=0.874, a_3=0658, and a_4=0.576. An array antenna is designed on a RT/Duroid 6010 with a relative dielectric constant of 10.2 and a thickness of 0.381 mm. All eight array elements are identical except the length for realizing the Dolph-Chebyshev distribution and designed for operating at 8 GHz. The dimensions of array element are as follows: the width of 7.92 mm, the length of 5.84 mm, the inset width of 0.32 mm, and the inset length of 1.86 mm. The width of 50 Ω microstrip feed line (w_0) is 0.35 mm. The lengths for realizing the excitation coefficients are l_{t1} = l_{t8} 1.58 mm, l_{t2} = l_{t7} = 1.28 mm, l_{t3} = l_{t6} = 0.6 mm, and l_{t5} = 0 mm (50 Ω feed line), respectively and the width (w) is 2 mm. The radiating elements of the antenna array are spaced at a distance d=0.5 λ_0 at 8 GHz.

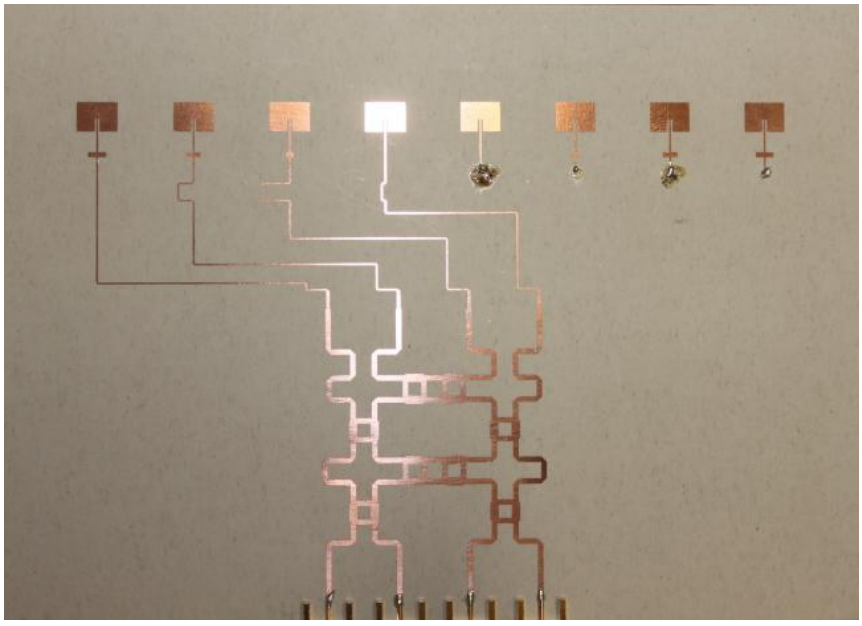

(a)

Fig. 48. Photos of the proposed switched beam array antenna: (a) top view and (b) bottom view.

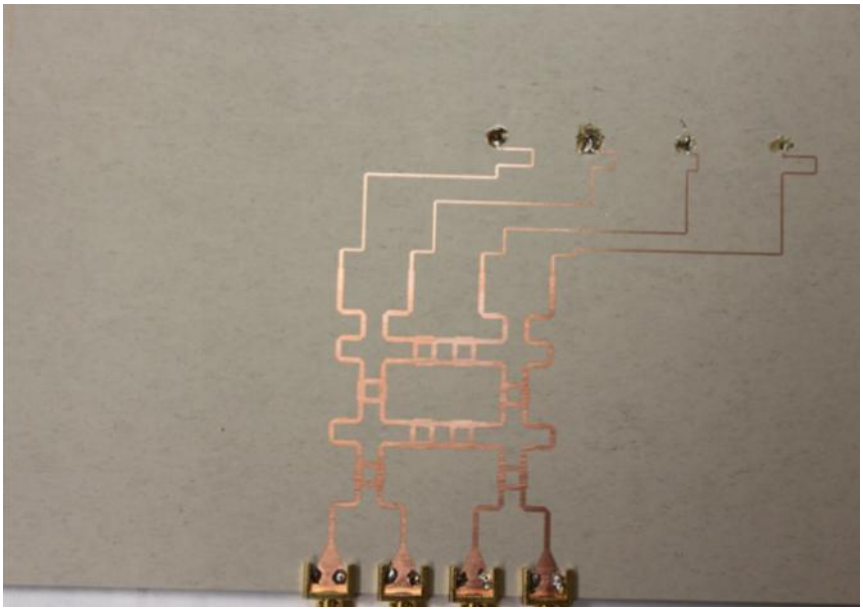

(b)

Fig. 48. Continued.

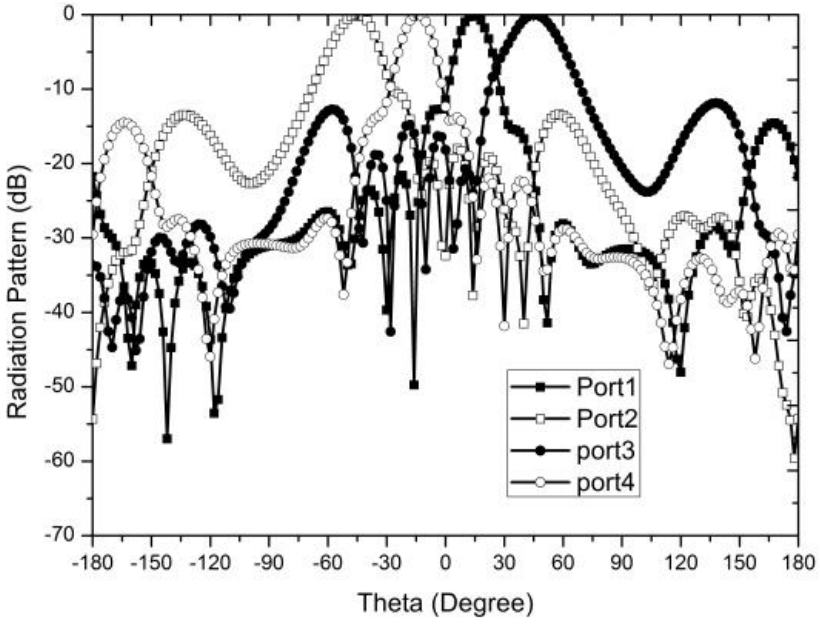

Fig. 49. Normalized radiation patterns of the switched beam antenna array.

Fig. 48 shows the photograph of the proposed 4 x 8 Butler matrix on a DSPSL and a DSPSL with the inserted ground plane. Fig. 49 shows the measured normalized radiation pattern. The SLLs of each beam are lower than -12.5 dB. In particular, the SLLs of port 1 and port 4 are lower than -18.2 dB. The boresight angles of the four beams are 14^{o}, -46^{o}, 46^{o}, and -14^{o}, respectively. The measured gain of the switched beam system is 13.5 dBi for port 1 & port 4 and 12.8 dBi for port 2 & port 3.

4.5 Conclusions

A design of a switched beam antenna array based on a DSPSL and a DSPSL with the inserted ground plane with a 4 x 8 Butler matrix is designed and manufactured. To increase the number of output port, the power dividers are used between a 4 x 4 Butler matrix and a microstrip antenna array. The proposed switched beam antenna array achieves a low sidelobe level with a high gain. This design structure is relatively simple and small compared to an 8 x 8 Butler matrix that is composed of two Butler matrixes. Experimental results show that a SLL of each switched beam is lower than -12.5 dB at all four beam directions.

CHAPTER V

BROADBAND CIRCULARLY POLARIZED APERTURE-COUPLED MICROSTRIP ANTENNA WITH DUAL-OFFSET FEEDLINES*

5.1 Introduction

With rapid growth of satellite and mobile communication systems, wideband circularly polarized (CP) antennas have been developed due to the flexibility of the oriented angle of transmitters and receivers. Although microstrip antennas have many advantages of low profile, low coast, easy fabrication, and conformability, they have the narrow impedance and the 3 dB axial ratio (AR) bandwidth [73, 74]. Therefore, the impedance and AR bandwidth have been the essential parts of a CP microstrip antenna. To obtain a wider axial ratio bandwidth, several different methods have been presented such as proximity-coupled L-probe feeding method [75-77], coaxial feeding method [78, 79], aperture-coupled feeding method [80]. The impedance and axial ratio bandwidths of 38% are obtained by L-probe feed method with broadband feed network using Wilkinson power divider. In [79], a stacked microstrip antenna with C-type feed is used to obtain a wider bandwidth and achieves a 3 dB axial ratio bandwidth of 13% and an impedance bandwidth of 21%. The aperture-coupled feeding method is an attractive

---

* Part of this chapter is reprinted with permission from J. -K. Lee, C. –H. Ahn, and K. Chang, "Broadband circularly polarized aperture-coupled microstrip antenna with dual-offset feedlines", *IEEE AP-S. International Symposium*, pp. 1127-1130, Jul. 2011, Copyright 2011 by IEEE.

feeding type due to isolation of spurious feed line radiation generating cross-polarized radiations [80]. Therefore, the aperture-coupled method is suitable to CP antenna design. It is easy to control the input impedance of aperture-coupled antenna by changing the size and the location of aperture slot. The aperture-coupled microstrip antenna with crossed coupling slot achieves the impedance bandwidth of 30% and the 3 dB axial ratio bandwidth of 12% [80].

In this chapter, the aperture-coupled stacked microstrip antennas with dual-offset feedlines are proposed. These antennas are fed by two orthogonal feedlines through cross coupling slot. In the aperture-coupled microstrip antenna, the cross-polarization can be increased because the aperture can be operated as a radiator. By using crossed coupling slot with the dual-offset feedlines, the cross-polarization levels produced by single-offset feedline can be decreased [81]. To obtain the circular polarization, the Wilkinson power divider and the branch-line coupler are used as the feed network [75, 80]. In these type couplers, it is difficult to obtain the broad bandwidth of phase and magnitude response. In this work, a multi-section slot-coupled quadrature hybrid is used to drive the crossed coupling slot for the broad bandwidth response. This directional coupler can obtain tight couplings such as 3 dB and is suitable to the broadband applications [82].

5.2 Design of the broadband feed network

Broadband quadrature hybrids are one of the important passive components of microwave circuits. These directional couplers are widely used in the microwave

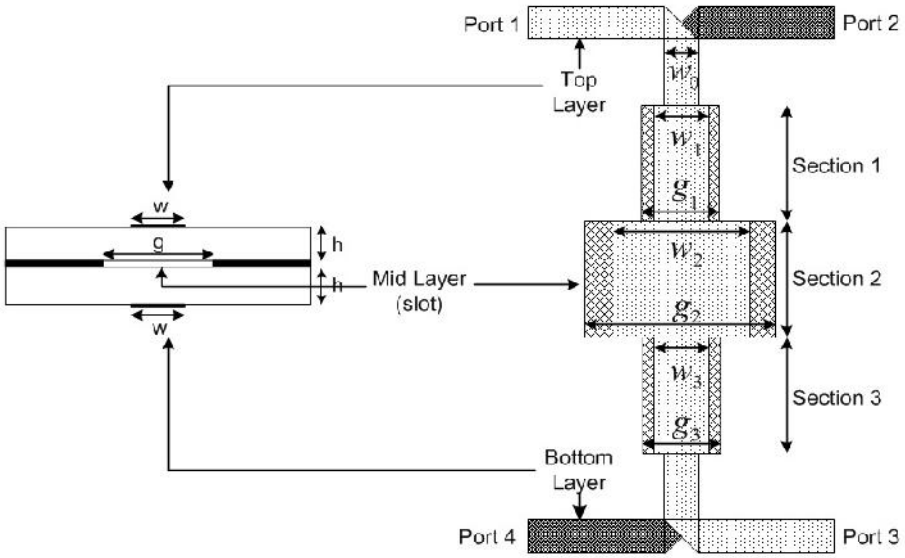

Fig. 50. Cross-section and top view of the slot-coupled coupler.

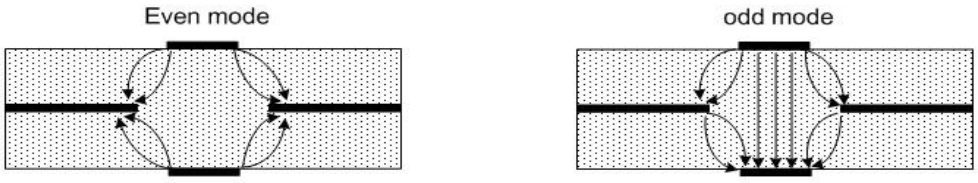

(a) (b)

Fig. 51. Electric field distribution of (a) even mode and (b) odd mode.

subsystems such as balanced amplifiers, beamforming networks for antenna arrays, and mixers. An interesting structure of the broadband directional coupler is the slot-coupled directional coupler. There has been published about the slot-coupled directional coupler and slot-coupled microstrip lines [82-87]. Since the slot-coupled microstrip line has the advantages of wide bandwidth, small size, and flexible control over even and odd mode

impedances, it can be easily applied to realize the directional couplers with tight and loose coupling value [84]. This coupler can be used in the feed network to make the microstrip antenna to have CP capability. The geometry of a broadband feed network is shown in Fig. 50. The slot-coupled quadrature hybrid has the advantages of broad bandwidth, easy control of impedance, and compact size. For the circularly polarized radiation, the feed network has equal magnitudes and a 90° phase shift through the crossed coupling slot. Port 1 is input port located at top layer, port 2 is coupled port located at bottom layer, port 3 is direct port located at top layer, and port 4 is isolated port located at bottom layer. This three-section directional coupler is symmetrical and can be analyzed on the basis of the even and odd mode analysis method. The proposed coupler consists of two microstrip lines and the common ground plane with rectangular slot at the middle layer as shown in Fig. 50. Two microstrip lines of top layer and bottom layer are coupled through slot in the common ground plane. Fig. 51 shows the electric field of the even and odd mode. The even mode impedance (z_{0e}) and the odd mode impedance (z_{0o}) of each section can be calculated by quasi-TEM wave analysis. The design equation of TEM mode directional coupler can be used. The characteristic impedance and the coupling coefficient are given below [44]:

$$z_0 = \sqrt{z_{0e} z_{0o}} = 1 \tag{31}$$

$$C = \frac{z_{0e} - z_{0o}}{z_{0e} - z_{0o}} \tag{32}$$

The substrate materials used in this coupler are Roger RT/duroid 5880 with ε_r=2.2 and h=0.254 mm. The even mode impedance of each section can be found in [83]. For 0.15 dB ripple symmetrical -3.01 dB coupler, z_{0e1} and z_{0e3} are equal to 1.19 Ω and z_{0e2} is equal to 3.34 Ω. From Eq. (31) and (32), odd mode impedance and coupling coefficient

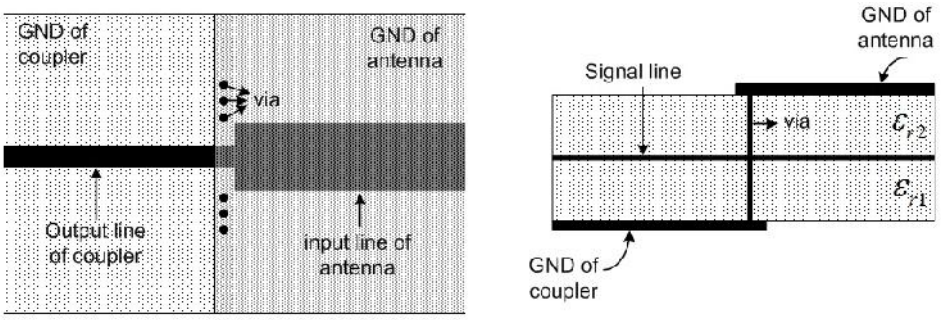

Fig. 52. (a) Top view and (b) cross view of the transition between two signal lines.

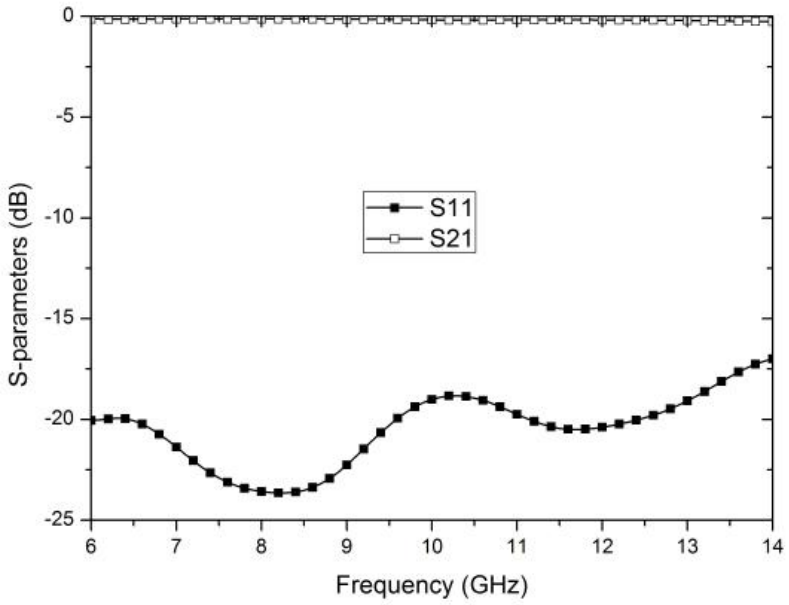

Fig. 53. Transition between the output line of coupler and the input line of antenna.

(C) can be calculated (z_{0o1}=z_{0o3}=0.84 Ω, z_{0o2}=0.3 Ω, c_1=c_3=0.173, and c_2=0.835). From the above values, the width of microstrip line (w) and slot (g) can be obtained. By using the odd mode impedance, the width of microstrip line can be easily obtained from microstrip line formulas (w_2=3.51 mm and $w_{1,3}$=1 mm). The length of three sections is about quarter-wavelength of even and odd mode impedance at center frequency (f_0=10 GHz). By using Ansoft HFSS v12, the slot widths (g) in the middle layer are evaluated from the even mode impedance and coupling coefficient (g_2=6 mm and $g_{1,3}$=0.8 mm). After tuning several parameters, the final dimensions of the coupler are w_0=0.78 mm, w_2=3.38 mm, g_2=5.8 mm, $w_{1,3}$=0.94 mm, $g_{1,3}$=0.75 mm, and the length of each section=3.75 mm.

The common ground of the coupler and the ground of antennas are located at different layer. As shown in Fig. 52, two grounds are connected by via. Fig. 53 shows the simulated S-parameters of the transition between the output line of the directional coupler and the input line of an antenna. The return loss is greater than -18 dB and the insertion loss is less than -0.2 dB from 6 GHz to 14 GHz as shown in Fig. 53. In consideration of this transition, the simulated S-parameter responses of the proposed directional coupler are achieved by Ansoft HFSS v12 as shown in Fig. 54 and Fig. 55. In Fig. 54, it is observed that S_{11} and S_{41} are greater than -14.5 dB and the range of S_{21} and S_{31} are -3.18 dB to -3.68 dB over X frequency band. The maximum imbalance of the insertion loss is ±0.18 dB at 12 GHz. Fig. 55 shows the phase response of the output ports and the maximum phase error of the directional coupler is ±1.65°.

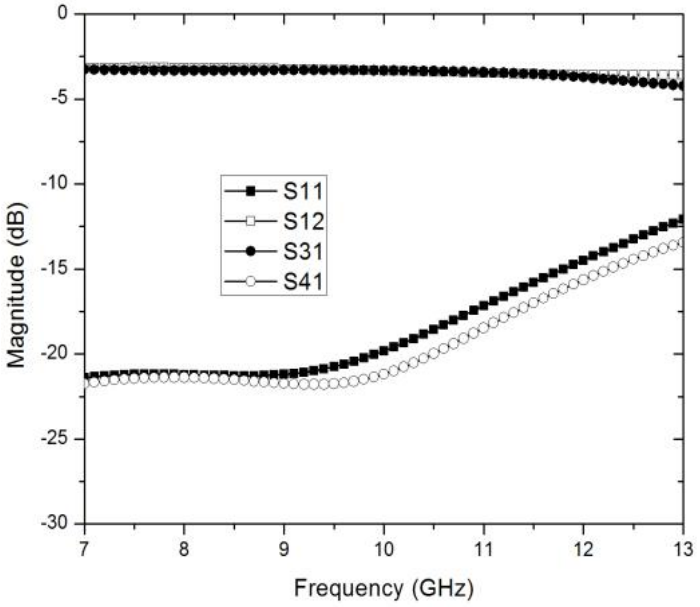

Fig. 54. Simulated magnitude responses of the slot-coupled directional coupler.

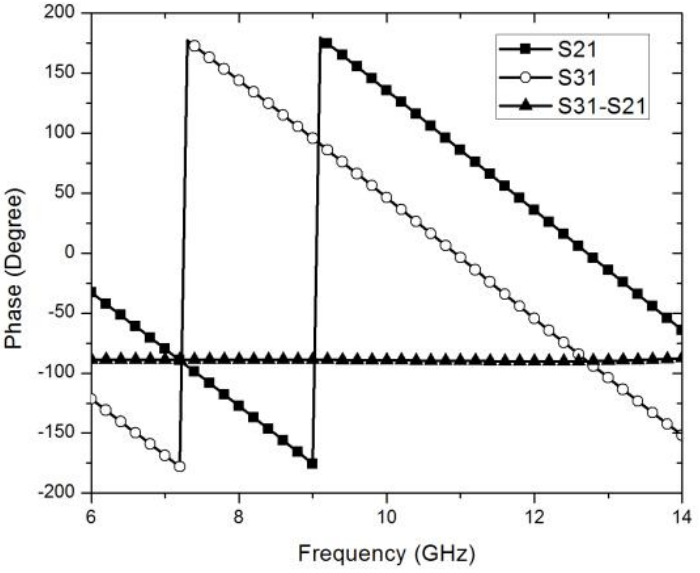

Fig. 55. Simulated phase responses of the slot-coupled directional coupler.

5.3 Design of the aperture coupled microstrip antenna

The configuration of the proposed dual-fed antenna is shown in Fig. 56. It is composed of two microstrip antennas, ground plane with a crossed coupling slot, two foam layers, and two feed lines. Two feed lines with dual-offset feedlines are located at different layers. For circularly polarization, the square patch antennas are used and two feed lines must have the phase difference of 90°. These feed lines are connected with the output port of the quadrature hybrid which is mentioned in previous section. Two square antennas are fed through crossed coupling slot and feed lines are located symmetrically

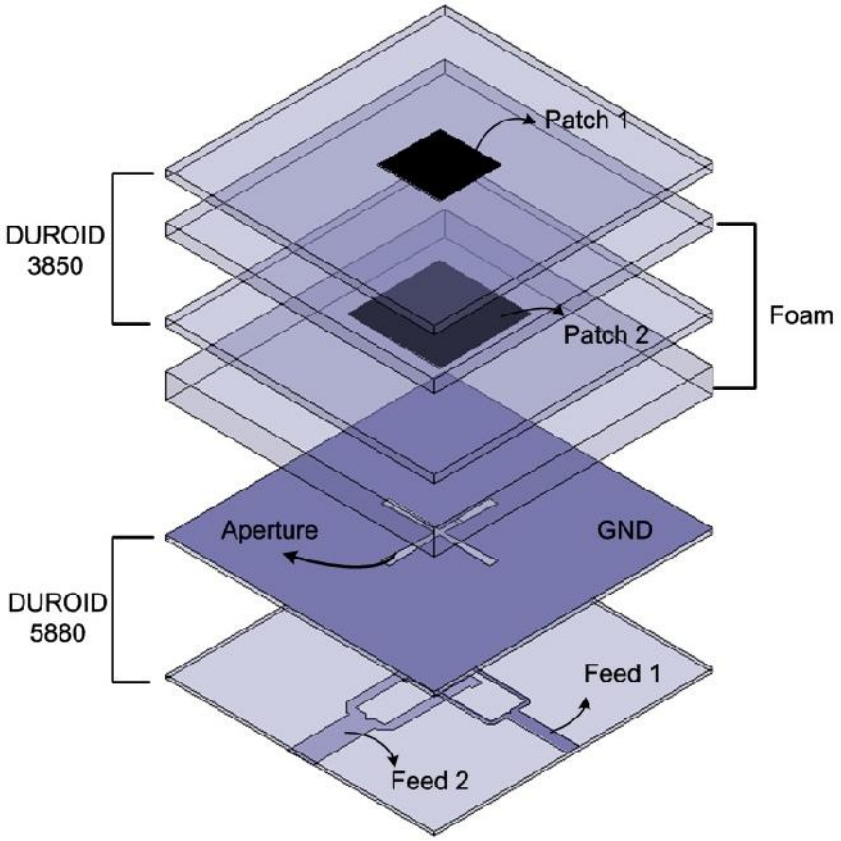

Fig. 56. Geometry of the proposed multi-layer microstrip antenna.

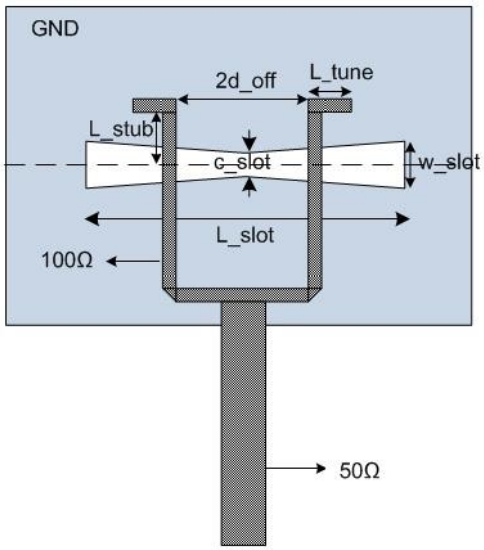

Fig. 57. Geometry of feedline and slot of the aperture-coupled microstrip antenna.

at the center of each. The aperture is located at the center of the patches. For the upper and lower patch, Rogers ULTRALAM 3850 substrate with h=0.0508 mm and ε_r=2.9 are chosen. For the aperture, Rogers RT/duroid with h=0.508 mm and ε_r=2.2 is used. The substrate materials used in two feed lines are Roger RT/duroid 5880 with ε_r=2.2 and h=0.254 mm. The relative dielectric constant of a foam is 1.06 and the heights are 1.6 and 3.2 mm. The antennas with the foam layers can have wider bandwidth. The stacked microstrip antennas consist of two square patches of slightly different resonant frequencies. Patch sizes are chosen using simple formulas. It is difficult to find the ideal value because two patches interact with each other and are affected by apertures. Fig. 57 shows slot and feedline configuration for the aperture-coupled microstrip antenna. The dimensions of the antenna are as follows: Patch 1=8.9 mm, Patch 2=10.1 mm, the 50 Ω line width of feed 1=1.56 mm, the 50 Ω line width of feed 2=3.3 mm, the 100 Ω line

width of feed 1=0.5 mm, the 100 Ω line width of feed 2=1.2 mm, c_slot=0.6 mm, w_slot=1 mm, L_slot=9.8 mm, 2d_off=5 mm, L_stub=0.8 mm, L_tune of feed 1=1.4 mm, and L_tune of feed 2=1.7 mm. Fig. 58 shows the simulated radiation patterns of the aperture- coupled microstrip antenna at 8.5 GHz, 10 GHz, and 11.5 GHz. The maximum gain of the antenna is 5.87 dBi at 8.5 GHz, 6.49 dBi at 10 GHz, and 6.98 dBi at 11.5 GHz at the boresight angle.

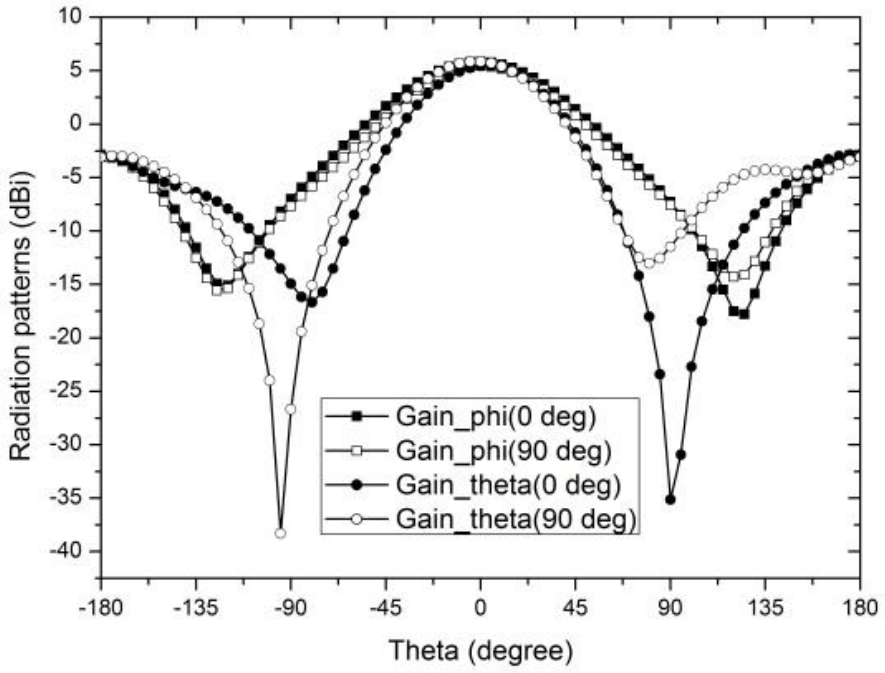

(a)

Fig. 58. Simulated radiation patterns of the microstrip stacked antenna: (a) at 8.5 GHz, (b) at 10 GHz, and (c) at 11.5 GHz.

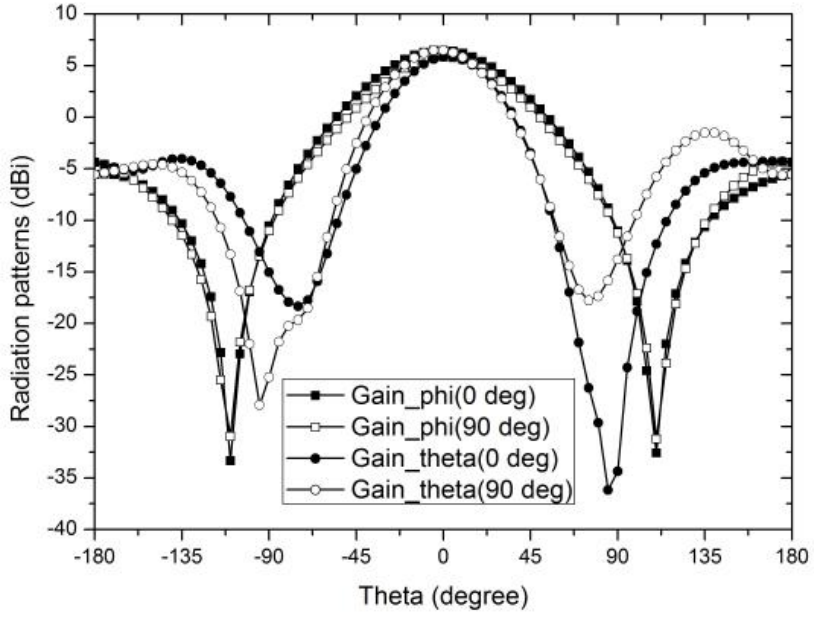

(b)

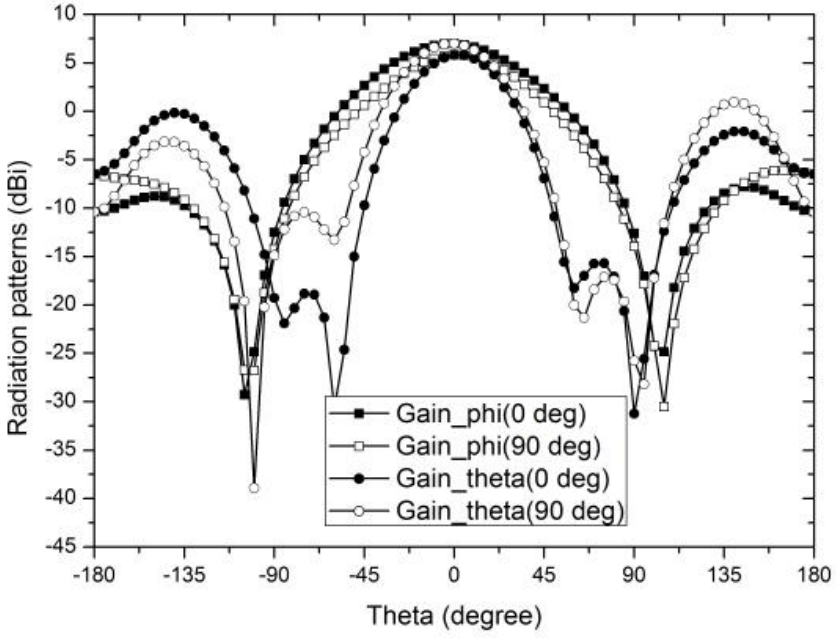

(c)

Fig. 58. Continued

5.4 Results of the broadband CP aperture-coupled microstrip antenna

Fig. 59 shows the simulated results of S-parameters and the axial ratio of the aperture-coupled microstrip antenna. The 10 dB return loss bandwidth is 35.5% (8.1 GHz to 11.6 GHz) and the isolation of two feed lines is greater than 20 dB as shown in Fig. 59 (a). As shown in Fig. 59 (b), the simulated 3 dB axial ratio bandwidth is over 40%. Fig. 60 shows the radiation patterns of the broadband CP antenna in both principle planes. The right-hand circular polarization (RHCP) gain is 8.47 dBi at 8.5 GHz, 9.17 dBi at 10 GHz and 9.13 dBi at 11.5 GHz at the boresight angle. Moreover, a 3dB gain bandwidth is over 35%. The gain difference between left-hand circular polarization (LHCP) and RHCP is greater than 23 dB at frequency bands at the broadside direction. The simulation results are based on Ansoft HFSS v12.

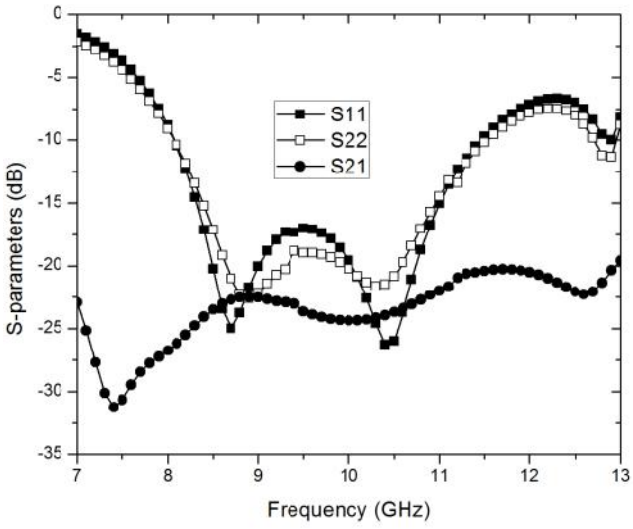

(a)

Fig. 59. Performance of the broadband CP microstrip antenna: (a) S-parameters and (b) axial ratio.

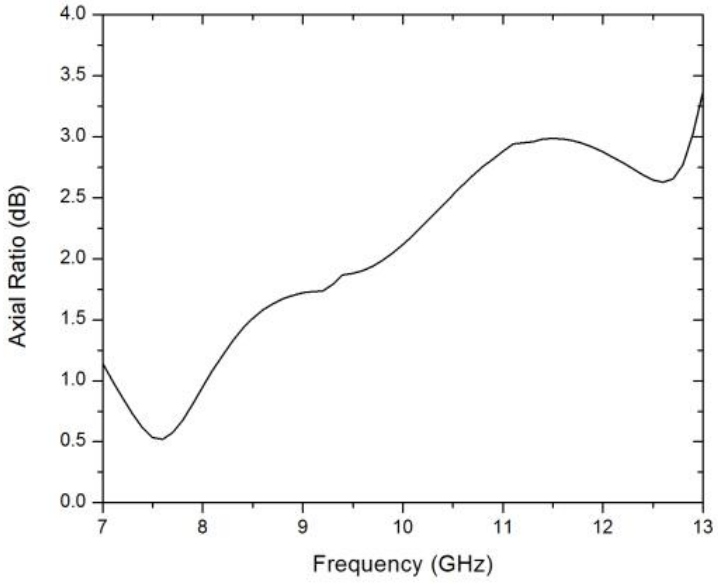

(b)

Fig. 59. Continued.

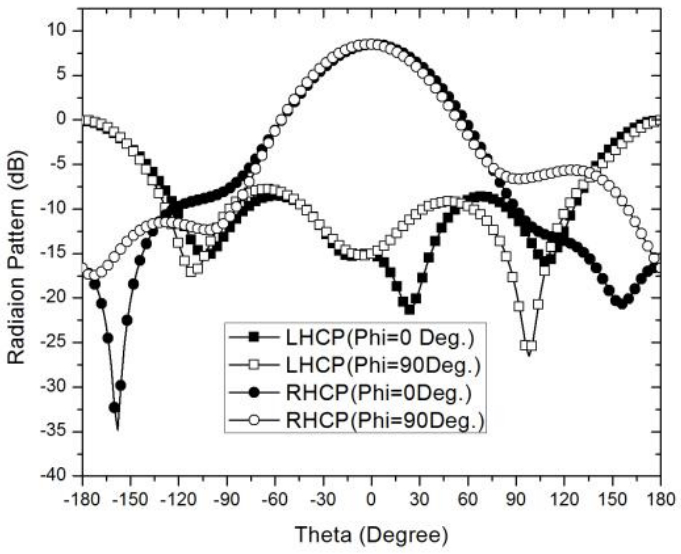

(a)

Fig. 60. Radiation pattern of the broadband CP antenna at (a) 8.5 GHz, (b) 10 GHz, and (c) 11.5 GHz.

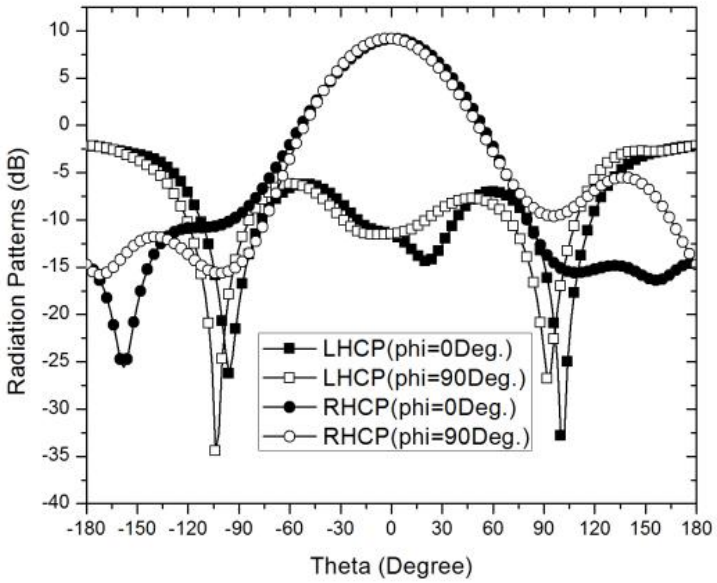

(b)

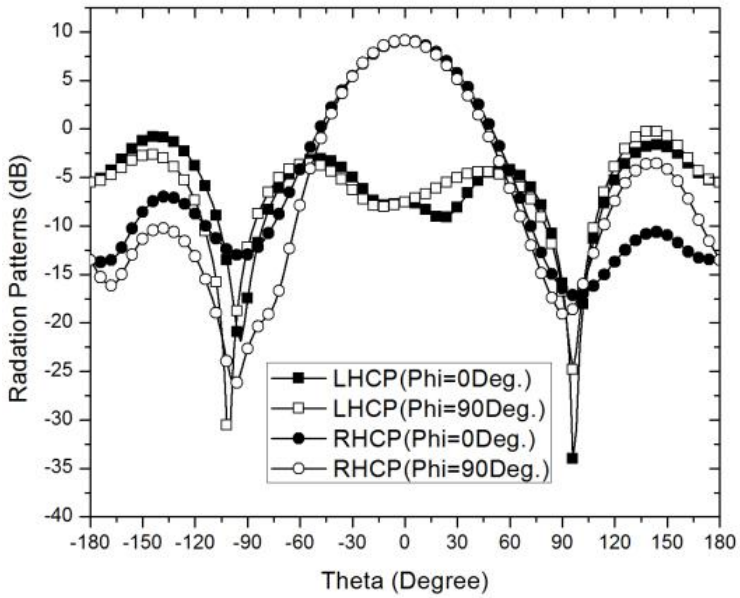

(c)

Fig. 60. Continued.

5.5 Conclusions

In this work, we propose a broadband circularly polarized aperture-coupled microstrip antenna. Crossed coupling slots with dual-feedlines are used to feed the stacked antenna. First, a broadband slot-coupled quadrature hybrid has been presented for the CP operation and has shown good simulated results of magnitude and phase response. Then, the stacked square patches with crossed coupling slot have been presented. This proposed antenna has the 10 dB return loss bandwidth of 35.5 % and the axial ratio bandwidth of 40 %. Moreover, the antenna has a good gain bandwidth over all frequency bands.

CHAPTER VI

SIX-BAND MICROSTRIP REFLECTARRAY ON TWO LAYERS*

6.1 Introduction to multiband reflectarray

A reflectarray is a flat, light-weight, and high gain antenna and often replaces the conventional parabolic reflectors. The main concept of a reflectarray is to make the reflected wave from elements cophasal wave as controlling the phase of the reflected wave from its element. The microstrip reflectarray has a narrow bandwidth because of the bandwidth limits of microstrip antenna and different spatial phase delay according to different frequencies. To overcome the limitations, this work presents a multi-band microstrip reflectarray that covers six bands on two layers. The phase of reflected wave from each frequency element and coupling effects from other frequency elements are described.

The objective of this project is to study, analysis and design for the development of a multi-frequency shared-aperture reflectarray antenna for the National Oceanic and Atmosphere Administration's (NOAA) future large-aperture radiometer and imaging antenna at Medium Earth Orbit (MEO). Table 6 shows the performance goals of the multiband reflectarray. This reflectarray should support at least 6 frequency bands and

---

* Part of this chapter is reprinted with permission from S. –W. Oh, J. -K. Lee, J. Huang, and K. Chang, "A six-band reflectarray antenna", *IEEE AP-S. International Symposium*, pp. 1-4, Jun. 2009, Copyright 2009 by IEEE.

Table 6. Performance goals.

Parameter	
No. of frequency bands	Minimum of 6 to maximum of 10
Aperture size	0.75 meter (scalable to larger size)
Bandwidth	Not available (generally narrow)
Efficiency	40 %
Polarization	See Table I - 2
Peak side lobe level	-30 dB

no more than 10 frequency bands.

6.2 Configuration of reflectarray

Six more important frequency bands selected for this reflectarray are 6.625, 18.7 52.5, 57.5, 166, and 183.31 GHz. The polarization required for each frequency band is listed in Table 7.

Table 7. Frequency plan and polarization.

Frequency (GHz)	Polarization
6.625	Dual linear polarization (V and H)
18.7	Dual linear (V and H) and Dual CP (RHCP and LHCP)
52.5	Single linear (V)
57.5	Single linear (H)
166	Single linear (V)
183.31	Single linear (V)

The types of the elements selected at different frequency will have significant effects on the amount of coupling among elements and arrangements of each layer. Possible element types at each frequency band are listed in Table 8. The dual ring configuration can be used for achieving a wider phase range.

Table 8. Element types at different frequency bands.

Frequency (GHz)	Element type
6.625	Ring or cross dipole
18.7	Cross dipole
52.5	Ring with gap, dipole
57.5	Ring with gap
166	Dipole
183.31	Dipole

The reflectarray will consist of two thin substrate layers and two foam spacers. The substrate selected for the proposed design is Roger/flex 3850 circuit material with the thickness of 0.0508 mm. The thicknesses of the foam layers are pre-determined to be 0.6 mm and 1 mm for the top and bottom layer respectively after optimized simulations. Each substrate layer will accommodate three frequency bands as shown in Fig. 61. Element spacing for each frequency band will be determined later with considerations of the coupling effects, grating lobes, and limited real estate of the array.

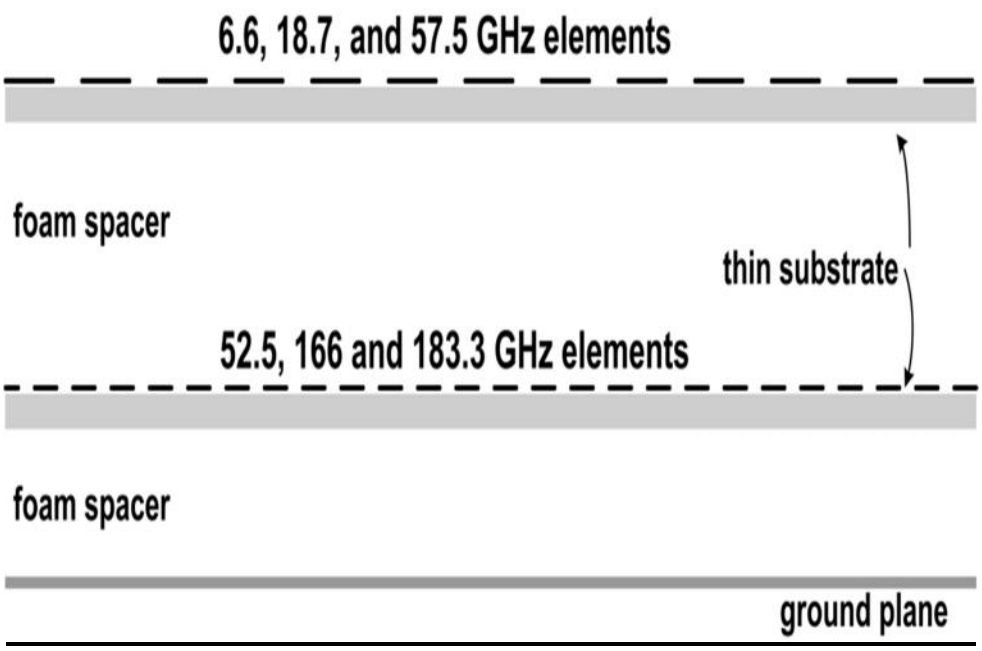

Fig. 61. Configuration of the six-band microstrip reflectarray.

6.3 Top layer element design

In order to minimize the blockage produced by the elements at the top layer, the elements at the top layer was designed to reduce the thickness and to increase the element spacing. Fig. 62 shows the arrangement of elements on the top layer. A 18.7 GHz element, the element of middle frequency band at the top layer, will be designed first and then other elements will be designed afterward.

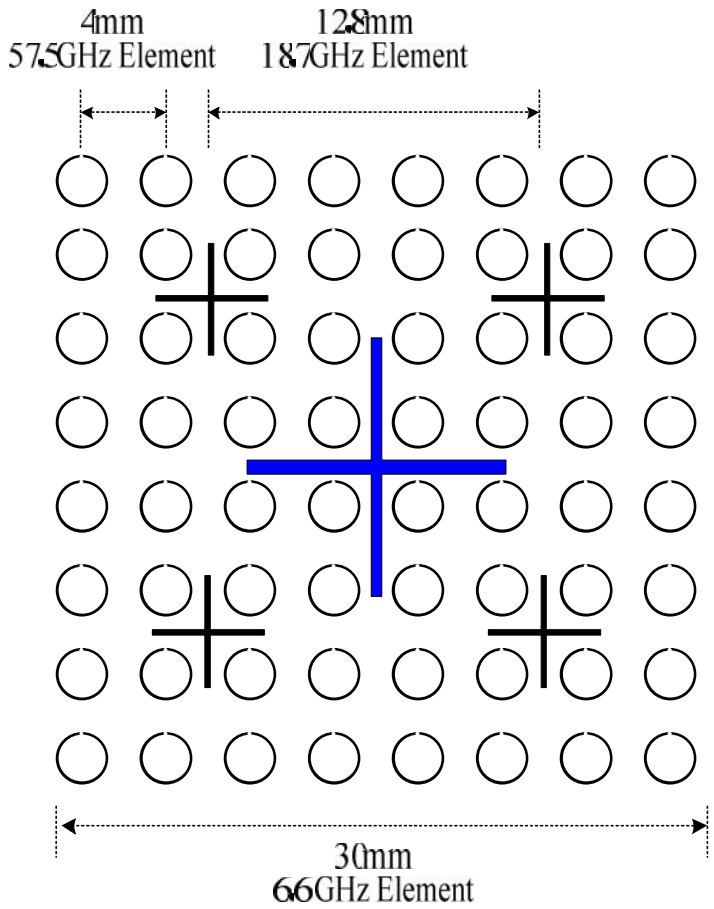

Fig. 62. Arrangement of the top layer elements.

A. 18.7 GHz element

Fig. 63 shows the simulation setup of the unit cell at 18.7 GHz. The dimensions of the unit cell are chosen to be 12.8 mm (0.8 λ_o) x 12.8 mm (0.8 λ_o) and the arm length of the cross dipole are varied for different phases of the reflected wave. Results of reflected phases versus lengths with different widths of arms are shown in Fig. 64. As can be seen from the results, the phase variation range for 0.2 mm to 1.6 mm of width can be from 327º to 286º. 0.2 mm element arm width is chosen for 18.7 GHz for reducing the blocking the bottom layer elements.

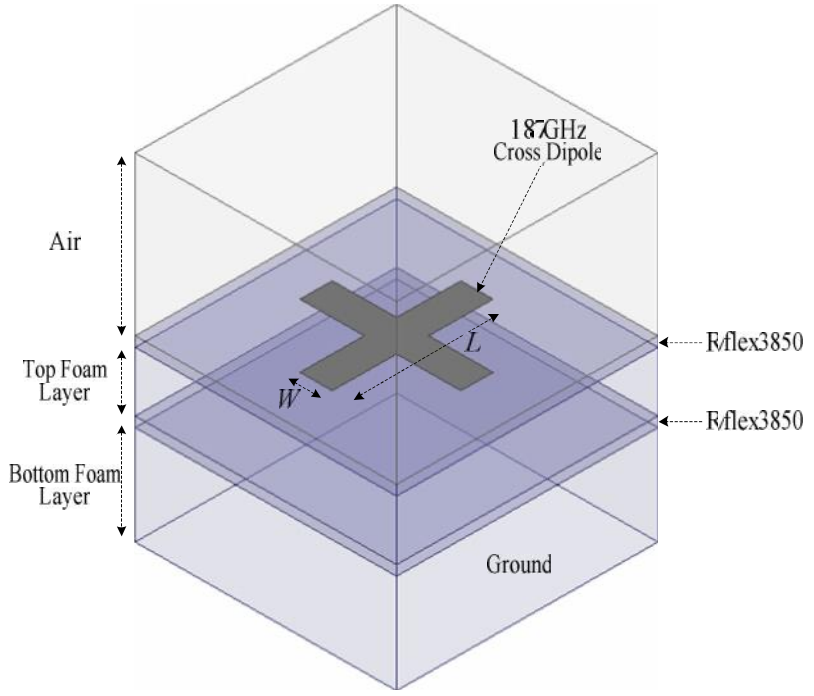

Fig. 63. Simulation setup of unit cell of the 18.7 GHz element.

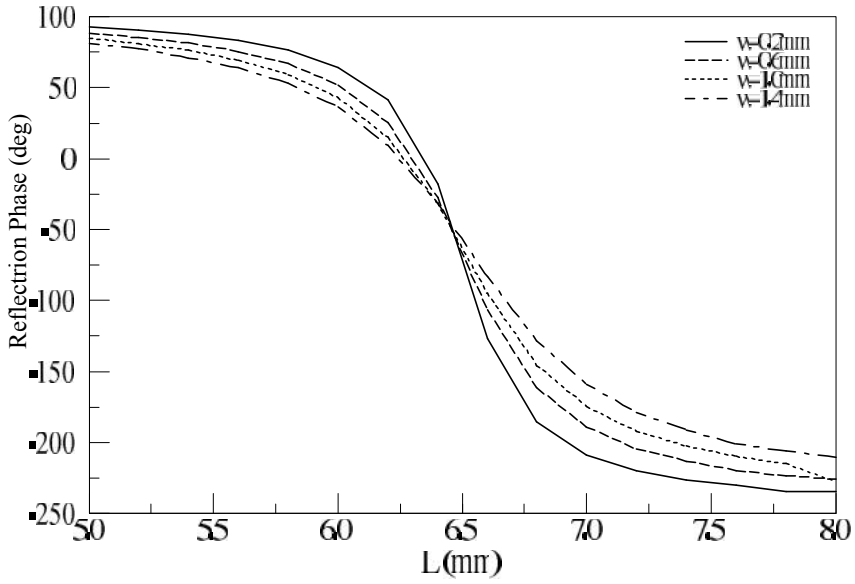

Fig. 64. Phase responses as a function of the dipole width (*w*).

B. 57.5 GHz element

The simulation setup of the 57.5 GHz is shown in Fig. 65. The dimensions of the unit cell are chosen to be 4 mm (0.77 λ_o) × 4 mm (0.77 λ_o). According to Fig. 66, the total phase variation ranges of the circular loop for different loop width (2) vary from 294º to 118º. Therefore loop width is chosen to 0.1 mm for large phase variation range and less blockage. Gap width (Gw) also is selected to 0.1 mm.

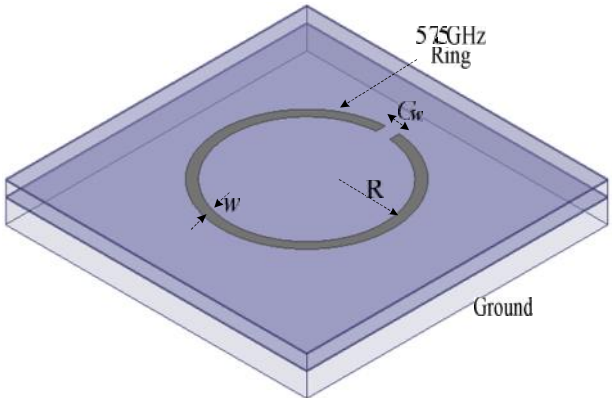

Fig. 65. Simulation setup of unit cell of the 57.5 GHz element.

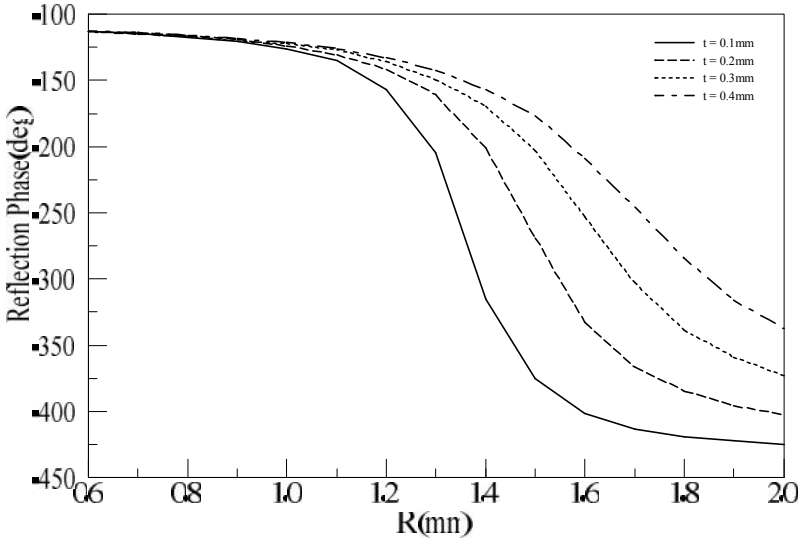

Fig. 66. Phase responses as a function of the ring width (*w*).

C. 6.6 GHz element

The dimensions of the unit cell are chosen to be 26 mm (0.79 λ_o) × 26 mm (0.79 λ_o) and the arm length of the cross dipole are varied for different phases of the reflected wave. Fig. 67 and Fig. 68 show the simulation setup of a unit cell working at 6.6 GHz and the reflected phase responses, respectively. The result indicate the width of the cross dipole does not effect on the total reflected phase range significantly, but the dipole width is chosen to 0.4 mm for fewer blockages.

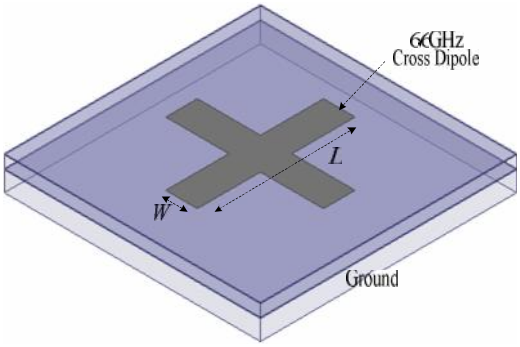

Fig. 67. Simulation setup of a unit cell of the 6.6 GHz element.

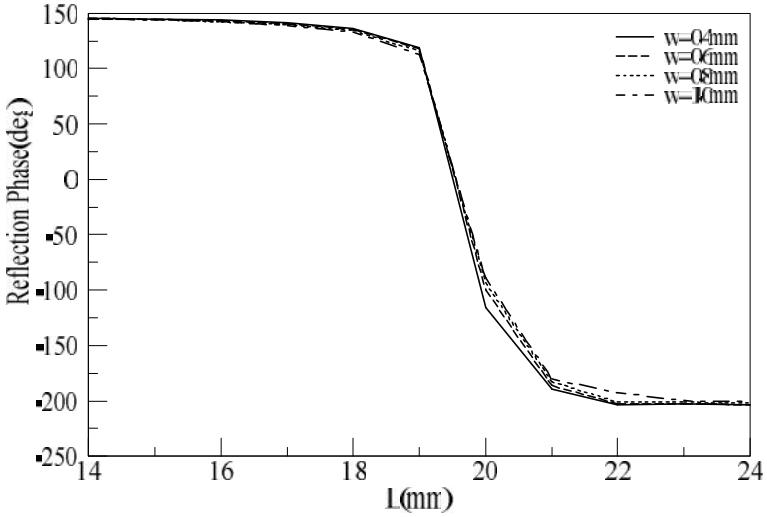

Fig. 68. Phase responses as a function of the arm width (*w*).

6.4 Bottom layer element design

The focus of the bottom layer design is on the elements of 52.5, 166, and 183 GHz. At such high frequencies, the element selection and design could be very critical. Simple element shapes, i.e. rectangular patches and dipoles, are chosen as the reflectarray elements at the high frequencies. Fig. 69 shows the arrangement of the bottom layer elements.

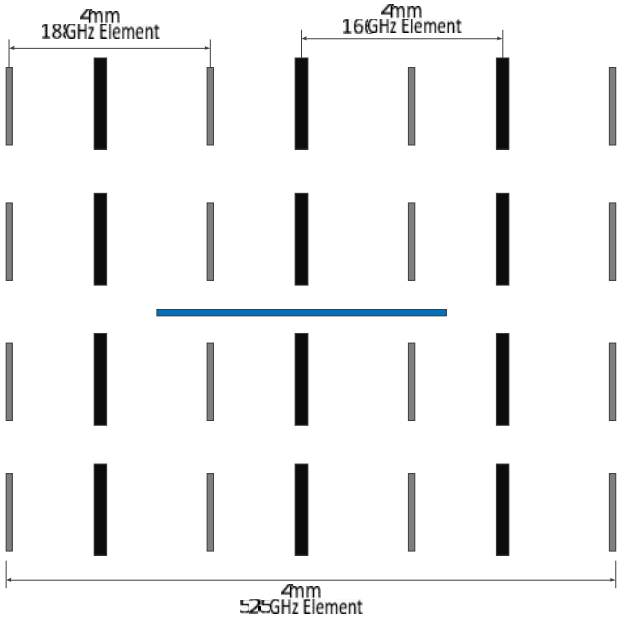

Fig. 69. Arrangement of the bottom layer elements.

A. 166 GHz element

The geometry of 166 GHz elements is shown in Fig. 70, which show the simulation setup of a unit cell. The dimensions of the unit cell are chosen to be 1.3 mm (0.72 λ_0) x 1.3 mm (0.72 λ_0) to take into account coupling with adjacent unit cell. Both the 166 and 183 GHz elements are placed in the unit cell so that the effects of one element on the other could be taken into considerations. The thickness of the copper cladding is also

considered in the simulations for better accuracy. The width of the rectangular patch is fixed at 0.22 mm and the length is varied for different phases of the reflected waves. The height of top and bottom foam layer is 0.6 mm and 1.1 mm, respectively. The phase variation range is about 315^{o} as shown in Fig. 71.

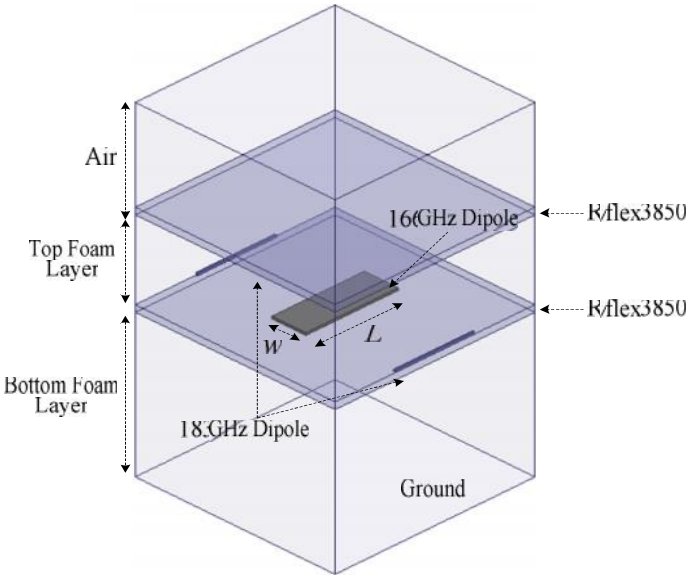

Fig. 70. Simulation setup of unit cell of the 166 GHz element.

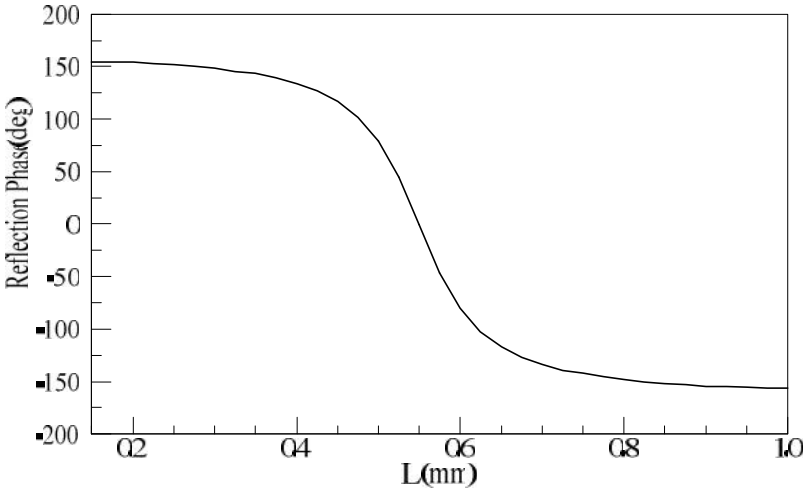

Fig. 71. Phase response as a function of the dipole length (L).

B. 183 GHz element

As what have been done in the previous simulations, the unit cell also includes the 166 GHz elements to take into account the possible mutual coupling effects in Fig. 72. The unit cell size is the same as the size at 166 GHz and the width of the dipole is 0.1 mm. As shown in Fig. 73, the phase variation range is about 320 ^{o}.

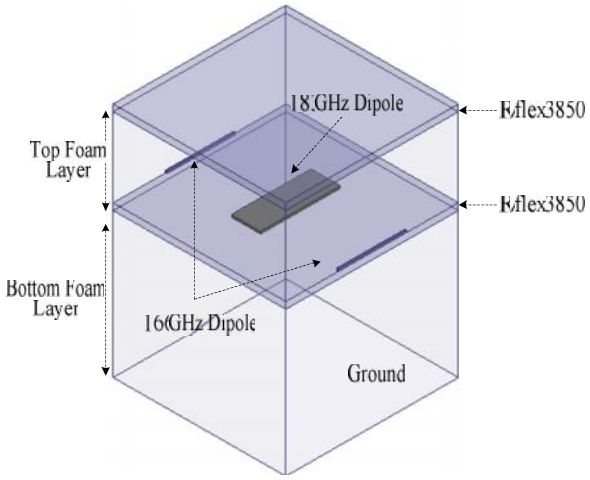

Fig. 72. Simulation setup of unit cell of the 183 GHz element.

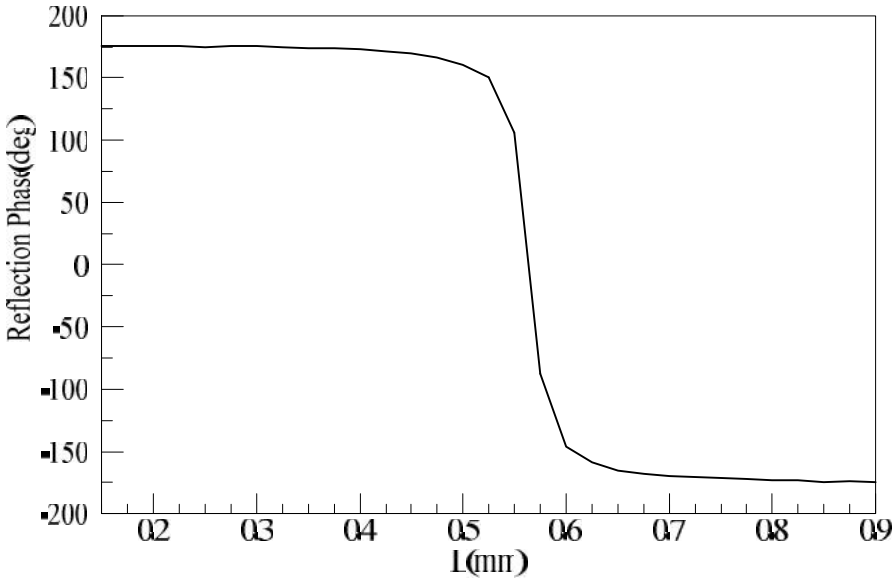

Fig. 73. Phase response as a function of the arm length (L).

C. 52.5 GHz element

Dipoles with variable lengths are used for the 166 and 183 GHz bands. The choices of the element type at the 52.5 GHz are limited by the 166 and 183 GHz elements which are located at the same layer. Dipole elements are used again for the 52.5 GHz as shown in Fig. 74, but they are oriented vertically in perpendicular to the 166 GHz and 183 GHz elements. Fig. 75 shows the phase variation range of 290° which is achieved by changing the dipole length.

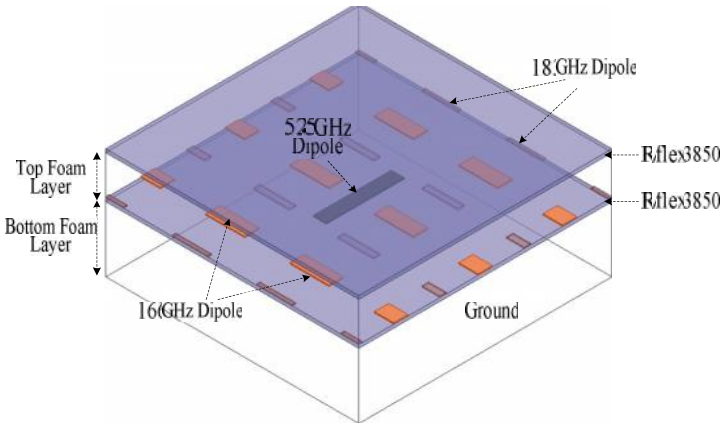

Fig. 74. Simulation setup of unit cell of the 52.5 GHz element.

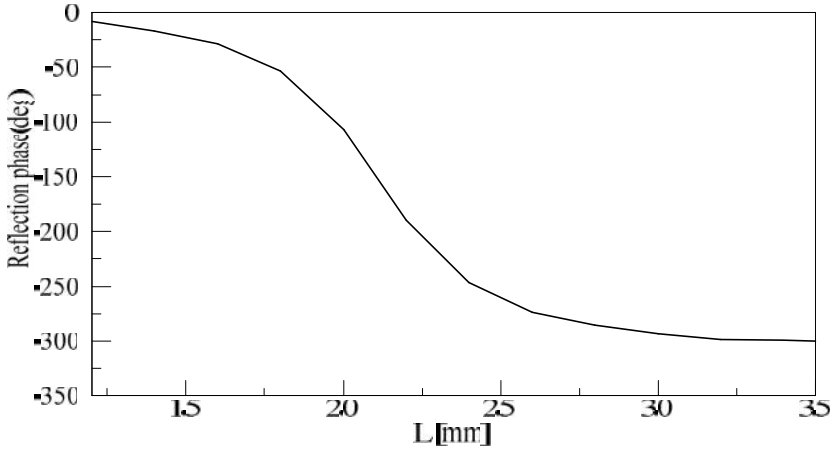

Fig. 75. Phase response as a function of the dipole length (L).

6.5 Coupling effects with neighborhood elements

In this chapter, various cases of intersections are investigated, for example, cases between elements at different frequencies band on top layer, cases between elements on bottom layer, and cases between elements on top layer and ones on bottom layer. As shown in Fig. 76 and Fig. 77, though the top and bottom elements are placed together in a unit cell of radiating elements, each element can obtain the necessary reflection phase. The reflection phases are shifted but the phase variation ranges are similar.

6.6 Conclusions

This chapter presents a reflectarray configuration which supports the operation of six frequency bands. The proposed reflectarray has two substrate layers and each layer accommodates array elements of three frequency bands. The reflection phase curves of the array elements of different frequency bands are simulated and summarized in Table 9. Interactions among the elements are also explored. Detailed results of the reflection phase curves in different situations have been presented in this chapter. Based on the high accuracy of the simulation software, these results are believed to be reliable and are ready for real implementation of the reflectarray.

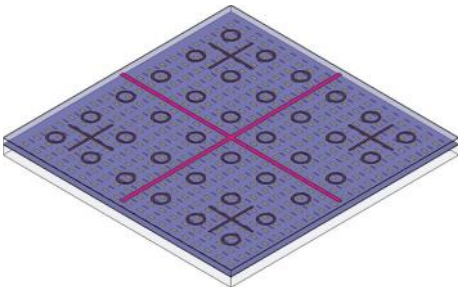

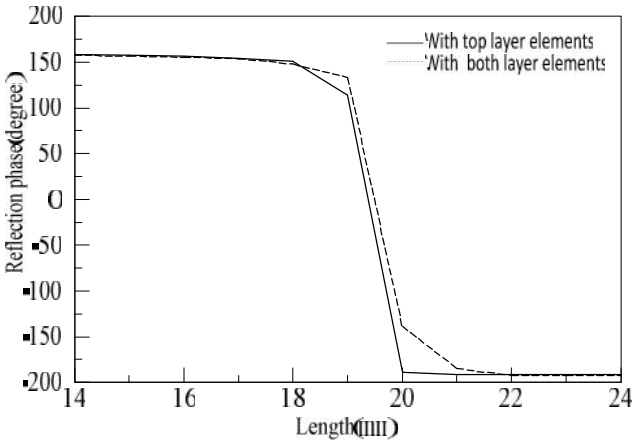

(a)

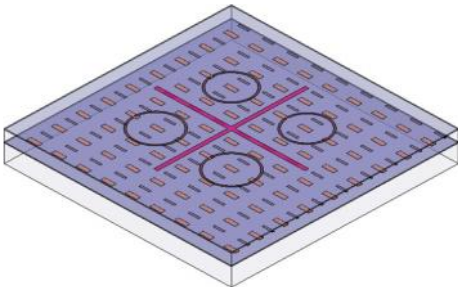

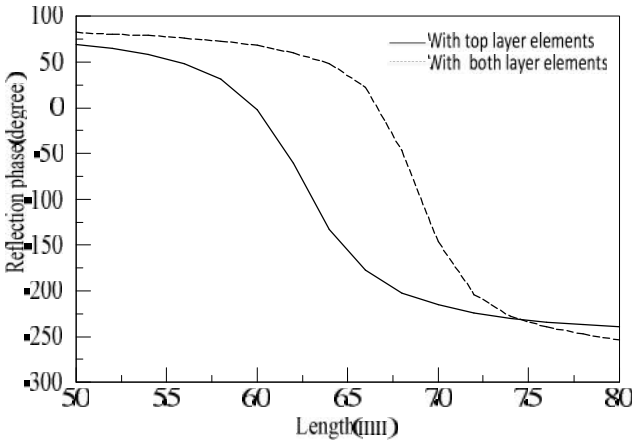

(b)

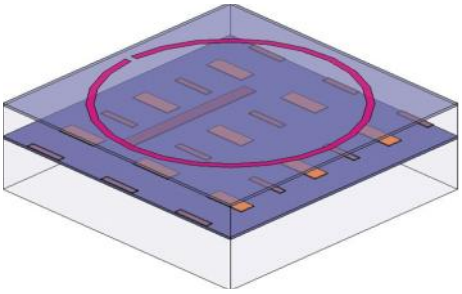

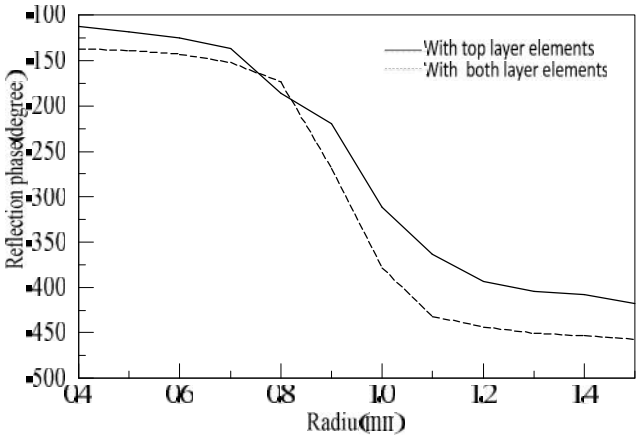

(c)

Fig. 76. Coupling effects on the elements on top layer: (a) 6.6 GHz, (b) 18.7 GHz, and (c) 57.5 GHz.

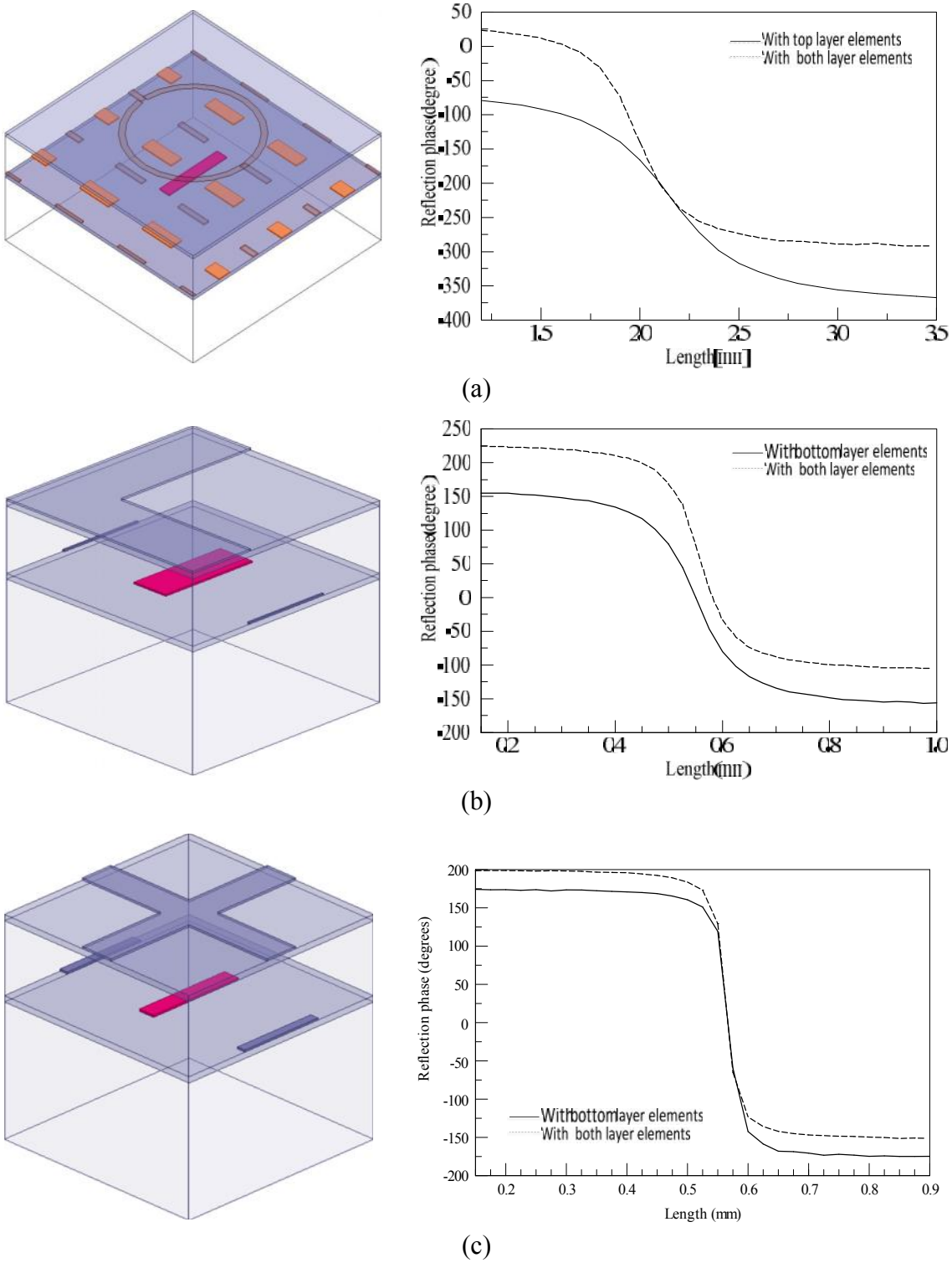

Fig. 77. Coupling effects on the elements on bottom layer: (a) 52.5 GHz, (b) 166 GHz, and (c) 183 GHz.

Table 9. Design parameters of the reflectarray elements.

Top layer				
Freq.	Shape	Element description	Element spacing	Single element achievable reflection phase range
6.6 GHz	Cross dipole	Equal arm length Width: .0.4mm	0.79 λo	355°
18.3 GHz	Cross dipole	Equal arm length Width: 0.2mm	0.80 λo	327°
57.5 GHz	Circular ring with gap	Width: 0.1mm Gap: 0.1mm	0.77 λo	295°
Bottom layer				
Freq.	Shape	Element description	Element spacing	Single element achievable reflection phase range
52.5 GHz	Horizontal Dipole	Width: 0.2mm	0.68 λo	290°
166 GHz	Vertical Dipole	Width: 0.22mm	0.72 λo	315°
183 GHz	Vertical dipole	Width: 0.1mm	0.79 λo	320°

CHAPTER VII

DUAL-BAND BRANCH-LINE COUPLER USING DSPSL

7.1 Introduction

With the rapid growth of wireless communications, many microwave circuits are developed using microstrip line, coplanar waveguide, slotline, coplanar strips, and double-sided parallel-strip line (DSPSL). As mention in chapter IV, DSPSL is proposed by H. A. Wheeler in 1964 [70] and is simply analyzed by using the uniform current approximation by J. M. Rochelle [88]. Recently, various interesting passive components using DSPSL have been developed such as power divider, diplexer, filters and branch line coupler [89]. Moreover, DSPSL can be used for design of differential Monolithic Microwave Integrated Circuits (MMIC) technology for low cost implementation [89].

The branch line coupler is one of the most fundamental and popular circuits in microwave applications. In the modern wireless systems, multiple frequency band performance has been demanded. Dual-band branch line couplers using cross coupled line, short and open stubs, and two branch lines have been published. In this chapter, a dual-band branch line coupler using DSPSL is proposed. By using this transmission line, high impedance lines can be easily realized. The proposed circuit has three branch lines and the lengths of the horizontal line and vertical line are different for the dual-band applications.

7.2 Analysis of DSPSL and offset DSPSL

Fig. 78 shows double-sided parallel-strip line and offset double-sided parallel-strip Line. DSPSL transmission line is a balanced line and offset DSPSL is separated by distance (d) between top and bottom lines as shown in Fig. 78. The effective dielectric constant of DSPSL is the same as that of the microstrip line (MSL) and the wavelength is shorter than that of microstrip line [15]. The impedances of a DSPSL and offset DSPSL versus the width (w) and offset distance (d) with the same width are extracted by Zeland IE3D and are shown in Fig. 79 and Fig. 80. These characteristic impedances are calculated by using the substrate with ε_r = 10.2 and h=0.635 mm. As shown in Fig. 79, the characteristic impedance of DSPSL is higher than that of microstrip line with the same width. Similarly, the characteristic impedance of offset DSPSL can be increased by increasing offset distance (d) of top and bottom lines as shown in Fig. 80. It can be seen that the wider the offset distance is, the weaker the coupling between top and bottom strip lines is [90].

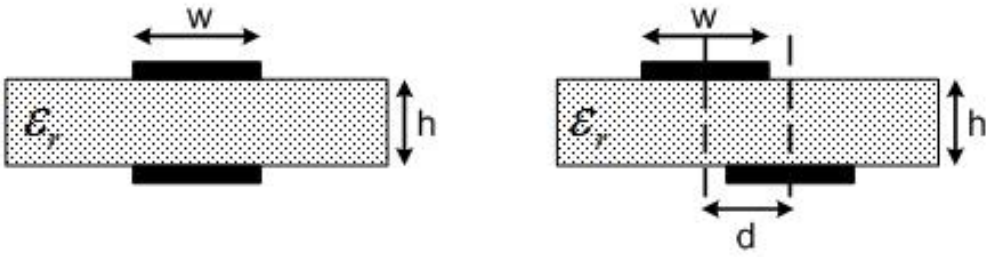

(a) (b)

Fig. 78. Cross section view of (a) the conventional DSPSL and (b) offset DSPSL.

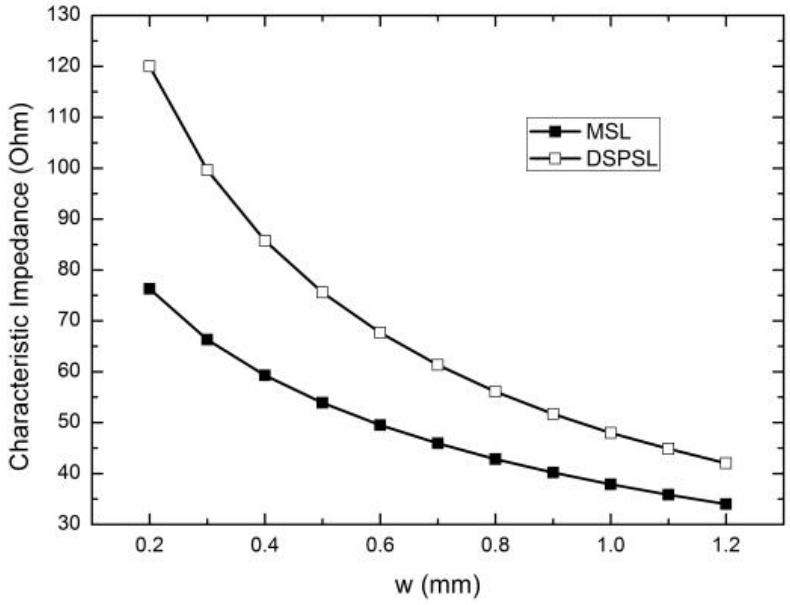

Fig. 79. Characteristic impedances of the microstrip line and DSPSL.

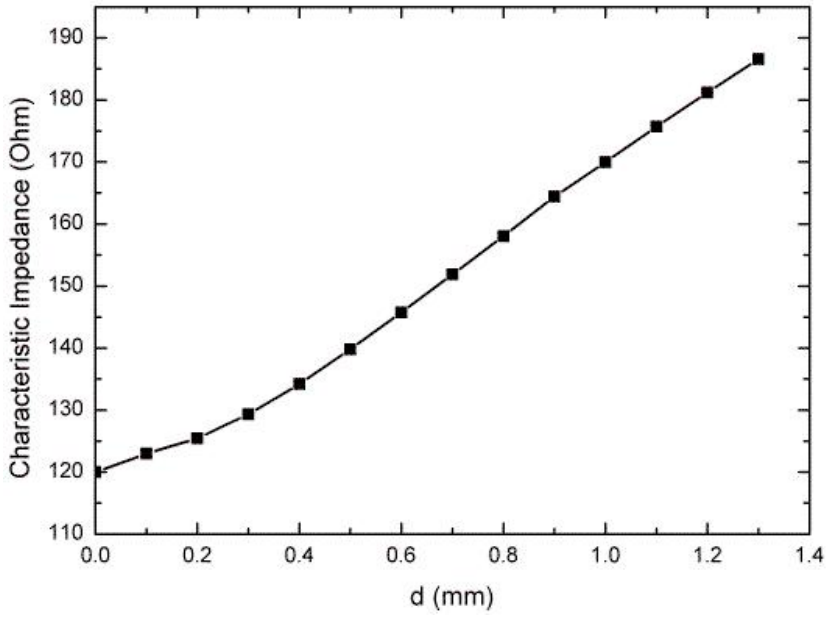

Fig. 80. Characteristic impedances of an offset DSPSL (w=0.2 mm).

7.3 Analysis of dual-band branch-line coupler

The even and odd mode decomposition method can be used for a symmetrical four port network analysis. Fig. 3 and Fig. 4 show the schematic diagram and even and odd mode equivalent circuits of the proposed directional coupler. The electrical length of the conventional branch line coupler is a quarter-wavelength long. In this case, the multiple quarter wavelengths of vertical and horizontal branches are used for the dual-band coupler at the center frequency (f_o) of the two operating frequencies (f_1, f_2). As shown in Fig. 4, these cascaded lines and stubs can be analyzed by the ABCD matrix method.

In the four port coupler, the following amplitude and phase conditions should be satisfied: $|S_{21}| = |S_{31}|$, $|S_{41}| = 0$, and $\angle S_{21} - \angle S_{31} = \pm 90^\circ$. We need to find θ, Z_1, Z_2, and Z_3 that satisfy the above conditions at the frequencies f_1 and f_2. For simplification, it is assumed that the vertical lengths of three branches are the same ($\theta_2 = \theta_3$) and we choose $\theta_1 = m\pi/2$ and $\theta_2 = n\pi/2$ where n and m are positive integers. The magnitudes of S parameter can be solved numerically to find the value of Z_1, Z_2, and Z_3 using Eq. (1)-(8). Fig. 81 shows the normalized impedance Z_1, Z_2, and Z_3 versus the fractional bandwidth (($f_2 - f_1$)/($f_2 + f_1$)).

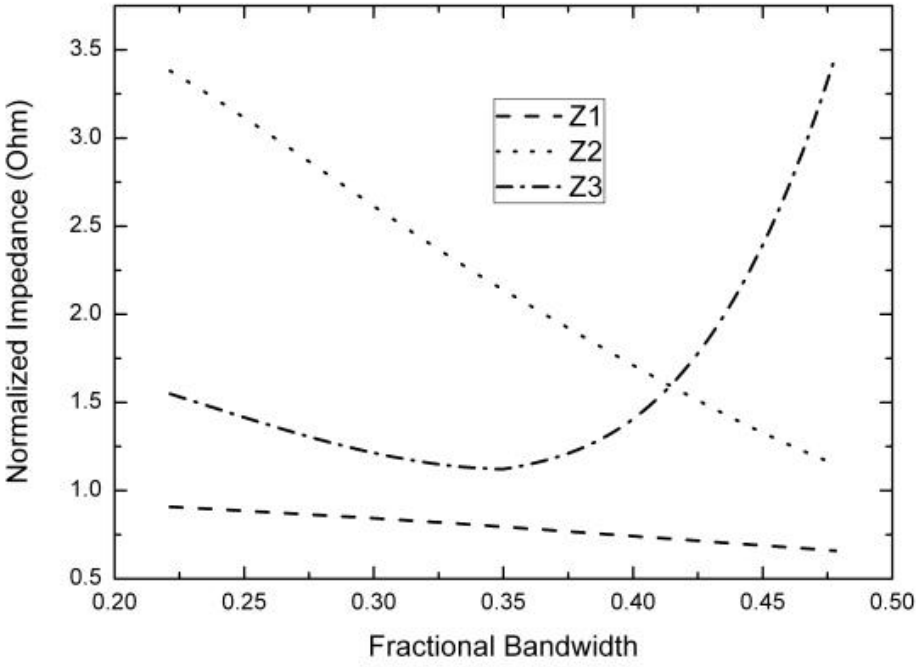

Fig. 81. Normalized impedances versus the fractional bandwidth (δ).

7.4 Design of dual-band branch-line coupler

Conventionally, the range of characteristic impedances on a microstrip line could be limited by technological constraint. However, as DSPSL and offset DSPSL are used, the limit can be reducible. For examples, a dual-band coupler is considered to operate at f_1=3 GHz and f_2=5.7 GHz on a substrate with the dielectric constant 10.2 and the thickness 0.635 mm. The center frequency (f_o) is 4.35 GHz and the fractional bandwidth (δ) is 0.31. The line impedance for this coupler can be found from Fig. 81: Z_1 =42 Ω, Z_2 =125 Ω, and Z_3=57 Ω. The widths of line impedance Z_1 and Z_3 can be obtained using Fig. 79: 1.2 mm and 0.82 mm. The width of line impedance Z_2 can be obtained using

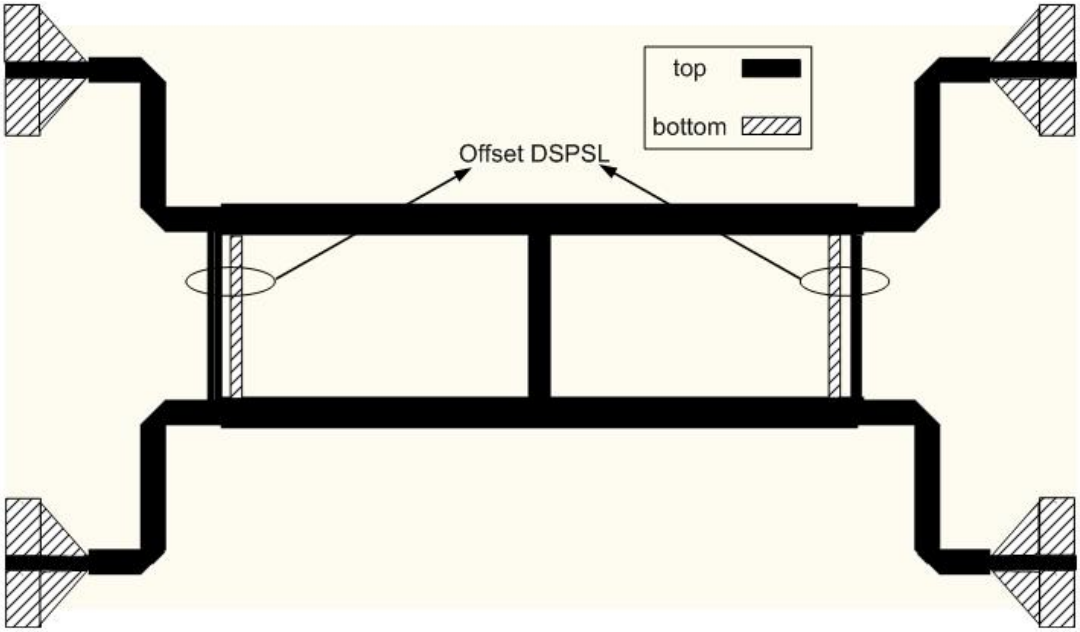

Fig. 82. Layout of the proposed dual-band branch-line coupler on DSPSL.

Fig. 80: 0.2 mm with a 0.3 mm offset distance (d). The physical dimensions of each line length with m=2 and n=1 are θ_1 = 12.3 mm and θ_2= 6.2 mm at the center frequency. Fig. 82 shows a layout of the proposed dual-band branch-line coupler.

The measurements are accomplished by using an Agilent 8510C vector network analyzer. The proposed dual-band coupler is designed based on the above results. As shown in Fig. 83 (a), the measured S_{21} and S_{31} at two output ports are about -3.35 dB at 3 GHz and -3.65 dB at 5.77 GHz. The return loss (S_{11}) and the isolation (S_{41}) are better than -19 dB at 3 GHz and -16 dB at 5.77 GHz. Fig. 83 (b) shows the phase difference of output ports ($\angle S_{21}$ and $\angle S_{31}$). The output phase difference ($\angle S_{21} - \angle S_{31}$) is 89.5^o at 3 GHz and 89.2^o at 5.77 GHz which are very closed to the desired value of 90^o.

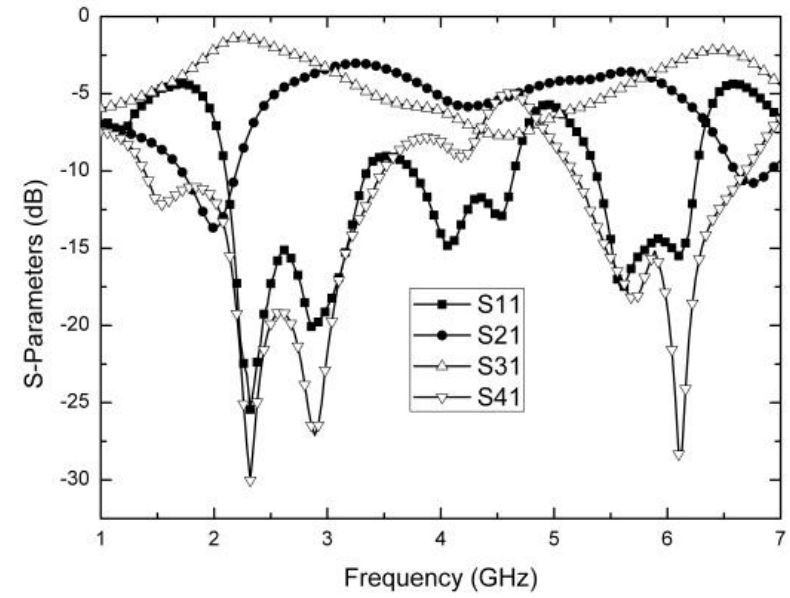

(a)

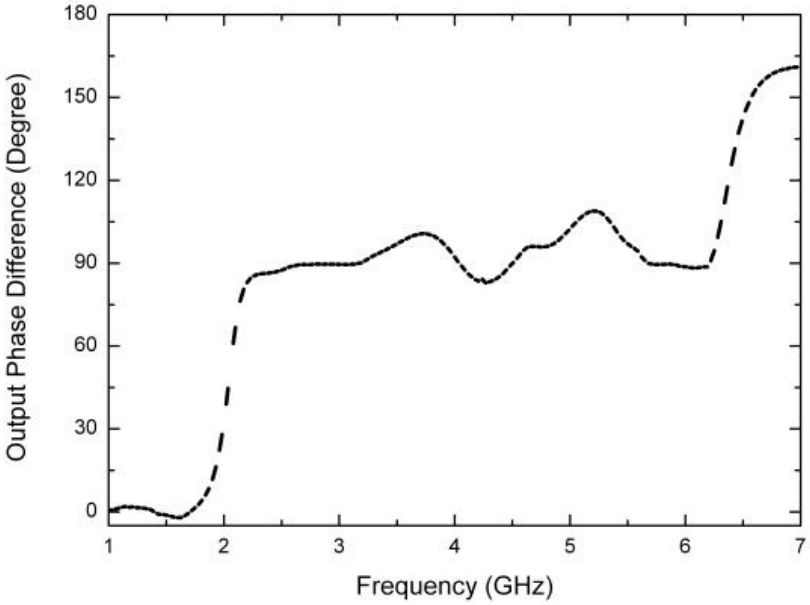

(b)

Fig. 83. Measured results of the proposed dual-band coupler: (a) magnitude and (b) phase difference between the output ports.

7.5 Conclusions

In this chapter, a dual-band branch line coupler using double-sided parallel-strip line is proposed and verified. The proposed coupler can work at two arbitrary design frequencies. The insertion losses at both frequency bands are a little higher than that of other dual-band branch line couplers. We believe that it is due to the transition loss between microstrip lines and double-sided parallel-strip lines. The results of the return loss, isolation, and phase difference are reasonable. By using DSPSL, the proposed circuit may be applied to coupler design with both small and large separated frequency bands.

CHAPTER VIII

SUMMARY AND CONCLUSIONS

8.1 Summary

As an alternative of a parabolic reflect antenna, the microstrip reflectarray has recently being investigated for high-gain applications because of low profile, light weight, and small masses. However, the microstrip reflectarray suffers from narrow bandwidth caused by its inherited limit and differential spatial phase delay. To improve the bandwidth and obtain the beam scanning capability, multi-band reflectarray and beam switching reflectarray was proposed.

In this dissertation, an offset cylindrical reflectarray fed by linear polarized phased array has been developed. The electrically beam scanning microstrip reflectarray has been designed and fabricated. The microstrip reflectarray is fed by a phased array antenna with the 4 x 4 Butler matrix. The feed antenna has the boresight angles of four beams at 16^{o}, -32^{o}, 31^{o},and -15^{o}. The sidelobe level (SLL) is -11.5 dB for port 1 & port 4 and -8.8 dB for port 2 & port 3. The unit cell, a ring and circular patch, has the reflection phase of 612^{o} in case of normal incidence. The boresight angles of beam switching microstrip reflectarray fed by a phased array antenna are 14^{o}, -29^{o}, 35^{o},and -12^{o}. The sidelobe levels are -12.9 dB for port 1 & port 4 and -5.1 dB for port 2 & port 3.

As a microstrip reflectarray for the multi-band application, a six-band reflectarray has been developed on two layers. Each three different frequency band elements are

located on each layer. The array elements of 6.6 GHz, 18.7 GHz, and 57.5 GHz are located on top layer and the array elements of 52.5 GHz, 166 GHz, and 183.3 GHz are located on bottom layer. The capabilities of phase variation range of each element and the coupling among elements have been investigated.

A single-band and dual-band phased array antenna fed by the Butler matrix is proposed. A single-band array antenna is designed on a double-sided parallel-strip line (DSPSL) and DSPSL with the inserted ground plane. In this case, the power divider is used to increase the number of the array element, which can reduce the sidelobe level. The SLLs of each beam are lower than -12.5 dB. In particular, the SLLs of port1 and port4 are lower than -18.2 dB. The boresight angles of the four beams are 14^{o}, -46^{o}, 46^{o}, and -14^{o}, respectively. In case of dual-band systems, modified Butler matrix is used to reduce the circuit size. The Butler matrix and antenna array have dual-band characteristic and connected the back-to-back substrate. The main beam direction of 4 GHz antenna array is $\pm 14^{o}$ for port 1 & 4 and $\pm 47^{o}$ for port 2 & 3. The main beam direction of 7.3 GHz antenna array is tilted by $\pm 10^{o}$ for port 1&4 and $\pm 28^{o}$ for port 2 & 3. The side lobe level (SLL) of 4 GHz array antenna is -13 dB at port 1 & 4 and -7.5 dB at port 2&3. The SLL of 7.3 GHz system is -12.5 dB at port 1&4 and -7.2 dB at port 2&3. The frequency ratio between the two frequency bands is around 1:1.85.

Lastly, a broadband circularly polarized microstrip antenna has been developed. The microstrip antenna uses the feed method of the aperture-coupled type and has dual-offset feedlines on bottom layer. The stacked microstrip patch antennas are fed by the slot-coupled directional coupler for the circular polarization. This coupler has showed the

broadband characteristic. The 10 dB return loss bandwidth of the proposed CP antenna is 35.5% and the 3 dB axial ratio is over 40 %. The right-hand circular polarization (RHCP) gain is 8.47 dBi at 8.5 GHz, 9.17 dBi at 10 GHz and 9.13 dBi at 11.5 GHz at the boresight angle.

8.2 Recommendations for future research

In the previous study, the offset-fed beam scanning reflectarray is presented. The sidelobe level of a beam switching reflectarray has less than – 10 dB when port 2 and port 3 are excited. The sidelobe level of the feed antenna was -8.8 dB at port 2 and port 3. Therefore, if the sidelobe level of the feed array antenna may be reduced, the sidelobe level of the beam scanning reflectarray can be reduced.

Moreover, the beam shaping of reflectarrays can be achieved by adjusting the phase of the reflection coefficient at each element on the reflectarray surface. A Particle Swarm Optimization can be used to obtain the required phase distribution on the reflectarray surface which generates the shaped beam pattern.

The previous work verifies that the DSPSL has many advantages in designing RF circuits and components. To increase the versatility, the future work will construct the applications of the DSPSL and its variant forms in Monolithic Microwave Integrated Circuit (MMIC). To reduce the cost of MMIC design, the compact size is the important factor for the transition between the DSPSL and CPW. In consequence, a DSPSL in MMIC application can be realized in a compact and convenient method for wireless communication system.

REFERENCES

[1] T. A. Denidni and T. E. Libar, "Wide band four-port Butler matrix for switched multibeam antenna arrays," *IEEE Proc. Personal Indoor and Mobile Radio Communi.,*pp. 2461-2463, 2003.

[2] J. H. Winter, "Smart antenna for wireless systems*," IEEE Personal commun.*, vol. 5, pp. 23-27, Feb. 1998.

[3] H. Ming-gu, G. L. Stuber, and M. D. Austin, "Performance of switched beam smart antennas for cellular radio systems," *IEEE Trans. Vehi. Tech.*, vol. 47, no. 1, pp. 10-19, Feb. 1998.

[4] S. Mosca, F. Bilotti, A. Toscano, and L. Vegni, "A novel design method for Blass matrix beam-forming networks," *IEEE Trans. Anteanns Propagat.*, vol. 50, no. 2, pp. 225-232, Feb. 2002.

[5] Y. T. Lo and S. W. Lee, *Antenna Handbook*, New York: Van Nostrand Reinhold, 1988.

[6] W. Rotman and R. F. Turner, "Wide-angle microwave lens for line source applications," *IEEE Trnas. Antennas Propagat*., vol. AP-11, no. 6, pp. 623-632, Nov. 1963.

[7] H. Hayashi, D. A. Hitko, and C. G. Sodini, "Four-element planar Butler matrix using half-wavelength open stubs," *IEEE Microw. Wireless Compon. Lett*., vol. 12, no. 3, pp. 73-75, Mar. 2002.

[8] K. Wincza, S. Gruszczynski, and K. Sachse, "Integrated four-beam dual-band antenna array fed by broadband Butler matrix, " *Electron. Lett*., vol. 43, pp. 7-8, 2007.

[9] W. R. Li, C. Y. Chu, K. H. Lin, and S. F. Chang, "Switched-beam antenna based on modified Butler matrix with low sidelobe level," *Electron. Lett*., vol. 40, no. 5, pp. 290-292, Mar. 2004.

[10] S. Zheng, W. S. Chan, S. H. Jeung, and Q. Xue, "Broadband Butler matrix with flat coupling," *Electron. Lett*., vol. 43, no. 10, pp. 576-577, May 2007.

[11] M. Bona, L. Manholm, J. P. Starski, and B. Svensson, "Low-loss compact Butler matrix for a microstrip antenna, " *IEEE Trans. Microw. Theory Tech*., vol. 50, no. 9, pp. 2069-2075, Sep. 2002.

[12] M. Nedil, T. A. Denidni, and L. Talbi, "Novel Butler matrix using CPW multi-layer technology," *IEEE Trans. Microw. Theory Tech*., vol. 54, no. 1, pp. 499-507, Jan. 2006.

[13] J. Remez and R. Carmon, "Compact designs of waveguide Butler matrix," *IEEE Antennas Wireless Propagat. Lett.*, vol. 5, pp. 27-31, 2006.

[14] C. Chang, R. Lee, and T. Shih, "Design of a beam switching/steering Butler matrix for phased array system," *IEEE Trans. Antennas Propagat.*, vol. 58, no. 2, pp. 367-374, Feb. 2010.

[15] S. Kim and K. Chang, "Ultrawide-band transition and new microwave components using double-sided parallel-strip lines," *IEEE Trans. Microw. Theory Tech.*, vol. 52, no. 9, pp. 2148-2152, Sep. 2004.

[16] J. Chen, C. K. Chin, and Q. Xue, "Double sided parallel stripline with an inserted conductor plane and its application," *IEEE Trans. Microw. Theory Tech.*, vol. 55, no. 9, pp. 1899-1904, Sep. 2007.

[17] L. Chiu and Q. Xue, "Wideband parallel-strip 90^{o} hybrid coupler with swap," *Electron. Lett.*, vol. 44, no. 11, pp. 687-688, May 2008.

[18] L. Chiu and Q. Xue, “A parallel strip ring power divider with high isolations and arbitrary power dividing ratio,” *IEEE Trans. Microw. Theory Tech.*, vol. 55, no 11, pp. 2419-2426, Nov. 2007.

[19] D. Berry, R. Malech, and W. Kennedy, "The reflectarray antenna," *IEEE Trans. Antennas Propagat.,* vol. 11, pp. 645-651, Nov. 1963.

[20] D. M. Pozar, "Bandwidth of reflectarrays," *Electron. Lett.,* vol. 39, pp. 1490-1491, Oct. 2003.

[21] J. Huang, "Bandwidth study of microstrip reflectarray and a novel phased reflectarray concept," in *Antennas and Propagation Society International Symposium, AP-S. Digest*, 1995, pp. 582-585.

[22] C. Han, C. Rodenbeck, J. Huang, and C. Kai, "A C/Ka dual frequency dual layer circularly polarized reflectarray antenna with microstrip ring elements," *IEEE Trans. Antennas Propagat.,* vol. 52, pp. 2871-2876, Nov. 2004.

[23] Y. Fan, K. Yanghyo, Y. Ang, J. Huang, and A. Elsherbeni, "A single layer reflectarray antenna for C/X/Ka bands applications," in *ICEAA 2007 International Conference on Electromagnetics in Advanced Applications*, 2007, pp. 1058-1061.

[24] A. Yu, F. Yang, A. Z. Elsherbeni, and J. Huang, "Experimental demonstration of a single layer tri-band circularly polarized reflectarray," in *Antennas and Propagation Society International Symposium (APSURSI)*, 2010, pp. 1-4.

[25] E. Carrasco, M. Barba, and J. A. Encinar, "Reflectarray element based on aperture-coupled patches with slots and lines of variable length," *IEEE Trans. Antennas Propagat.,* vol. 55, pp. 820-825, Mar. 2007.

[26] M. R. Chaharmir, J. Shaker, N. Gagnon, and D. Lee, "Design of broadband, single layer dual-band large reflectarray using multi open loop elements," *IEEE Trans. Antennas Propagat.,* vol. 58, pp. 2875-2883, Sep. 2010.

[27] J. A. Encinar and J. A. Zornoza, "Broadband design of three-layer printed reflectarrays," *IEEE Trans. Antennas Propagat.,* vol. 51, pp. 1662-1664, Jul. 2003.

[28] J. Huang, "Capabilities of printed reflectarray antennas," *IEEE AP-S Sympo.*, pp. 131-134, Oct. 1996.

[29] J. Huang, "Microstrip reflectarray antenna for a SCANSCAT radar applications," Jet Propulsion Lab., Pasadena, CA, no. 90-45, Nov. 1990.

[30] R. D. Javor, X. D. Wu, and K. Chang, "Beam steering of a microstrip flat reflect-array antenna," *IEEE AP-S Symp.*, pp. 956-959, June 1994.

[31] R. D. Javor, X. D. Wu, and K. Chang, "Design and performance of a microstrip reflectarray antenna," *IEEE Trans. Antennas Propagat.*, vol. 43, pp. 932-939, Sept. 1995.

[32] J. Huang and R. Pogorzelski, "A Ka-band microstrip reflectarray with elements having variable rotation angles," *IEEE Trans. Antennas Propagat.*, vol. 46, pp. 650-656, May 1998.

[33] D. M. Pozar and T. Metzler, "Analysis of A reflectarray antenna using microstrip patches of variable size," *Electron. Lett.*, pp. 657-658, Apr. 1993.

[34] D. M. Pozar, S. D. Targonski, and H. D. Syrigos, "Design of millimeter wave microstrip reflectarrays," *IEEE Trans. Antennas Propagat.*, vol. 45, pp. 287-296, Feb. 1997.

[35] M. Riel and J. Laurin, "Design of an electronically beam scanning reflect array using aperture-coupled elements," *IEEE Trans. Antennas Propagat*., vol. 55, no. 5, pp. 1260-1266, May 2007.

[36] S. Hsu, C. Han, J. Huang, and K. Chang, "An offset linear-array fed Ku/Ka dual-band reflectarray for planet cloud/precipitation radar," *IEEE Trans. Antennas Propagat.*, vol. 55, no. 11, pp. 3114-3122, Nov. 2007.

[37] D.M. Pozar and B. Kaufman, "Design considerations for low side lobe microstrip antenna," *IEEE Trans. Antennas Propagat.*, vol. AP-39, pp. 1176-1185, Aug. 1990.

[38] N. M. Jizat, S. A. Rahim, and T. A. Rahman, "Dual band beamforming network integrated with array antenna," *Math. Modeling and Comp. Simu.(AMS), 2010 Fourth Asia Intern. Conf.*, pp. 561-566, 2010.

[39] HFSS ™ V12.0, 3D Full wave Electro-magnetic Field Simulation, Ansoft, Inc., [Online]. Available at. http://www.ansoft.com/products/hf/hfss

[40] F. L. Wong and K. Cheng, "A novel planar branch-line coupler design for dual-band application," *IEEE MTT-S Int. Microw. Sym. Dig.*, vol. 2, pp. 1176-1185, Jun. 2004.

[41] K. –K. Cheng and F. –L. Wong, "A novel approach to the design and inplementation of dual-band compact planar 90^{o} branch-line coupler," *IEEE Trans. Microw. Theory Tech.*, vol. 52, no. 11, pp. 2458-2463, Nov. 2004.

[42] M. J. Park, and B. J. Lee, "Dual-band, cross coupled branch line coupler," *IEEE Microw. Wireless Compon. Lett.*, vol. 15, no. 10, pp. 655-657, Oct. 2005.

[43] C. Collado, A. Grau, and F. D. Flaviis, "Dual-band planar quadrature hybrid with enhanced bandwidth response," *IEEE Trans. Microw. Theory Tech.*, vol. 54, no. 1, pp. 180-188, Jan. 2006.

[44] D. M. Pozar, *Microwave Engineering*, New York: John Wiley & Sons, 1998.

[45] Shivnarayan and B. R. vishvakarma, "Analysis of dual-band patch antenna for mobile communication," *Microw. and Optical Tech. Lett.*, vol. 47, no. 6, pp. 558-564, Dec. 2005.

[46] S. C. Gao, L. W. Li, and P. Gardner, "Analysis of a dual-frequency microstrip antenna," *IEEE Antennas and Propagat. Sociey Interna. Sympo.*, vol. 31, Jun. 2002.

[47] K. S. Kim, T. W. Kim, and J. H. Choi, "Dual-frequency aperture-coupled square patch antenna with doble notches," *Microw. and Optical Tech. Lett.*, vol. 24, no. 6, pp. 370-374, Mar. 2000.

[48] C. Jung and F. D. Flaviis, "A dual band antenna for WLAN application by double rectangular patch with 4-bridges," *IEEE Antennas and Propagat. Society, Interna. Sympo.*, vol. 4, pp. 20-25, Jun. 2004.

[49] B. Strassner, C. Han, and K. Chang, "Circularly poliarized reflectarray with microstip ring elements having variable rotation angles," *IEEE Trans. Antennas Propagat*., vol. 52, pp. 1122-1125, Apr. 2004.

[50] J. Huang, "Analysis of a microstrip reflectarray antenna for micro spacecraft applications," Spacecraft Telecommunications Equipment Section, TDA Progress Report 42-210, pp. 153-173, Feb. 1995.

[51] J. Huang and J. A. Encinar, *Reflectarray Antenna*. Hoboken, New Jersey: Wiely-IEEE Press, 2007

[52] S. W. Oh, Wideband reflectarray using compact coupled element and rectifying antenna combined with reflectarray, Ph. D. Dissertation, Texas A&M University, College Station, TX, Aug. 2011.

[53] R. Javor, X. Wu, and K. Chang, "Offset-fed microstrip reflectarray antenna," *Electron. Lett.*, vol. 30, no. 17, pp. 1363-1365, Aug. 1994.

[54] C. Han, J. Huang, and K. Chang, "A high efficiency offset-fed X/Ka-dual-band reflectarray using this membranes," *IEEE Trans. Antennas Propagat.*, vol. 53, no. 9, pp. 2792-2798, Sep. 2005.

[55] J. Huang, C. Han, and K. Chang, "A Cassegrain offsetfed dual band reflectarray," *IEEE AP-S Symp*., pp. 2439-2442, Jul. 2006.

[56] C. Han, J. Huang, and K. Chang, "Cassegrain offset subreflector-fed X/Ka dual-band reflectarray with thin membranes," *IEEE Trans. Antennas Propagat*., vol. 54, no. 10, pp. 2838-2844, Oct. 2006.

[57] J. Zuccarelli, V. Martorelli, O. D'Arcangelo, A. D. Rosa, N. Mandolesi, and L. Valenziano, "Onset & offset configuration for Ka-band reflectarray antenna," *Antennas and Propagation*, 2009. EuCAP 2009. 3rd European Conference, pp. 1234-1238, 2009.

[58] D. –C, Chang and M. –C. Huang, "Microstrip reflectarray antenna with offset feed," *Electron. Lett*., vol. 28, no. 16, pp. 1489-1491, Jul. 1992.

[59] C. A. Balanis, *Antenna Theory Analysis and Design*, New Jersey: Wiley-Interscience, 2005.

[60] R. S. Elliott, *Antenna Theory and Design*, Englewood Cliffs, New Jersey: Prentice-Hall, 1981.

[61] W. L. Stutzman and G. A. Thiele, *Anenna Theory and Design*, New York: Wiley, 1998.

[62] S. Silver, *Microwave Antenna Theory and Design*, New York: McGraw-Hill, Inc., 1949.

[63] Y. Rahmat-samii, J. Huang, B. Lopez, M. Lou, E. Im, S. L. Durden, and K. Bahadori, "Advanced precipitation radar antenna: Array-fed offset membrane cylindrical reflector antenna," *IEEE Trans. Antennas Propagat.*, vol. 53, pp. 2503-2515, Aug. 2005.

[64] Y. –J. Park and W. Wiesbeck, "Offset cylindrical reflector antenna fed by a parallel-plate Luneburg lens for automotive radar applications in millimeter-wave," *IEEE Trans. Antennas Propagat.*, vol. 51, no. 9, pp. 2481-2483, Sep. 2003.

[65] K. Y. Sze, Analysis of line-source-fed single-layer microstrip reflectarray, Ph. D. dissertation, Dept. Elect. Comp. Eng., Univ. Manitoba, Winnipeg, Canada, 2001.

[66] F.E. Tsai and M.E. Bialkowski, "An equivalent waveguide approach to designing of reflect array with the use of variable size microstrip patches," *Microwave Opt. Technol. Lett.*, vol 34, pp. 172-175, Aug. 2002.

[67] P. L. Carro and J. D. Mingo, "Analysis and synthesis of double-sided parallel - strip transitions," *IEEE Trans. Microw. Theory Tech.*, vol. 58, no. 2, pp. 372-380, Feb. 2010.

[68] J. X. Chen, C. H. Chin, K. W. Lau, and Q. Xue, "90^{o} out-of-phase power divider based on double-sided parallel striplines," *Electron. Lett.*, vol. 42, no. 21, pp. 1229-1230, Oct. 2006.

[69] T. Yang, J. X. Chen, X. Y. Zhang, and Q. Xue, "A dual-band out-of-phase power divider," *IEEE Microwave Wireless Comp. Let.*, vol. 18, no. 3, pp. 188-190, Mar. 2008.

[70] H.W. Wheeler, "Transmission-line properties of parallel strips separated by a dielectric sheet," *IEEE Trans. Microw. Theory Tech.*, vol. 13, pp. 172-185, Mar. 1965.

[71] IE3D, Zeland Softwave Inc., Fermont, CA.

[72] C. L. Dolph, "A current distribution for broadside arrays which optimizes the relationship between beamwidth and side-lobe-level," *Proc. IRE and Waves and Electrons,* Jun. 1946.

[73] D. M. Pozar and D. H. Schaubert, *Microstrip antennas: The analysis and design of microstrip antenna and arrays*, Piscataway, NJ: IEEE Press, 1995.

[74] N. C. Karmakar and M. E. Bialkowski, "Circularly polarized aperture-coupled circular microstrip antennas for L-band applications," *IEEE Trans. Antennas Propagat.*, vol. 47, no. 5, pp. 933-940, May 1999.

[75] L. Bian, Y. X. Guo, L. C. Ong, and X. Q. Shi, "Wideband circularly polarized patch antenna," *IEEE Trans., Antennas Propagat*., vol. 54, pp. 2682-2686, Sep. 2006.

[76] Y. X. Guo, L. Bian, and X. Q. Shi, "Broadband circularly polarized annular-ring microstrip antenna," *IEEE Trans. Antennas Propagat*., vol. 57, no. 8, pp. 2474-2477, Aug. 2009.

[77] K. –L. Lau and K. –M. Luk, "A wide-band circularly polarized L-probe coupled patch antenna for dual-band operation," *IEEE Trans. Antenna Propagat*., vol. 53, no. 8, pp. 2636-2644, Aug. 2005.

[78] Nasimuddin, K. P. Esselle, and A. K. Vema, "Wideband circularly polarized stacked microstrip antenna," *IEEE Antennas Wireless Propag. Lett*., vol. 6, pp. 21-24, 2007.

[79] N. Herscovici, Z. Sipus, and D. Bonefacic, "Circularly polarized singl-fed wide-band microstrip patch," *IEEE Trans. Antennas Propagat*., vol. 51, no. 6, pp. 1277-1280, Jun. 2003.

[80] S. D. Targonski and D. M. Pozar, "Design of wideband circularly polarized aperture-coupled microstrip antenna," *IEEE Trans. Antennas Propagat*., vol. 41, pp. 214-220, Feb. 1993.

[81] S. D. Targonski, R. B. Waterhouse, and D. M. Pozar, "Design of wide-band aperture-stacked patch microstrip antennas," *IEEE Trans. Antennas Propagat*., vol. 46, no. 9, pp. 1245-1251, Sep. 1998.

[82] A. Moscoso-Martir, J. G. Wanguemert-Perez, I. Molina-Fernandez, and E. Marquez-Segura, "Slot-coupled multisection quadrature hybrid for UWB application," *IEEE Microw. Wireless Compon. Lett*., vol. 19, no. 3, pp. 143-145, Mar. 2009.

[83] E. G. Cristal and L. Young, "Theory and tables of optimum symmetrical TEM-mode coupled-transmission-line directional coupler," *IEEE Trans. Microw. Theory Tech*., vol. MTT-17, no. 5, pp. 544-558, Sep. 1965.

[84] T. Tanaka, K. Tsunoda, and M. Aikawa, "Slot-coupled directional couplers between double-sided substrate microstrip lines and their applications," *IEEE Trans. Microw. Theory Tech.*, vol. 36, no. 12, pp. 1752-1757, Dec. 1988.

[85] M. –F. Wong, O. Picon, and H. Baudrand, "Analysis and design of slot-coupled directional couplers between double-sided substrate microstrip lines," *IEEE Trans. Microw. Theory Tech*., vol. 29, no. 12, pp. 2123-2129, Dec. 1991.

[86] C. E. Smith and R. –S. Chang, "Microstrip transmission line with finite-width dielectric and ground plane," *IEEE Trans. Microw. Theory Tech*., vol. MTT-33, no. 9, pp. 835-839, Sep. 1985.

[87] C. –H. Tseng and Y. –C. Hsiao, "A new broadband marchand balun using slot-coupled microstrip lines," *IEEE Microw. Wireless Compon. Lett*., vol. 20, no. 3, pp. 157-159, Mar. 2010.

[88] J. M. Rochelle, "Approximations for the symmetrical parallel-strip transmission line," *IEEE Trans. Microw. Theory Tech*., vol. MTT-23, pp. 712-714, Aug. 1975.

[89] Q. Xue, "Double side parallel strip line and its application," *IEEE MTT-S Inter. Microw. Workshop Series*, IMS 2008, pp. 55-58, Dec. 2008.

[90] S. Sun and L. Zhu, "Stopband-enhanced and size-miniaturized low-pass filters using high-impedance property of offset finite-ground microstrip line," *IEEE Trans. Microw. Theory Tech*., vol. 53, no. 9, pp. 2844-2850, Sep. 2005.

VITA

Jungkyu Lee was born in Gimpo, Republic of Korea. He received a B.S. degree in electrical engineering from the Kwangwoon University, Korea in 2001. He received an M.S. degree in electrical and computer engineering from the University of California, Irvine, in 2006. From August 2007, he started working towards his Ph. D. degree in electrical and computer engineering at Texas A&M University, College Station, TX, and was advised and guided by Prof. Kai Chang in the Electromagnetics and Microwave Laboratory. His present research includes microstrip reflectarrays, a phased array antenna, and a wideband microstrip antenna and array. He can be reached through Prof. Kai Chang, Department of Electrical and Computer Engineering, Texas A&M University, College Station, TX 77843-3128. His email address is ljk7410@gmail.com.